UNIVERSIDADE FEDERAL DE SANTA CATARINA

CENTRO TECNOLÓGICO

PROGRAMA DE PÓS-GRADUAÇÃO EM ENGENHARIA MECÂNICA

THIAGO MORHY CAVALCANTE

EVALUATION OF NOVEL AND ESTABLISHED METHODS USED IN COMPLEX VIBRO-ACOUSTIC ANALYSIS

FLORIANÓPOLIS

2022

Thiago Morhy Cavalcante

EVALUATION OF NOVEL AND ESTABLISHED METHODS USED IN COMPLEX VIBRO-ACOUSTIC ANALYSIS

Dissertação submetida ao Programa de Pós-Graduação em engenharia mecânica da Universidade Federal de Santa Catarina como requisito parcial para a obtenção do Grau de mestre em Vibrações e Acústica.

Orientador: Prof. Júlio Apolinário Cordioli, Dr.Eng.

Florianópolis

2022

Ficha de identificação da obra elaborada pelo autor,
através do Programa de Geração Automática da Biblioteca Universitária da UFSC.

Cavalcante, Thiago Morhy
Evaluation of novel and established methods used in complex vibro-acoustic analysis / Thiago Morhy Cavalcante ; orientador, Júlio Apolinário Cordioli, 2022.
103 p.

Dissertação (mestrado) - Universidade Federal de Santa Catarina, Centro Tecnológico, Programa de Pós-Graduação em Engenharia Mecânica, Florianópolis, 2022.

Inclui referências.

1. Engenharia Mecânica. 2. Finite Element Method. 3. Statistical Energy Analysis. 4. Hybrid FE-SEA Method. 5. General power-flow framework. I. Cordioli, Júlio Apolinário. II. Universidade Federal de Santa Catarina. Programa de Pós-Graduação em Engenharia Mecânica. III. Título.

Thiago Morhy Cavalcante

Evaluation of novel and established methods used in complex vibro-acoustic analysis

O presente trabalho em nível de mestrado foi avaliado e aprovado por banca examinadora composta pelos seguintes membros:

Prof. Arcanjo Lenzi, Dr. Eng.
Universidade Federal de Santa Catarina, Brasil

Prof. Bryce Gardner, Dr. Eng.
ESI US R&D, Inc., Estados Unidos

Certificamos que esta é a **versão original e final** do trabalho de conclusão que foi julgado adequado para obtenção do título de Mestre em Engenharia Mecânica.

Documento assinado digitalmente
Henrique Simas
Data: 16/12/2022 08:59:52-0300
CPF: ***.194.639-**
Verifique as assinaturas em https://v.ufsc.br

Prof. Henrique Simas, Dr. Eng.
Coordenador do Programa

Documento assinado digitalmente
Julio Apolinario Cordioli
Data: 16/12/2022 13:58:41-0300
CPF: ***.276.989-**
Verifique as assinaturas em https://v.ufsc.br

Prof. Júlio Apolinário Cordioli, Dr.Eng.
Orientador

Florianópolis, 2022.

ACKNOWLEDGEMENTS

Queria primeiro agradecer profundamente aos meus pais, Laila e Carlos, pelo suporte ao longo da minha mudança e estadia em Florianópolis. Sem isso, não teria condições de me manter em grande parte da minha formação no mestrado na UFSC. Muito obrigado, além de todo amor que recebo de ambos, o qual é verdadeiramente recíproco. Te amo, pais! Queria agradecer também ao resto da minha família, como meu tio Omar, Mario e tia Lilia, pois são pessoas que compartilho um carinho e amor ao longo da minha vida inteira e devo muito a eles. Ao meus avós, Omar e Carlos, e minhas avós, Vera e Nazaré, também os amo muito e agradeço pelo carinho. Aos familiares ou próximos que eu não mencionei, saibam que vocês me ajudaram em algum peso para eu estar aonde estou.

Também queria agradecer encarecidamente aos meus amigos. Sejam os de Belém: Gustavo, Luana, Kalynda, Gema, Pedro, Maia, João, Carlos, Thales, Gugu, Felipe, Caio, Breno, Artur, Wlad, Gema, Zé, Thiago, entreoutros. Sejam os de Florianópolis: Ana, Bruna, Bernardo, Victória, Nick, Beatriz Sousa, Beatriz Amin, Thamires. Sejam os do LVA: Marcelo, Racquel, Mathias, Bonomo, Martin, Isabella, Meireles, Maria Victoria, Camila, Joanna, Caldeira, Recruta, Eduardo, Maria Fernanda, Renan Moura, Gil, Guilherme Treco, Chefe e, claramente, meu orientador, Júlio Coridoli.

Queria agradecer também à CAPES pela bolsa de mestrado e à ESI Group pela parceria no projeto de pesquisa, o qual financiou o projeto e nos proporcionou discussões muito frutiferas no tema da pesquisa.

"Antes de realizar qualquer sonho em vida, é preciso primeiro se permitir ter um. Não tenha medo de sonhar alto."

RESUMO

Sistemas vibro acústicos complexos contemplam grande parte dos designs de engenharia em várias áreas de produção e transporte industriais e tecnológicas atualmente, e certamente em atividades futuras que permearão nossa sociedade. Tais sistemas são compostos de diversos componentes físicos com diferentes níveis de complexidade e geometria irregular. Para compreender e controlar o ruído e vibração desses sistemas complexos, múltiplas técnicas analíticas e numéricas foram desenvolvidas para simulá-las e analisá-las. Este trabalho busca apresentar uma visão global com comparações e análises para alguns destes procedimentos consagrados de modelagem e incrementa a discussão com uma técnica numérica nova adicional para problemas de média e alta frequência, com o objetivo de realçar competências e desvantagens específicas de cada método, orientando onde cada um é mais indicado para uso. Os métodos consagrados apresentados são: Método de Elementos Finitos (FEM), o qual é a referência principal da dissertação, Análise Estatística Energética (SEA) para problemas de alta frequência, e o método Híbrido FE-SEA para interações de média frequência. O método novo é uma estrutura genérica de fluxo de potência, baseado na relação de reciprocidade de campo difuso, permitindo que os subsistemas estatísticos sejam modelados diretamente de modelos de elementos finitos tradicionais ou periódicos. Isto abre a oportunidade para analisar estruturas complexas como subsistemas estatísticos, e apresenta um forte competidor para SEA e Híbrido FE-SEA para, respectivamente, problemas de média e alta frequência. Os métodos e estruturas foram analisados em alguns casos numéricos, nos quais, em cada caso, suas competências e robustez foram exploradas. A abordagem de Monte Carlo com Método de Elementos Finitos foi utilizada para representar a solução de referência. Resultados exibiram seus distintos custos de processamento computacional e quantidade de informação considerada nas soluções. A nova estrutura demonstrou quando flexibilidade e resultados robustos em comparação com métodos consagrados de análise de sistemas vibro acústicos em ambos os problemas de média e alta frequência, demonstrando grande potencial para futuras aplicações.

Keywords: Método de Elementos Finitos. Análise Estatística Energética. Método Híbrido FE-SEA. Estrutura genérica de fluxo de potência. Custo computacional.

RESUMO EXPANDIDO

Introdução

Sistemas vibro acústicos em indústrias de engenharia (como por exemplo, automotiva, aeroespacial e marinha) são analisadas através do uso de múltiplos método numéricos. A aplicações a ser exploradas guia predominantemente a escolha do método a ser utilizado para a análise. A configuração ou nível de complexidade do sistema são também aspectos que conduzem o uso de um método específico ou uma combinação de múltiplos. Por mim, apesar de um método específico ser capaz de ótimos resultados, o custo de processamento requerido pelo método pode ser inviável para o contexto e, consequentemente, não ser adequado para a tarefa.

Normalmente, estes aspectos mencionados são relacionados com o espectro de frequência adotado para a aplicação: para análises em baixa frequência, menos modos são representados, resultando em menos custo computacional e em uma deformação mais espacialmente e estatisticamente coerente. Métodos como Elementos Finitos (MEF ou FEM) para aplicações estruturais e Elementos de Contorno (MEC ou BEM) para acústicos demonstram ótima performance, já que malhas menos densas são necessárias para essas faixas de frequências. Esses métodos são também capazes de descrever o maior nível de detalhamento para a configuração do sistema. Para os casos de análise em alta frequência, a deformação altamente incoerente e maior concentração de modos demanda do modelo um expressivo detalhamento do sistema. Abordagens como Análise Estatística Energética (AEE ou SEA) se tornaram uma importante alternativa para esse tipo de cenário, já que descrições de média espacial e conjunto feitas no método servem como uma aproximação adequada para o campo difuso incerto produzido na deformação do sistema. Além disso, essas descrições são obtidas por formulações analíticas, resultando em um custo de processamento reduzido.

Se problemas de média frequência são considerados (quando deformações com comprimentos de ondas pequenos e grandes estão presentes ao mesmo tempo em diferentes componentes do sistema), o método padrão que presenta uma ótima performance é o método Híbrido FE-SEA, o qual conecta o equilíbrio dinâmico do sistema com um modelo de fluxo de potência. Isto é elegantemente idealizado com o uso da relação de reciprocidade entre a radiação do campo direto e o carregamento reverberante difuso, o qual permite

que o campo reverberante difuso dos components sejam diretamente calculados pela impedância do campo direto no seu contorno. Além disso, a maioria das implementações do método em softwares comerciais assumem que deformações em campo difuso sejam consideradas de serem espacialmente e estatísticamente incoerentes, resultando em uma redução computacional enorme, já que permite o modelo de fluxo de potência seja calculado pelas formulações robustas e analíticas já consagradas de SEA.

Apesar dessas formulações provarem de serem aproximações excelentes para as descrições do campo difuso, o raio de possíveis configurações de serem descritas é limitado apenas no espectro de condições elementares. Isto é uma consequência dessas formulações serem analíticas, as quais são incapazes de obter soluções conhecidas para deformações consideravelmente complexas. Por este motivo, os componentes irregulares que se assumem deformações com comprimento de onda pequeno no método Híbrido FE-SEA (e em SEA também) são divididos em mútiplos subcomponentes/subsistemas elementares. Normalmente, os softwares comerciais oferecem um conjunto de opções para possiveis configurações de subsistemas: cavidade acústica, placas planas e curvadas são exemplos comuns.

Geralmente, estes componentes irregulares não apenas divididos, mas também consideravelmente simplificados para garantir uma mínima quantidade de modos em cada subsistema. Esta simplificação pode implicar em perca de importantes informações sobre a deformação do subsistema e, consequentemente, uma descrição genérica para os componentes do sistema se torma atrativa. Isso é obtivel com o uso de um modelo de elementos finitos desses components. No caso de um modelo períodico de elementos finitos, a impedância do campo direto pode ser obtida através das curvas de dispersão. Já se um modelo comum de elementos finitos é utilizado, técnicas de média de conjunto podem ser aplicadas para calcular a impedância do campo direto. Estas impedâncias são utilizadas para modelar a troca de energia entre os componentes do sistema, porem a potência dissipada por estes componentes se mantém sendo calculada analíticamente tanto no método Híbrido FE-SEA quanto em SEA. Ideias e formulações iniciais para uma descrição genérica e numérica para a potência dissipada já foram definidas e exploradas neste trabalho. Estas formulações já foram anteriormente aplicadas e avaliadas em problemas de alta frequência (neste contexto, esse novo método é denominado de "Numerical SEA") e mostraram resultados robustos e encorajadores.

No caso de terem componentes no sistema vibrando em altos comprimentos de

onda, além dos vibrando em baixo comprimento de onda, uma formulação híbrida é aplicada ao novo método (neste contexto, esse novo método é denominado de "Generalized Hybrid FE-SEA" e o "Numerical SEA" acaba se tornando um subcaso deste híbrido). A implementação necessária para o método híbrido também é apresentada neste trabalho e possui a capacidade de estender a aplicabilidade dessas análises de sistemas vibroacústicos por descrever mais precisamente os subsistemas e junções com configurações irregulares em média e alta frequência com custo computacional competitivo.

Objetivos

Este trabalho tem como objetivo a avaliação da perfomance dos métodos consagrados (FEM, SEA e Híbrido FE-SEA) em análise vibroacústica em cenários específicos, permeando desde configurações elementares para irregulares, explorando suas capacidades e limitações. Este trabalho também explora um novo método generalizado, o qual foi apenas aplicado para problemas de alta frequência, e desenvolve além sua aplicabilidade para interações de média frequência, apresentando a devida implementação numérica necessária para um modelo eficiente e robusto.

Metodologia

A avaliação dos métodos consagrados e do método novo (tanto o híbrido e de alta frequência) foi feita a partir da modelagem de alguns casos específicos, sendo estes: um caso simples e clássico de média frequência, um caso mais complexo de média frequência (saindo do escopo elementar das configurações do sistema), um caso simples de alta frequência (fuselagem) e um caso de sistema com configuração irregular (parte inferior de um carro). Deixando claro cada uma das características de cada método em cenários bem distintos. Foi definido um método de referência para qualificar a performance dos métodos na modelagem dos casos. Este método se baseia em combinar FEM com uma abordagem estatística de conjunto, assim conseguindo abranger todos os possíveis casos com grande acurácia, porem ao custo computacional excessivo (o que não é um problema se o método é apenas uma referência). A abordagem utilizada neste método de referência é denominada de FE Monte Carlo. A implementação dos métodos foi feita a partir do uso do software de simulação VAOne. Os métodos FE Monte Carlo e o novo generalizado necessitaram de pos-processamentos no software Matlab para a implementação do conjunto estatístico e

formulações definidas, respectivamente.

Resultados e Discussão

Para problemas de média frequência, um conjunto de amostras e uma malha densa são requisitados para um definição robusta de componentes específicos do sistema. Para casos que consistem exclusivamente de configurações elementares, como propriedades materiais homogêneas e isotrópicas com geometria bem comportada, as formulações analíticas do método Híbrido FE-SEA são capazes de calcular uma caracterização robusta do campo de onda. Apesar do método generalizado também conseguir tal façanha, ele demanda um custo computacional bem superior para um sistema tão simples. Já em casos mais complexos, as descrições generalizadas do novo método se tornam necessárias para obter um resultado robusto. Em relação aos casos de alta frequência, a mesma lógica de resultados é obtida: para casos elementares, SEA com suas formulações analíticas é o método recomendado, já para casos mais complexos, o método generalizedo com suas formulações numéricas se torna necessário para uma modelagem robusta.

Considerações Finais

Em resumo, a ideia extraída na análise numérica feita neste trabalho foi que nenhum método vibro acústico específico possui uma performance ótima para todo cenário possível. Isto normalmente vai depender nas características do sistema e no contexto da análise. A dissertação conseguiu presentear algumas orientações relacionadas à escolha do método mais adequado a ser utilizado em alguns casos específicos. Claramente, terão casos aonde nenhum método apresentarão a performance desejada. Neste cenário, as vantagens e desvantagens deles devem ser ponderadas. O método novo generalizado apresentou uma ótima performance tanto em problemas de média como de alta frequências. Apesar disso, ele só foi avaliado em sistemas estruturais, então um sistema que contém também cavidades acústicas é de principal interesse para futuras análises. O que resta também é desenvolver formulações que abranjam tais subsistemas e junções.

Palavras-chave: Método de Elementos Finitos; Análise Estatística Energética; Método Híbrido FE-SEA; Estrutura genérica de fluxo de potência; Custo computacional.

ABSTRACT

Complex vibro-acoustic systems contemplate most of the engineering designs in several important industrial and technological areas of production and transportation at present days, and certainly will be on future activities permeating society. Such systems are composed of diverse physical components with different degrees of dynamic complexity and irregular geometries. To understand and control the noise and vibration from these complex systems, multiple analytical and numerical frameworks were developed to model and analyze them. The present work presents an overview with comparisons and evaluations for some of these established modelling methods and increments the discussion with an additional novel numerical framework to mid and high frequency problems, with the aim of highlighting specific features and limitations for each method, clarifying where each one is most suitable for use. The established frameworks and methods presented are: Finite Element Method (FEM), which is the main reference result of the paper; Statistical Energy Analysis (SEA) for high frequency problems; and the Hybrid FE-SEA Method for mid frequency interactions. The novel procedure is a general power flow framework, based on the diffuse field reciprocity relationship, allowing statistical subsystems being modeled directly from either standard or periodic FE models. This opens the opportunity to analyze complex structures at mid and high frequencies with increased precision and lower computational expenses, and presents a powerful competitor to SEA and Hybrid FE-SEA in, respectively, mid and high frequency problems. The methods and frameworks were evaluated in multiple numerical examples, in which, in each case, their modelling capabilities and reliability were explored. A FE Monte Carlo approach was used to represent the reference solutions. Results exhibited their distinct computational processing costs and detail amount considered on solutions. The novel framework showed great flexibility and reliable results in comparison to the established Vibro-acoustic analysis procedures for both mid and high frequency problems, exhibiting great potential for future applications.

Keywords: Finite Element Method. Statistical Energy Analysis. Hybrid FE-SEA Method. General power-flow framework. Computational expense.

LIST OF FIGURES

LIST OF TABLES

LIST OF SYMBOLS

General

$.^H$ Hermitian

$.^T$ Transpose

$\Delta\omega^i_{1/3}$ Width of the ith one-third band

η Damping loss factor

$\langle\, . \,\rangle$ Ensemble average

$\mathbf{f}$ Global force vector

$\mathbf{I}$ Identity matrix

$\mathbf{p}$ Global modal degrees of freedom

$\mathbf{q}$ Global nodal degrees of freedom

$\mathrm{Im}\{\, . \,\}$ Imaginary part

$\mathrm{Re}\{\, . \,\}$ Real part

$\mathrm{Tr}\{\, . \,\}$ Trace operator

ω Frequency in Rad/s

ω_n Natural mode

i Imaginary operator

n_i Modal density of the ith statistical subsystem

N_ω Number of one-third bands

Finite Element Method

$\mathbf{\Lambda}$ Modal stiffness matrix of a FE model

$\mathbf{D^p}(\omega)$ Modal dynamic stiffness matrix of a FE model

$\mathbf{D}(\omega)$ Dynamic stiffness matrix of a FE model

$\mathbf{K}$ Stiffness matrix of a FE model

$\mathbf{M}$ Mass matrix of a FE model

$\mathbf{N}$ Modal force of a FE model

$\mathbf{U}$ Modal shape matrix of a FE model

Statistical Energy Analysis

η_i Damping loss factor of ith subsystem

$\eta_{i,j}$ Coupling loss factor from jth statistical subsystem to ith statistical subsystem

$\Pi_{\mathrm{diss,i}}$ Dissipated power of ith statistical subsystem

$\Pi_{\mathrm{in,i}}$ Input power to ith statistical subsystem

$\Pi_{\mathrm{in,i}}^{\mathrm{coup}}$ Power radiated in to ith statistical subsystem due coupling

$\Pi_{\mathrm{in,i}}^{\mathrm{ext}}$ Power radiated in to ith statistical subsystem due external loads

$\Pi_{\mathrm{in,i}}^{\mathrm{ext}}$ Power radiated out from jth statistical subsystem to ith statistical subsystem

$\Pi_{\mathrm{out,i}}$ Output power from ith statistical subsystem

E_i Vibrational energy of ith statistical subsystem

Hybrid FE-SEA

$\mathbf{D_d}$ Global deterministic dynamic stiffness matrix

$\mathbf{D_{dir,i}}$ Direct field dynamic stiffness from ith statistical subsystem

$\mathbf{D_{dir}}$ Direct field dynamic stiffness

$\mathbf{D_{tot}}$ Total dynamic stiffness matrix

$\mathbf{f}^{\mathrm{ext}}$ Global force vector of external loads

$\mathbf{f}^{\mathbf{B}}$ Force vector to the deterministic boundary of a statistical subsystem

$\mathbf{f_d}$ Global force vector to deterministic subsystems

$\mathbf{f_{in,i}}$ Force force due to input loads to the ith statistical subsystem

$\mathbf{f_{rev,i}}$ Force vector from the *ith* statistical subsystem's reverberant field

$\mathbf{f_{rev}}$ Force vector from the reverberant field

$\mathbf{q^B}$ Global degrees of freedom from deterministic boundaries

$\mathbf{q_d}$ Global nodal deterministic degrees of freedom

$\mathbf{S_{ff}^{ext}}$ Cross-spectral force from external loads

$\mathbf{S_{qq,i}^{rev}}$ Cross-spectral response from the *ith* statistical subsystem's reverberant field

$\mathbf{S_{qq}}$ Cross-spectrum of the response

$\mathbf{S_{qq}}^{\text{ext}}$ Cross-spectrum response due to external loads

$\mathcal{M}_{d,i}$ Damping coefficient from deterministic coupling to the *ith* statistical subsystem

$\mathcal{M}_i$ Dissipation coefficient of the *ith* statistical subsystem

C_i Diffuse amplitude of the *ith* statistical subsystem

$h_{i,j}$ Power-transfer coefficient from *ith* statistical subsystem to the *jth* statistical subsystem

Generalized Hybrid Method

$\mathbf{B_i}$ Boolean matrix of the *ith* statistical subsystem to filter local coordinates from global ones

$\mathbf{D_i^J}$ Junction dynamic stiffness of *ith* statistical subsystem

$\mathbf{D_{dir,i}^L}$ Direct field dynamic stiffness of *ith* statistical subsystem in local coordinates

$\mathbf{D_i^{BB}}$ Boundary dynamic stiffness matrix of the *ith* statistical subsystem

$\mathbf{D_i^{BI}}$ Dynamic stiffness matrix of the *ith* statistical subsystem related to the internal degrees of freedom and forces to the boundary

$\mathbf{D_i^{IB}}$ Dynamic stiffness matrix of the *ith* statistical subsystem related to the boundary degrees of freedom and forces to the internal domain

$\mathbf{D_i^{II}}$ Internal dynamic stiffness matrix of the *ith* statistical subsystem

$\mathbf{D}^{\mathbf{II}}_{\mathbf{dir,i}}$ Internal dynamic stiffness of the *ith* statistical subsystem due to loading from its reverberant field

$\mathbf{D}^{\mathbf{II}}_{\mathbf{dir,i}}$ Internal dynamic stiffness of the *ith* statistical subsystem

$\mathbf{D_i}$ Dynamic stiffness matrix of the *ith* statistical subsystem

$\mathbf{D_{dir,i}}$ Direct field dynamic stiffness of the *ith* statistical subsystem in global coordinates

$\mathbf{f}^{\mathbf{B}}_{\mathbf{i}}$ Force vector to the boundary of *ith* statistical subsystem

$\mathbf{f}^{\mathbf{I}}_{\mathbf{i}}$ Force vector to the internal domain of *ith* statistical subsystem

$\mathbf{f}^{\mathbf{I}}_{\mathbf{diss,i}}$ Internal dissipative force of the *ith* statistical subsystem

$\mathbf{f_i}$ Force vector to the *ith* statistical subsystem

$\mathbf{H}^{\mathbf{II}}_{\mathbf{i}}$ Internal receptance of the *ith* statistical subsystem in local coordinates

$\mathbf{K}^{\mathbf{II}}_{\mathbf{i}}$ Internal stiffness matrix of the *ith* statistical subsystem

$\mathbf{K_i}$ Stiffness matrix of the *ith* statistical subsystem

$\mathbf{M}^{\mathbf{II}}_{\mathbf{i}}$ Internal mass matrix of the *ith* statistical subsystem

$\mathbf{M_i}$ Mass matrix of the *ith* statistical subsystem

$\mathbf{q}^{\mathbf{B}}_{\mathbf{i}}$ Boundary degrees of freedom to the *ith* statistical subsystem

$\mathbf{q}^{\mathbf{I}}_{\mathbf{i}}$ Internal degrees of freedom to the *ith* statistical subsystem

$\mathbf{q_i}$ Nodal degrees of freedom of the *ith* statistical subsystem

$\mathbf{S}_{\mathbf{q}^{\mathbf{I}}_{\mathbf{i}}\mathbf{q}^{\mathbf{I}}_{\mathbf{i}}}$ Cross-spectral response of the internal domain of the *ith* statistical subsystem

Numerical implementation - Modal projection (statistical subsystems)

$\widetilde{\mathbf{K}}^{\mathbf{BI,p}}_{\mathbf{i}}$ Partially modal stiffness matrix of the *ith* statistical subsystem related to the internal modal degrees of freedom and forces to the boundary with internal dissipation

$\widetilde{\mathbf{K}}^{\mathbf{IB,p}}_{\mathbf{i}}$ Partially modal dynamic stiffness matrix of the *ith* statistical subsystem related to the boundary degrees of freedom and modal forces to the interior domain with internal dissipation

$\widetilde{\mathbf{K}}_{\mathbf{i}}^{\mathbf{II,p}}$ Internal modal stiffness matrix of the *ith* statistical subsystem with internal dissipation

$\widetilde{\mathbf{K}}_{\mathbf{res,i}}$ Residual flexibility matrix of the *ith* statistical subsystem

$\mathbf{D}_{\mathbf{i}}^{\mathbf{BI,U}}$ Partially modal dynamic stiffness matrix of the *ith* statistical subsystem related to the internal modal degrees of freedom and forces to the boundary

$\mathbf{D}_{\mathbf{i}}^{\mathbf{IB,U}}$ Partially modal dynamic stiffness matrix of the *ith* statistical subsystem related to the boundary degrees of freedom and modal forces to the interior domain

$\mathbf{D}_{\mathbf{i}}^{\mathbf{II,p}}$ Modal dynamic stiffness matrix of the *ith* statistical subsystem

$\mathbf{D}_{\mathbf{i}}^{\mathbf{J,p}}$ Modal junction dynamic stiffness matrix of the *ith* statistical subsystem

$\mathbf{H}_{\mathbf{i}}^{\mathbf{II,p}}$ Internal modal receptance matrix of the *ith* statistical subsystem

$\mathbf{K}_{\mathbf{i}}^{\mathbf{BI,U}}$ Partially modal stiffness matrix of the *ith* statistical subsystem related to the internal modal degrees of freedom and forces to the boundary

$\mathbf{K}_{\mathbf{i}}^{\mathbf{BI}}$ Stiffness matrix of the *ith* statistical subsystem related to the internal degrees of freedom and forces to the boundary

$\mathbf{K}_{\mathbf{i}}^{\mathbf{II,p}}$ Internal modal stiffness matrix of the *ith* statistical subsystem

$\mathbf{M}_{\mathbf{i}}^{\mathbf{BI,U}}$ Partially modal mass matrix of the *ith* statistical subsystem related to the internal modal degrees of freedom and forces to the boundary

$\mathbf{M}_{\mathbf{i}}^{\mathbf{BI}}$ Mass matrix of the *ith* statistical subsystem related to the internal degrees of freedom and forces to the boundary

$\mathbf{p}_{\mathbf{i}}^{\mathbf{I}}$ Internal modal degrees of freedom of the *ith* statistical subsystem

$\mathbf{p}^{\mathbf{I}}$ Internal modal degrees of freedom

$\mathbf{q}^{\mathbf{I}}$ Internal nodal degrees of freedom

$\mathbf{S}_{\mathbf{f}_{\mathbf{rev,i}}^{\mathbf{I}},\mathbf{f}_{\mathbf{rev,i}}^{\mathbf{I}}}$ Cross-spectral modal response of the internal domain of the *ith* statistical subsystem due to its reverberant field

$\mathbf{S}_{\mathbf{p}_{\mathbf{i}}^{\mathbf{I}},\mathbf{p}_{\mathbf{i}}^{\mathbf{I}}}$ Cross-spectral modal response of the internal domain of the *ith* statistical subsystem

$\mathbf{U_i^I}$ Internal modal shape matrix of the *ith* statistical subsystem

Numerical implementation - Efficient matrix averaging

$\delta_{\mathbf{R,i}}$ Non-parametric randomization universal parameter

γ Lorentzian weighting function's shape parameter

$\gamma_{\mathbf{A}}$ Shape parameter defined according to the subsystems associated to $\mathbf{A}$

$\gamma_{1/3}$ Shape parameter defined according to one-third bandwidth

$L(\omega, \gamma)$ Lorentzian weighting function

$n_{\mathbf{A}}$ Modal density of the subsystems associated to $\mathbf{A}$

N_γ Integer related to γ

$W(\omega)$ Weighting function

Numerical implementation - Wavefield partition

$\mathbf{\hat{i}_i^L}$ First local coordinate's vector of the *ith* statistical subsystem

$\mathbf{\hat{i}}$ First global coordinate's vector

$\mathbf{\hat{j}_i^L}$ Second local coordinate's vector of the *ith* statistical subsystem

$\mathbf{\hat{j}}$ Second global coordinate's vector

$\mathbf{\hat{k}_i^L}$ Third local coordinate's vector of the *ith* statistical subsystem

$\mathbf{\hat{k}}$ Third global coordinate's vector

$\mathbf{\hat{v}_n}$ Flat plate's normal vector

$\mathbf{D_i^L}$ Dynamic stiffness of the *ith* statistical subsystem in local coordinates

$\mathbf{D_{in,i}^L}$ In-plane dynamic stiffness of the *ith* statistical subsystem in local coordinates

$\mathbf{D_{out,i}^L}$ Out-of-plane dynamic stiffness of the *ith* statistical subsystem in local coordinates

$\mathbf{D_{in,i}^{BI,U}}$ In-plane partially modal dynamic stiffness matrix of the *ith* statistical subsystem related to the internal degrees of freedom and modal forces to the boundary

$\mathbf{D}_{\mathbf{in,i}}^{\mathbf{IB,U}}$ In-plane partially modal dynamic stiffness matrix of the *ith* statistical subsystem related to the boundary degrees of freedom and modal forces to the internal domain

$\mathbf{D}_{\mathbf{cor,i}}^{\mathbf{II,P}}$ Modal internal dynamic stiffness matrix of the *ith* statistical subsystem that represents the correlation between out-of-plane and in-plane wavefields

$\mathbf{D}_{\mathbf{in,i}}^{\mathbf{II,P}}$ In-plane modal internal dynamic stiffness matrix of the *ith* statistical subsystem

$\mathbf{D}_{\mathbf{out,i}}^{\mathbf{II,P}}$ Out-of-plane modal internal dynamic stiffness matrix of the *ith* statistical subsystem

$\mathbf{D}_{\mathbf{in,i}}^{\mathbf{II}}$ In-plane internal dynamic stiffness matrix of the *ith* statistical subsystem

$\mathbf{D}_{\mathbf{out,i}}^{\mathbf{II}}$ Out-of-plane internal dynamic stiffness matrix of the *ith* statistical subsystem

$\mathbf{D}_{\mathbf{in,dir,i}}$ In-plane direct field dynamic stiffness of the *ith* statistical subsystem

$\mathbf{D}_{\mathbf{in,i}}$ In-plane dynamic stiffness of the *ith* statistical subsystem

$\mathbf{D}_{\mathbf{out,dir,i}}$ Out-of-plane direct field dynamic stiffness of the *ith* statistical subsystem

$\mathbf{D}_{\mathbf{out,i}}$ Out-of-plane dynamic stiffness of the *ith* statistical subsystem

$\mathbf{f}_{\mathbf{i}}^{\mathbf{L}}$ Force vector to the *ith* statistical subsystem in local coordinates

$\mathbf{f}_{\mathbf{in,i}}$ In-plane force vector to the *ith* statistical subsystem

$\mathbf{f}_{\mathbf{out,i}}$ Out-of-plane force vector to the *ith* statistical subsystem

$\mathbf{H}_{\mathbf{in,dir,i}}^{\mathbf{II,P}}$ In-plane modal internal direct field receptance of the *ith* statistical subsystem

$\mathbf{H}_{\mathbf{in,i}}^{\mathbf{II,P}}$ In-plane modal internal receptance of the *ith* statistical subsystem

$\mathbf{H}_{\mathbf{out,dir,i}}^{\mathbf{II,P}}$ Out-of-plane modal internal direct field receptance of the *ith* statistical subsystem

$\mathbf{H}_{\mathbf{out,i}}^{\mathbf{II,P}}$ Out-of-plane modal internal receptance of the *ith* statistical subsystem

$\mathbf{K}_{\mathbf{in,i}}^{\mathbf{II,P}}$ In-plane modal internal stiffness matrix of the *ith* statistical subsystem

$\mathbf{K}_{\mathbf{out,i}}^{\mathbf{II,P}}$ Out-of-plane modal internal stiffness matrix of the *ith* statistical subsystem

$\mathbf{K}_{\mathbf{in,res,i}}$ In-plane residual flexibility of the *ith* statistical subsystem

$\mathbf{K}_{\mathbf{out,res,i}}$ Out-of-plane residual flexibility of the *ith* statistical subsystem

$\mathbf{q}_{\mathbf{i}}^{\mathbf{L}}$ Nodal degrees of freedom of the *ith* statistical subsystem in local coordinate

$\mathbf{q_i^{B,L}}$ Boundary degrees of freedom of the *ith* statistical subsystem in local coordinates

$\mathbf{q_i^{I,L}}$ Internal degrees of freedom of the *ith* statistical subsystem in local coordinates

$\mathbf{T_i^I}$ Internal transformation matrix of the *ith* statistical subsystem from local to global coordinates

$\mathbf{T_i}$ Nodal transformation matrix of the *ith* statistical subsystem from local to global coordinates

$\mathbf{U_{in,i}^I}$ In-plane internal mode shape matrix of the *ith* statistical subsystem

$\mathbf{U_{out,i}^I}$ Out-of-plane internal mode shape matrix of the *ith* statistical subsystem

$\mathbf{U_{in,i}^{I,L}}$ In-plane internal modal shape matrix of the *ith* statistical subsystem in local coordinates

$\mathbf{U_{out,i}^{I,L}}$ Out-of-plane internal modal shape matrix of the *ith* statistical subsystem in local coordinates

θ_x Rotation degree of freedom in the x direction

θ_y Rotation degree of freedom in the y direction

θ_z Rotation degree of freedom in the z direction

u_x Displacement degree of freedom in the x direction

u_y Displacement degree of freedom in the y direction

u_z Displacement degree of freedom in the z direction

Numerical implementation - Modal projection (deterministic subsystems)

$\mathbf{B_{d,i}}$ Boolean matrix of the *ith* deterministic subsystem to filter nodal degrees of freedom from partially modal ones

$\mathbf{D_d^h}$ Deterministic dynamic stiffness in partially modal coordinates

$\mathbf{D_{dir,i}^h}$ Direct field dynamic stiffness of the *ith* statistical subsystem in partially modal coordinates

$\mathbf{D_{tot}^h}$ Total dynamic stiffness in partially modal coordinates

$\mathbf{K_{d,i}^{h}}$ Stiffness matrix of the *ith* deterministic subsystem in partially modal coordinates

$\mathbf{K_{d,i}^{II}}$ Internal stiffness matrix of the *ith* deterministic subsystem

$\mathbf{K_{d,i}^{IB}}$ Stiffness matrix of the *ith* deterministic subsystem related to the boundary degrees of freedom and modal forces to the internal domain

$\mathbf{K_{d,i}}$ Stiffness matrix of the *ith* deterministic subsystem

$\mathbf{M_{d,i}^{h}}$ Mass matrix of the *ith* deterministic subsystem in partially modal coordinates

$\mathbf{M_{d,i}^{II}}$ Internal mass matrix of the *ith* deterministic subsystem

$\mathbf{M_{d,i}}$ Mass matrix of the *ith* deterministic subsystem

$\mathbf{p_{d,i}^{I}}$ Internal modal degrees of freedom of the *ith* deterministic subsystem

$\mathbf{q_{d,i}^{h}}$ Partially modal degrees of freedom of the *ith* deterministic subsystem

$\mathbf{q^{h}}$ Partially modal degrees of freedom

$\mathbf{q_{d,i}^{B}}$ Boundary degrees of freedom of the *ith* deterministic subsystem

$\mathbf{q_{d,i}^{I}}$ Internal degrees of freedom of the *ith* deterministic subsystem

$\mathbf{q_{d,i}}$ Nodal degrees of freedom of the *ith* deterministic subsystem

$\mathbf{S_{ff}^{ext,h}}$ Cross-spectral force due to external loads in partially modal coordinates

$\mathbf{S_{q^h q^h}}$ Cross-spectral response in partially modal coordinates

$\mathbf{T_{U}}$ Transformation matrix from partially modal to nodal degrees of freedom

$\mathbf{T_{U,i}}$ Transformation matrix from partially modal to nodal degrees of freedom of *ith* deterministic subsystem

$\mathbf{U_{d,i}^{I}}$ Internal modal shape of the *ith* deterministic subsystem

$\mathbf{U_{d,i}}$ Free modal shape of the *ith* deterministic subsystem

$\mathcal{X}_{\mathbf{d,i}}$ Constrained modal shape of the *ith* deterministic subsystem

$\mathrm{N_d}$ Number of deterministic subsystems

$E_{d,i}$ Vibrational energy of the *ith* deterministic subsystem

$K_{d,i}$ Kinetic energy of the ith deterministic subsystem

$U_{d,i}$ Strain energy of the ith deterministic subsystem

CONTENTS

1 INTRODUCTION

1.1 A BRIEF TALK ABOUT VIBROACOUSTICS

Understanding the behavior and interaction of vibrating solid elastic structures and fluids is the goal of the field of study of steady-state vibroacoustics. Such physical systems have been the subject of extensive research over the last decades, partly due to the improvement of the computational capacity to model and analyze more complex structures (HAMBRIC; SUNG; NEFSKE, 2017), but also due to the increased applications and production regarding these systems in the industrial and daily environment. Some examples of applications to these systems are (shown in fig. 1): the industrial machinery's maintenance, which analyzes the structural vibration and sound field from a particular machine for the search to any possible faulty piece's appearance, the vibration control of a satellite during its launch to orbit, or simply the microphones and loudspeakers employed in the routine of the majority of society. The range of applications for the vibroacoustic field is vast and has yet a lot to be discovered, understood and applied.

There are several ways to model a vibroacoustic system (for now on, when vibroacoustic system is specified, it should be understood as one or more vibrating structure and/or acoustic fluid coupled). Each modeling approach defined will differ in terms of system's detailing scope and its interaction's idealization, which results in different types of formulations, processing demands and information retained to the model (HAMBRIC; SUNG; NEFSKE, 2017).

One common reference method for a vibro-acoustical numerical analysis is the Finite Element Method (FEM) and, although it was first developed to model static interactions, its versatility allows for any geometry or constrain to be described by the virtue of an appropriate discretization of the system domain, denoted as FE mesh grid. Due to the high computational processing expense required, the method is usually applied to low frequency vibrations, where a deterministic motion is associated (MEIROVITCH, 2010).

Higher frequency's analysis is constituted of smaller wavelengths deformations that not only demand a denser mesh grid, resulting in increased computational expense, but are also increasingly sensible to imperfections, leading to significant results variation when affected by manufacturing uncertainties (LYON; DEJONG, 1995). Deterministic approaches become then a misguiding alternative and statistical methods are pursued, e.g.

(a) Machinery analysis

Source: indiaMART

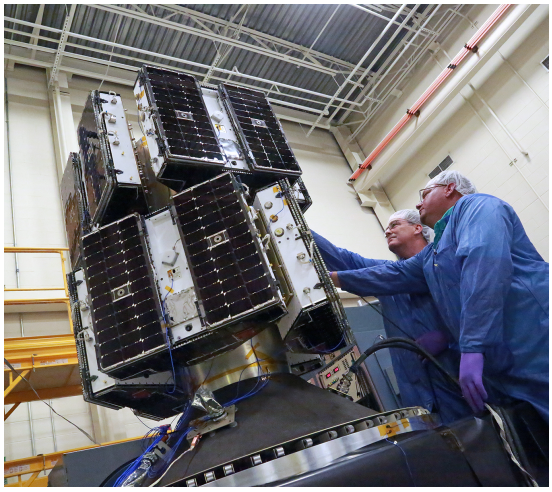

(b) Satellite over vibration analysis

Source: NASA

Figure 1 – Applications to vibro-acoustic systems

FE Monte Carlo simulations.

The reliability associated to the FE Monte Carlo approach, which assumes a population of systems, will mainly depend on the randomization techniques employed to each sample. This process is responsible to insert manufacturing uncertainties into the system. The approach, however, requires FE model to be solved multiple times in order to derive an ensemble average, which still makes the procedure highly unfeasible for practical and industrial applications at high frequencies (PAPADRAKAKIS; PAPADOPOULOS, 1996).

The established framework denoted as Statistical Energy Analysis (SEA) was developed to work as an alternative for these scenarios, where the uncertain mechanics linked to these sensible systems can be approximated by simply elementary analytical formulations (LE BOT, 2015). Essentially, SEA analyzes the energy storage and flow that occurs inside of a complex vibro-acoustic system. This power-flow balance is defined between the group of modes (or superposition of wavefields) of the physical components, denoted as "subsystems". The definitions of these groups of modes or subsystems are mainly done by the use of analytical formulations, which are only possible for physical components with elementary configurations, e.g, flat and (singly and doubly) curved plates, beams and cavities. Several other assumptions regarding damping, excitation and modal density (or wave diffusivity) are also required to reach known analytical solutions to such subsystem descriptions (HANSEN, 2018). Still, if all these configurations are met, the

framework is able to model the system's ensemble average response in reduced processing time, when compared to a single FE model.

Although real-life physical components usually present configurations outside of the elementary scope, in high frequencies, their complex wavefield motion tends to resemble of an elementary one, due to diffusivity, and therefore may be considerably approximated by the SEA analytical formulations (LYON; DEJONG, 1995). The SEA framework comes as an important tool for practical applications that are composed of physical components that reach high frequencies motions considerably fast in the frequency spectrum.

In case the system has, at the same time, physical components vibrating at distinct wavefield characteristics (some diffusive and others coherent), resulting either in a impracticable processing expense for a single FE model or in a poorly reliable SEA model, as the framework assumptions are clearly not met for every physical component, a different scenario emerges and is denoted as mid frequency interaction/problem. A method was then developed to handle such interaction and is denoted as Hybrid FE-SEA (SHORTER; LANGLEY, 2005b), whereas both the SEA power-flow balance and FE dynamic equilibrium are coupled and modelled to solve the system.

The Hybrid FE-SEA method idealizes the system as interaction between two different types of subsystems. Components that hold low modal densities (or highly spatially coherent wave-motions) and have configurations are denoted as the deterministic subsystems and are modelled by FE models, allowing any complex configuration to be described. The remaining components are defined as statistical subsystems and have their wave-motion described by a random diffuse reverberant field. If a maximum entropy distribution is assumed to the these subsystems' properties statistics, their fields (and consequently them) can be described by simply their direct field dynamic stiffness matrix $\mathbf{D}_{\text{dir}}$ and asymptotic modal density n. Moreover, as opposed to the deterministic subsystems, the statistical ones retain degrees of freedom only at their deterministic boundaries (junctions and excitation points), greatly reducing the computational processing expense involved in the model.

The direct field dynamic stiffness matrix $\mathbf{D}_{\text{dir}}$ had been derived analytically for some specific types of physical component's connections. In the case of flat plates, point (LANGLEY; SHORTER, 2003), interior line (CREMER; HECKL; PETERSSON, 2005) and flat boundaries line (LANGLEY; HERON, 1990) junctions have known solution for the parameter. It was also mentioned that $\mathbf{D}_{\text{dir}}$ could be indirectly derived by the use of another established vibro-acoustic modelling procedure, the Boundary Element Method

(SHORTER; LANGLEY, 2005b) (probably requiring a modification of the method to include ensemble statistics).

1.2 NOVEL DISCUSSIONS

The analytical descriptions of the statistical subsystems ($\mathbf{D}_{\text{dir}}$ and n) have only known solutions for elementary configurations, falling into the same limitation that SEA subsystems suffer. In a more recent publication (ALIMONTI et al., 2019), a novel generalized power-flow framework was introduced, which may be regarded as a more generic approach for the Hybrid FE-SEA method, as the statistical subsystems can be numerically described, encompassing more complex configurations. This new framework was then evaluated, in the reference, using periodic FE models to derive the statistical subsystems parameters and analyze the system.

An example of numerical derivation for $\mathbf{D}_{\text{dir}}$ using standard FE models was then formulated (DEVRIENDT et al., 2015). The approach assumes that ensemble average techniques are applied to the subsystems' FE matrices, which, if FE Monte Carlo simulations are adopted to this end, unfeasible processing expenses come involved into the derivation. Therefore, the paper also presented an average technique with reduced computational cost and based on frequency averages in conjunction with a Lorentzian weighted function. This function invokes a mathematical key feature enabling the ensemble average of FE models to be analytically computed, eliminating an enormous amount of computational processing time and allowing for the derivation to be applied into practical applications.

Parallel to this present thesis's work, a deeper investigation using this numerical description (with standard FE models) to the statistical subsystems was carried out (HINZ, 2021). The author also presented a numerical derivation for the dissipated power flow, which eliminated the need for a generic modal density definition, resulting in a full description for the statistical subsystem's power flow. Moreover, an alternative efficient ensemble averaging technique from the random matrix theory was evaluated. The work evaluated these generic descriptions into the novel generalized power-flow framework, applying it solely into fully statistical systems (no deterministic components), representing a direct comparison with SEA. In this context, the novel framework is denoted as numerical SEA.

There are still investigations left to be made, specially regarding to systems that

contains deterministic subsystems and how the novel generalized power-flow framework compares to other established methods, when analyzing their computational costs and versatility. The generalized power-flow framework, which is been denoted as "generalized hybrid FE-SEA method" here, serves as a generic framework for multiple and distinct vibroacoustic problems. It is a generalization of the Hybrid FE-SEA and, therefore, the SEA. It has the capability of extending the applicability of such vibroacoustic analysis by more accurately describing subsystems and junctions with irregular configurations in mid and high frequency problem at competitive processing time.

1.3 DISSERTATION OBJECTIVES

This work aims to evaluate the performance of the established methods in vibroacoustic analysis in specific scenarios, ranging from elementary to irregular configurations, exploring their features and limitations. The work also explores a novel generalized method, which had only been applied to high frequency problems, and further develops its applicability to mid frequency interactions, presenting the proper numerical implementation required for a proper robust model.

1.4 CHAPTERS OVERVIEW

This document is structured as follows:

- Chapter 2: Theoretical review. This chapter describes and clarifies the established numerical method and frameworks mentioned in the introduction: The Finite Element Method, the Statistical Energy Analysis and the Hybrid FE-SEA Method. No specific case scenario is investigated, just the main formulation and concept for each method and framework are presented.

- Chapter 3: Generalized hybrid FE-SEA method. The novel framework concepts and formulations are initially presented. The chapter then proceeds to discuss the fully numerical descriptions of the statistical subsystems used in the framework.

- Chapter 4: Numerical implementation. This chapter mostly explores the procedures and implementations applied to the novel method's model to assure competitive processing costs and a more robust definition of the subsystem's wavefield.

- Chapter 5: Numerical Examples. The three established methods and the novel framework are evaluated over four cases, involving both mid and high frequency problems. Features and limitations associated to each method or framework is discussed and compared.

- Chapter 6: Conclusion. Wrapping up this evaluation of vibroacoustic methods. Future works are suggested.

2 THEORETICAL REVIEW

The present chapter is just a brief presentation of the discussed methods. For a deeper and clearer understanding, the following references are suggested:

- Finite Element Method: (PETYT, 2019) and (FAHY; GARDONIO, 2007).
- Statistical Energy Analysis: (LYON; DEJONG, 1995) and (LE BOT, 2015).
- Hybrid FE-SEA Method: (SHORTER; LANGLEY, 2005b), (HAMBRIC; SUNG; NEFSKE, 2017) and (MARCELLA, 2018).

2.1 FINITE ELEMENT METHOD

FEM describes the continuous system's deformation as a superposition of local shape functions, resulting in a discretization of the system's domain into a finite set of smaller continuous elements. Energies contributions associated to each element are described in terms of generalized degrees of freedom $\mathbf{q}$ located at local specific points (usually at the element's vertices, but not only), denoted as nodes. Figure 2 illustrates a continuous plate discretized in a set of elements (rectangles) and nodes (dots). Shared nodes (and consequently degrees of freedom) between neighbor elements enforce compatibility into local dynamic mechanisms assuring a coupled deformation for the whole system.

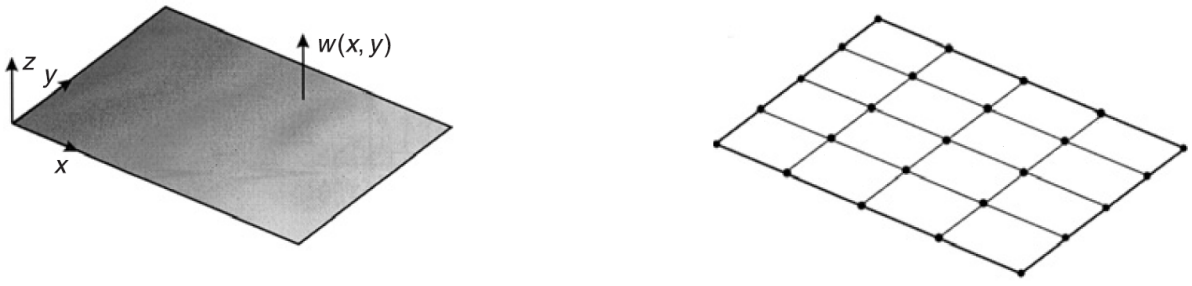

(a) (b)

Figure 2 – (a) Continuous and (b) discretized system.

Source: (FAHY; GARDONIO, 2007).

By representing the elementary energy expressions in quadratic forms, algebraic relations between the local mechanisms and the generalized degrees of freedom are introduced, which, if appropriate vetorization is defined, system's global matrices are assembled.

Assuming an internal damping η and harmonic motion ω, the system's equation of motion is defined as

$$\left[-\omega^2\mathbf{M} + (1 + \mathrm{i}\eta)\mathbf{K}\right]\mathbf{q} = \mathbf{D}(\omega)\mathbf{q} = \mathbf{f}, \tag{2.1}$$

where $\mathbf{M}$, $\mathbf{K}$ are, respectively, the mass and rigidity matrices and represent the inertia's and restoration's contributions of the forces exerted by the internal mechanisms of the system. Moreover, the force vector $\mathbf{f}$ and structural damping matrix $\mathrm{i}\eta\mathbf{K}$ are, respectively, derived from non-conservative forces of externally applied sources and internal friction mechanisms. Solving Eq. 2.1 simply involves the inversion of the dynamic stiffness matrix $\mathbf{D}(\omega)$ at every analyzed frequency. However, at higher frequencies, the number of degrees of freedom required for appropriate wave deformation's representations increases, resulting in larger matrices and, as mentioned, unfeasible computational processing expense.

A diagonalization process is invoked to improve the method performance and obtain a deeper understanding of the problem (SHABANA, 2010). A set of modal degrees of freedom $\mathbf{p}$ and a transformation matrix $\mathbf{U}$, i.e. $\mathbf{q} = \mathbf{U}\mathbf{p}$, are defined and derived from following the generalized eigenproblem of undamped free vibration

$$\left[\mathbf{K} - \omega_n^2\mathbf{M}\right]\mathbf{u} = \mathbf{0}, \tag{2.2}$$

where $\mathbf{U}$ is obtained from the collection of all eigenvectors from above equation, i.e. $\mathbf{U} = [\mathbf{u_1}, \ldots, \mathbf{u_N}]$. Due to the orthogonality property $\mathbf{U}$ has to both $\mathbf{M}$ and $\mathbf{K}$ matrices (resulted form the eigenproblem above), by multiplying the left side of Eq. 2.1 by $\mathbf{U}^{\mathrm{T}}$ and by applying a change of coordinates ($\mathbf{q} = \mathbf{U}\mathbf{p}$), the subsequent decoupled equation of motion is obtained

$$\left[-\omega^2\mathbf{I} + (1 + \mathrm{i}\eta)\mathbf{\Lambda}\right]\mathbf{p} = \mathbf{D^p}(\omega)\mathbf{p} = \mathbf{N}, \tag{2.3}$$

where the resulted modal mass $\mathbf{I}$ and modal stiffness $\mathbf{\Lambda}$ matrices are diagonal matrices and, therefore, the above equation can easily solved by simply inverting each diagonal element from the modal dynamic stiffness matrix $\mathbf{D^p}(\omega)$. In the context of vibro-acoustics, the columns of the transformation matrix $\mathbf{U}$ represent the nodal deformations (shape) associated to each mode of the system, underlying essential information to the analysis. Computational processing expense's improvements obtained from computing the system's response in modal coordinates can be further increased if a truncation of eigenvalues

retrieved from Eq. 2.2 is performed. Usually, the rule of thumb is to compute natural frequencies that have values up to twice the highest frequency analyzed (PETYT, 2019). Moreover, the vector $\mathbf{N}$ represents the modal force ($\mathbf{N} = \mathbf{U}^T\mathbf{f}$). After the modal coordinates $\mathbf{p}$ are determined from Eq. 2.3, a change back to nodal coordinates is possible ($\mathbf{q} = \mathbf{U}\mathbf{p}$) to extract physical understanding from the system's response.

The vibrational energy stored in each component of the system is then computed as the superposition of each of their nodal degrees of freedom's strain and kinetic energies (MEIROVITCH, 2010). However, it's possible to derive these same component's energies directly in modal coordinates through modally projected mass and stiffness matrices (MACE; SHORTER, 2000).

As mentioned, high frequency analysis requires that the influence from manufacturing imperfections be embedded into the FE model in order to derive reliable results. Statistical approaches like FE Monte Carlo become intuitive options to simulate an appropriate model, where, instead of a single deterministic system, the FE Monte Carlo defines a population of similar systems, leading to ensemble average results.

2.2 STATISTICAL ENERGY ANALYSIS

In SEA, the system's domain is sectioned in specific physical components of similar wave properties, e.g., a set of plates, beams and/or cavities. The subsystems of these components are idealized as energy containers that store, dissipate and exchange energy between other subsystems. Usually, in the case of a beam component, its subsystems are defined from the axial, the two bending and the rotational wavefields. Figure 3 illustrates an example of two beam's components coupled, displaying each of their four wavefields ("B" standing for bending, "L" for longitudinal and "T" for torsional).

The statistical framework assumes a population of nominally identical systems, resulting in the following ensemble average power-flow balance for the *ith* subsystem (considering only steady-state dynamics)

$$\langle \Pi_{\mathrm{diss,i}} \rangle + \langle \Pi_{\mathrm{out,i}} \rangle = \langle \Pi_{\mathrm{in,i}} \rangle, \tag{2.4}$$

where $\langle \Pi_{\mathrm{diss,i}} \rangle$, $\langle \Pi_{\mathrm{out,i}} \rangle$ and $\langle \Pi_{\mathrm{in,i}} \rangle$ are, respectively, the ensemble average dissipated, output and input power of the *ith* subsystem. The $\langle . \rangle$ brackets are used here in this work to represent the ensemble average estimation. In order to derive the response for these subsystems,

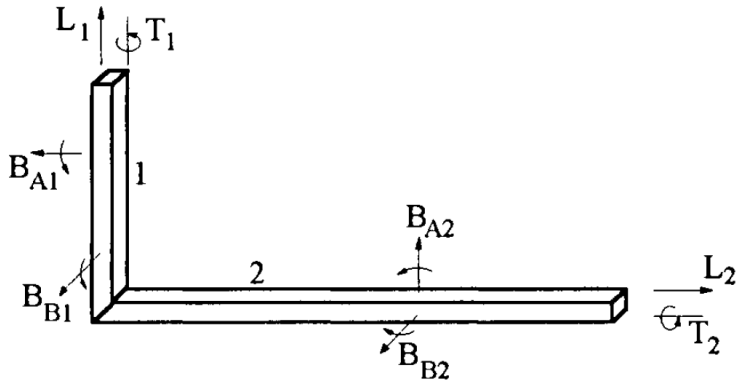

Figure 3 – Beam components and wavefields

Source: (LYON; DEJONG, 1995)

relations between these power coefficients and their energy are defined. Initially, the input power is composed of a coupling $\langle \Pi_{\mathrm{in,i}}^{\mathrm{coup}} \rangle$ and an external source $\langle \Pi_{\mathrm{in,i}}^{\mathrm{ext}} \rangle$ contribution

$$\langle \Pi_{\mathrm{in,i}} \rangle = \langle \Pi_{\mathrm{in,i}}^{\mathrm{coup}} \rangle + \langle \Pi_{\mathrm{in,i}}^{\mathrm{ext}} \rangle = \sum_{j \neq i} \langle \Pi_{\mathrm{j,i}} \rangle + \langle \Pi_{\mathrm{in,i}}^{\mathrm{ext}} \rangle, \tag{2.5}$$

where $\langle \Pi_{\mathrm{j,i}} \rangle$ is the ensemble average power radiated from *jth* subsystem to the *ith* subsystem. In SEA, the relationship between the radiated power and the radiator subsystem's energy is written as

$$\langle \Pi_{\mathrm{i,j}} \rangle = \omega \eta_{i,j} \langle E_i \rangle. \tag{2.6}$$

The SEA coefficient coupling loss factor $\eta_{i,j}$ is related to the ensemble average impedance of both subsystems at their connection. The output power is simply written as the superposition of radiated power from the *ith* to all the other subsystems

$$\langle \Pi_{\mathrm{out,i}} \rangle = \sum_{i \neq j} \langle \Pi_{\mathrm{i,j}} \rangle. \tag{2.7}$$

The ensemble average power being dissipated by internal losses is proportional to the kinetic energy and is derived using the definition of the *ith* subsystem's damping loss factor η_{i} (equivalent to the one from FEM) (LE BOT, 2015)

$$\langle \Pi_{\mathrm{diss,i}} \rangle = \omega \eta_{\mathrm{i}} \langle E_{\mathrm{i}} \rangle. \tag{2.8}$$

The external input power $\langle \Pi_{\mathrm{in}}^{\mathrm{ext}} \rangle$ is proportional to the ensemble average impedance of the subsystem in the excited location, similar to the coupling loss factor derivation. Furthermore, these ensemble average impedances actually converge to the impedances of infinite extended subsystems, which have less tedious and time consuming derivations and

are usually the standard approach used in commercial software routines to obtain such parameters. Accordingly, by substituting Eq. 2.5 to 2.8 into Eq. 2.4, the ensemble average power-balance equation is written as

$$\omega \left[\eta_{\mathrm{i}} \langle E_{\mathrm{i}} \rangle + \sum_{i \neq j} \left(\eta_{\mathrm{i,j}} \langle E_{\mathrm{i}} \rangle - \eta_{\mathrm{j,i}} \langle E_{\mathrm{j}} \rangle \right) \right] = \langle \Pi^{\mathrm{ext}}_{\mathrm{in,i}} \rangle, \tag{2.9}$$

which if written in matrix form

$$\begin{bmatrix} \eta_1 + \sum_{j \neq 1} \eta_{\mathrm{j},1} & -\eta_{1,2} & \cdots & -\eta_{1,\mathrm{N}} \\ -\eta_{2,1} & \eta_2 + \sum_{j \neq 2} \eta_{\mathrm{j},2} & & \\ \vdots & & \ddots & \vdots \\ -\eta_{\mathrm{N},1} & \cdots & & \eta_{\mathrm{N}} + \sum_{j \neq N} \eta_{\mathrm{j,N}} \end{bmatrix} \begin{bmatrix} \langle E_1 \rangle \\ \langle E_2 \rangle \\ \vdots \\ \langle E_{\mathrm{N}} \rangle \end{bmatrix} = \frac{1}{\omega} \begin{bmatrix} \langle \Pi^{\mathrm{ext}}_{\mathrm{in},1} \rangle \\ \langle \Pi^{\mathrm{ext}}_{\mathrm{in},2} \rangle \\ \vdots \\ \langle \Pi^{\mathrm{ext}}_{\mathrm{in,N}} \rangle \end{bmatrix}, \tag{2.10}$$

where a simple inversion, per frequency, of the left matrix computes the ensemble average vibrational energy from each subsystem. The computational processing time associated in solving Eq. 2.10 is fairly short, due to the small number of energy degrees of freedom defined (one per subsystem). Engineering units results (displacements for structures and pressure for cavities) can be derived from simple kinetic relations applied to the obtained vibrational energies.

2.3 HYBRID FE-SEA METHOD

The method initially describes the system's physical components in accordance to their wavefield characteristics. Components that have short wavelength's deformations, i.e. high sensibility to imperfections early on the frequency spectrum and require denser FE mesh grids for a reliable representation, have their subsystems described statistically. The rest of the components, which admit reasonably coherent deformations and demand smaller computational processing expenses, are modelled as deterministic subsystems.

These deterministic subsystems are described using FE models and, therefore, have their whole domain's response described by a set of generalized degrees of freedom $\mathbf{q_d}$. In the case of statistical subsystems, it's assumed that their domains are subdivided into two distinct characteristic regions. The first region is the deterministic boundary and contains all connection regions to other subsystems or/and external loads (i.e. all regions that admit flow of energy in or out of the subsystem). The second region, denoted as random boundary/domain, represents the remaining of the subsystem's domain. Due to the intrinsic sensibility to manufacturing imperfections and high degree of complexity that the

statistical subsystems possess, it's not intended for this region to be known precisely, but rather have an assumed statistical description across an ensemble. This shall be discussed further in this chapter.

An additional set of degrees of freedom $\mathbf{q^B}$ is then defined to describe displacement field across the deterministic boundaries of the statistical subsystems. Figure 4 exhibits these sets of generalized coordinates for an elementary system, where we can observe the $\mathbf{q_d}$ degrees of freedom defined for the (a) deterministic subsystem, and the $\mathbf{q^B}$ degrees of freedom describing the displacement field along the junction between (b) and (c) statistical subsystems and the excitation point (1) at the (c) subsystem. A global set of degrees of freedom $\mathbf{q}$ is then defined as the collection of both $\mathbf{q_d}$ and $\mathbf{q^B}$ generalized coordinates, i.e. $\mathbf{q} = [\mathbf{q_d}^T \, \mathbf{q^B}^T]^T$. Nevertheless, it is important to point out that, under specific conditions, the definition of the coordinate vector $\mathbf{q^B}$ becomes unnecessary, as the power-flow contributions on these regions could be directly calculated from analytical formulations of SEA. This is discussed in the end of this section and is how the method is usually implemented.

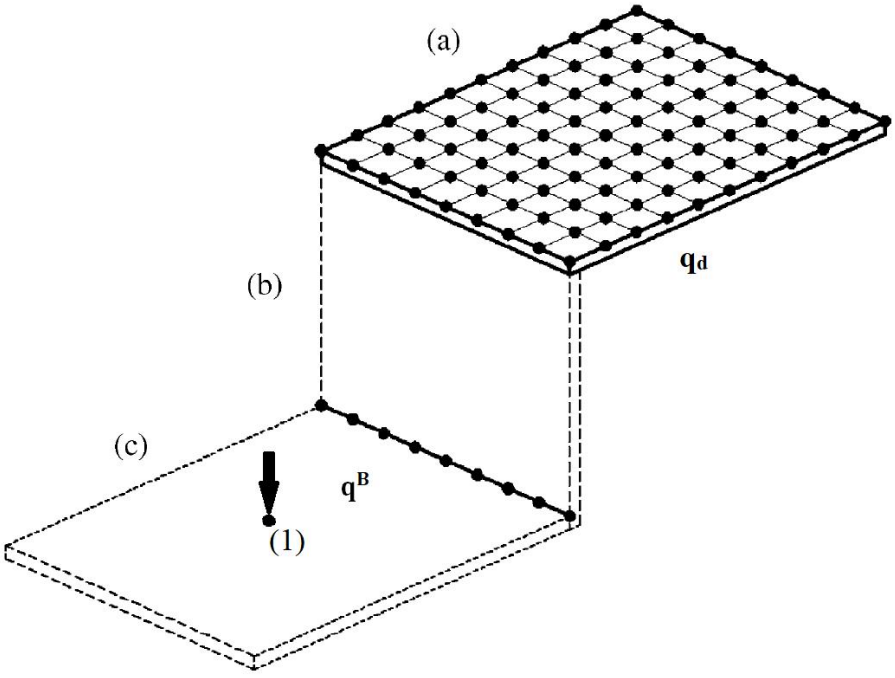

Figure 4 – Degrees of freedom used to describe the (a) subsystem, the junction between (b) and (c) subsystems, and the (1) excitation on the (c) subsystem.

Source: (SHORTER; LANGLEY, 2005b) (Modified)

2.3.1 Equations of motion

The uncoupled equation of motion that governs the deterministic subsystems is written as

$$\mathbf{D_d}(\omega)\mathbf{q} = \mathbf{f_d}, \tag{2.11}$$

where $\mathbf{D_d}$ and $\mathbf{f_d}$ represent, respectively, the dynamic stiffness matrix and external force vector applied to the deterministic subsystems. These contributions are computed similarly to Eq. 2.1. Regarding the statistical subsystems, their responses are defined from the energetics of random reverberant wavefields (every statistical subsystem is assumed to have, at least, one). Also, a direct field is generated from the prescribed displacement of the deterministic boundary and represents the radiation of energy into the subsystem's domain (i.e. reverberant field) assuming no reflections from the random boundary/domain are present. The dynamics of the deterministic boundary due to this direct field radiation/load is controlled by the dynamic stiffness $\mathbf{D_{dir}}$ that depends on the respective boundaries's configurations.

In order to characterize the wavefield, the reflections that arise from the direct field coming upon contact to the random boundary/domain are required to be considered and are represented by the reverberant wavefield. The influence of this wave scattering over the deterministic boundary is represented by the reverberant force $\mathbf{f_{rev}}$. Moreover, the uncoupled equation of motion of the statistical subsystem is defined as

$$\mathbf{D_{dir}}(\omega)\mathbf{q} = \mathbf{f^B} + \mathbf{f_{rev}}, \tag{2.12}$$

where $\mathbf{f^B}$ is the external load applied to the deterministic boundary. As mentioned, defining an exact configuration for the random boundary/domain of statistical subsystems is unfeasible, indicating that a more intuitive and practical definition for their influence is to actually assume that their configuration is uncertain and adopt a statistical description for them (SHORTER; LANGLEY, 2005a). For that reason, it is assumed that $\mathbf{f_{rev}}$ is random.

The coupled equation of motion is then written as follows

$$\mathbf{D_{tot}}(\omega)\mathbf{q} = \mathbf{f_{ext}} + \sum_i \mathbf{f_{rev,i}}, \tag{2.13}$$

where the total dynamic stiffness is the superposition of all subsystem's impedances defined, i.e. $\mathbf{D_{tot}} = \mathbf{D_d} + \sum_i \mathbf{D_{dir,i}}$. The *ith* subscript stands for *ith* statistical subsystem's contribution. Furthermore, the external force vector $\mathbf{f_{ext}}$ is the collection of all external loads to the deterministic regions of the system. Due to the uncertain characteristic associated to the reverberant fields, the reverberant force $\mathbf{f_{rev}}$ is random and, therefore, the interest lies in ensemble average response of the system. The cross-spectrum of the response ($\mathbf{S_{qq}} = \langle \mathbf{q}\mathbf{q}^H \rangle$) is written as

$$\mathbf{S_{qq}} = \mathbf{D_{tot}^{-1}}(\mathbf{f_{ext}}\mathbf{f_{ext}}^H + \sum_i \mathbf{f}\langle \mathbf{f_{rev,i}} \rangle^H + \sum_i \langle \mathbf{f_{rev,i}} \rangle \mathbf{f}^H + \sum_{i,j} \langle \mathbf{f_{rev,i}}\mathbf{f_{rev,j}}^H \rangle)\mathbf{D_{tot}^{-H}}. \tag{2.14}$$

2.3.2 Diffuse reverberant field

Defining proper ensemble statistics for the reverberant fields is tricky, as we would have to assume known information regarding the random boundary/domain. Moreover, the ensemble response is directly related to the amount of uncertainty defined for these regions, which should reach a limit when a maximum of entropy is considered. This results in the reverberant fields, across an ensemble, assuming a "diffuse" characteristic, where minimum information regarding the random boundaries/domains is defined (SHORTER; LANGLEY, 2005b).

It was shown that a specific and powerful relation arises from a diffuse reverberant field condition: the cross-spectral reverberant force can be fully described in terms of the direct field dynamic stiffness (SHORTER; LANGLEY, 2005a). This relation is denoted as "Reciprocity relationship between the diffuse reverberant field radiation and the direct field loading", which not only enables Eq. 2.14 to be deterministic defined, but also greatly simplifies it.

In this condition of diffuse field, the ensemble average reverberant force converges to zero, i.e. $\langle \mathbf{f_{rev,i}} \rangle = 0$, and the coupled cross-spectrum of diffuse reverberant force is given by

$$\sum_{i,j} \left\langle \mathbf{f_{rev,i}}\mathbf{f_{rev,j}}^H \right\rangle = \sum_i 4C_i \, \mathrm{Im}\left\{\mathbf{D_{dir,i}}\right\}. \tag{2.15}$$

The constant C_i is denoted as the diffuse field's amplitude and was proven to be directly proportional to the ensemble average energy $\langle E_i \rangle$ associated to the population of reverberant fields (SHORTER; LANGLEY, 2005a)

$$C_i = \frac{\langle E_i \rangle}{\pi \omega n_i}, \tag{2.16}$$

where n_i is the ith statistical subsystems modal density. The cross-spectral response of the coupled system is then written as

$$\mathbf{S_{qq}} = \mathbf{S_{qq}^{ext}} + \sum_i \mathbf{S_{qq,i}^{rev}} = \mathbf{D_{tot}}^{-1} \left[\mathbf{f_{ext}} \mathbf{f_{ext}}^H + \sum_i \frac{4\langle E_i \rangle}{\pi \omega n_i} \operatorname{Im} \{\mathbf{D_{dir,i}}\} \right] \mathbf{D_{tot}}^{-H}. \tag{2.17}$$

2.3.3 Power-flow model

In order to determine the energy contained in the diffuse reverberant fields and obtain the response of the deterministic regions (Eq. 2.17), a power-flow model between the statistical subsystems is idealized, similar to SEA. Figure 5 exhibits the power-flow balance for a statistical subsystem, where the power flowing into the subsystem is generated by the direct field radiation from the deterministic regions and is caused by either externally applied loads or coupling interaction to other subsystems. The reverberant field, which arises from the scattering of the direct field onto the random boundary/domain, is responsible to internally dissipate the contained energy in the subsystem and to radiate it to other subsystems through connection regions at the deterministic boundary. It is assumed that the most of the statistical subsystem's energy is contained at the reverberant field and, therefore, determining the latter's energy is enough to fully describe the energetics of the subsystem.

Assuming a population of systems, the time and ensemble average input power is expressed as (MACE; SHORTER, 2000)

$$\langle \Pi_{\text{in},i} \rangle = \frac{1}{2} \left\langle \operatorname{Re} \left\{ \mathrm{i}\omega \mathbf{f_{in,i}}^H \mathbf{q} \right\} \right\rangle. \tag{2.18}$$

The force generating energy to the ensemble average container is then described in terms of a direct field

$$\langle \Pi_{\text{in},i} \rangle = \frac{1}{2} \left\langle \operatorname{Re} \left\{ \mathrm{i}\omega \mathbf{q}^H \mathbf{D_{dir,i}}^H \mathbf{q} \right\} \right\rangle. \tag{2.19}$$

As the real part of a complex number multiplied by the imaginary operator i is equal to its imaginary part multiplied by -1, the equation can be rewritten as

$$\langle \Pi_{\text{in},i} \rangle = -\frac{1}{2} \left\langle \operatorname{Im} \left\{ \omega \mathbf{q}^H \mathbf{D_{dir,i}}^H \mathbf{q} \right\} \right\rangle, \tag{2.20}$$

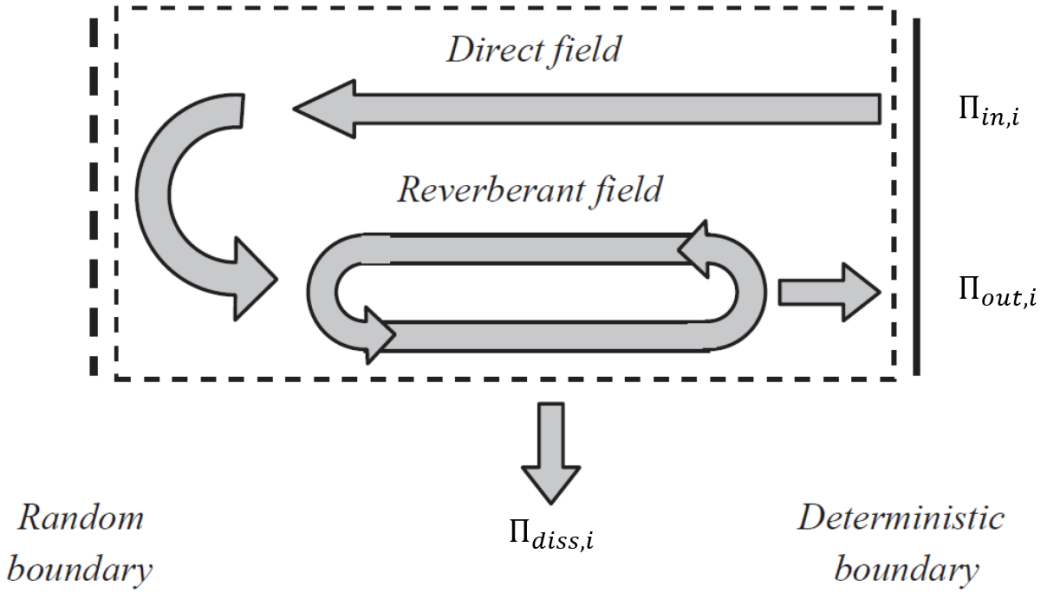

Figure 5 – Power-flow balance for a statistical subsystem

Source: (SHORTER; LANGLEY, 2005b) (Modified)

which if represented in index notation (conjugate operator on the dynamic stiffness is cancelled by the minus sign outside braces)

$$\langle \Pi_{\mathrm{in},i} \rangle = \frac{\omega}{2} \operatorname{Im} \left\{ \sum_{k,j} D_{\mathrm{dir,i}}^{(k,j)} \left\langle q^{(j)} q^{(k)*} \right\rangle \right\}. \tag{2.21}$$

As the direct field dynamic stiffness is not affected by the random reflections that arise from the subsystem's interior domain, i.e., is deterministic, it is not influenced by the ensemble average operator. Moreover, by remembering that the expression inside the brackets is the definition of a single element of the cross-spectrum matrix, the expression is rewritten as

$$\langle \Pi_{\mathrm{in},i} \rangle = \frac{\omega}{2} \sum_{k,j} \operatorname{Im} \left\{ D_{\mathrm{dir,i}}^{(k,j)} \right\} S_{qq}^{(k,j)}, \tag{2.22}$$

where a real response is assumed to the system. Rewriting the expression using matrix notation and the trace operator

$$\langle \Pi_{\mathrm{in},i} \rangle = \frac{\omega}{2} \operatorname{Tr} \left[\operatorname{Im} \left\{ \mathbf{D_{dir,i}} \right\} \mathbf{S_{qq}} \right], \tag{2.23}$$

and substituting Eq. 2.17 in above equation, the input power to the *ith* statistical subsystem is given by

$$\langle \Pi_{\mathrm{in},i} \rangle = \langle \Pi_{\mathrm{in},i}^{\mathrm{ext}} \rangle + \sum_{j} h_{j,i} \frac{\langle E_j \rangle}{n_j}, \tag{2.24}$$

where the externally applied load is given by (assuming deterministic excitation)

$$\langle \Pi_{\mathrm{in,i}}^{\mathrm{ext}} \rangle = \frac{\omega}{2} \operatorname{Tr}\left[\operatorname{Im}\left\{ \mathbf{D_{dir,i}} \right\} \mathbf{D_{tot}}^{-1} \mathbf{S_{ff}^{ext}} \mathbf{D_{tot}}^{-H} \right]. \tag{2.25}$$

The input power applied from the jth to the ith statistical subsystem by coupling is quantified by the power transfer coefficient $h_{j,i}$, which is given by

$$h_{\mathrm{i,j}} = \frac{2}{\pi} \operatorname{Tr}\left[\operatorname{Im}\left\{ \mathbf{D_{dir,i}} \right\} \mathbf{D_{tot}}^{-1} \operatorname{Im}\left\{ \mathbf{D_{dir,j}} \right\} \mathbf{D_{tot}}^{-H} \right] = h_{\mathrm{j,i}}. \tag{2.26}$$

The power being flown out of the ith statistical subsystem is completely composed of the exchange of energy between the other subsystems. In this case, the force that introduces the energy flow is generated by the ith statistical subsystem's reverberant field's displacement $\mathbf{S_{qq,i}^{rev}}$ in the boundary regions and is controlled by the total dynamic stiffness $\mathbf{D_{tot}}$ (as we are assuming coupling to both deterministic and statistical subsystems). Similarly to Eq. 2.23, the ensemble and time average output power leaving the ith is given by

$$\langle \Pi_{\mathrm{out},i} \rangle = \frac{\omega}{2} \operatorname{Tr}\left[\operatorname{Im}\left\{ \mathbf{D_{tot}} \right\} \mathbf{S_{qq,i}^{rev}} \right]. \tag{2.27}$$

By substituting reverberant term of Eq. 2.17 above, the expression can therefore also be written as

$$\langle \Pi_{\mathrm{out},i} \rangle = \left[\mathcal{M}_{d,i} + \sum_j h_{i,j} \right] \frac{\langle E_i \rangle}{n_i}, \tag{2.28}$$

where the damping coefficient $\mathcal{M}_{d,i}$ quantifies the amount of power radiated by the ith statistical subsystem that is dissipated by the deterministic subsystems in terms of modal energy and is given by

$$\mathcal{M}_{\mathrm{d,i}} = \frac{2}{\pi} \operatorname{Tr}\left[\operatorname{Im}\left\{ \mathbf{D_{d,j}} \right\} \mathbf{D_{tot}}^{-1} \operatorname{Im}\left\{ \mathbf{D_{dir,i}} \right\} \mathbf{D_{tot}}^{-H} \right]. \tag{2.29}$$

Similar to SEA, the power being dissipated internally by intrinsic mechanisms is given by Eq. 2.8. In the Hybrid FE-SEA method however, the diffuse reverberant fields of the statistical subsystems are represented by the ratio of their ensemble average energy and modal densities $\langle E_j \rangle / n_j$ (in (LYON; DEJONG, 1995), this ratio is denoted as modal power potential). Hence a more appropriate expression is given by

$$\langle \Pi_{\mathrm{diss,i}} \rangle = \mathcal{M}_{\mathrm{i}} \frac{\langle E_i \rangle}{n_i}, \tag{2.30}$$

where the dissipation coefficient $\mathcal{M}_{\mathrm{i}}$ of the ith statistical subsystem is equal to modal overlap factor, i.e,

$$\mathcal{M}_{\mathrm{i}} = \omega \eta_{\mathrm{i}} n_{\mathrm{i}}, \tag{2.31}$$

where n_{i} is the *ith* statistical subsystem's modal density. Finally, in order to derive the ratio of the energy and modal density associated to the *ith* statistical subsystem, Equation 2.23, 2.28 and 2.30 are substituted in Eq. 2.4, resulting in the following power-flow balance expression

$$\left[\left(\mathcal{M}_{\mathrm{i}} + \mathcal{M}_{\mathrm{d,i}} + \sum_{i \neq j} h_{\mathrm{i,j}}\right)\frac{\langle E_i \rangle}{n_i} - \left(\sum_{i \neq j} h_{\mathrm{j,i}} \frac{\langle E_j \rangle}{n_j}\right)\right] = \langle \Pi^{\mathrm{ext}}_{\mathrm{in,i}} \rangle, \tag{2.32}$$

which if written in matrix form

$$\begin{bmatrix} \mathcal{M}_1 + \mathcal{M}_{\mathrm{d,1}} + \sum_{j \neq 1} h_{\mathrm{j,1}} & \dots & -h_{1,\mathrm{N}} \\ \vdots & \ddots & \vdots \\ -h_{\mathrm{N},1} & \dots & \mathcal{M}_{\mathrm{N}} + \mathcal{M}_{\mathrm{d,N}} + \sum_{j \neq N} h_{\mathrm{N,j}} \end{bmatrix} \begin{bmatrix} \langle E_1 \rangle / n_1 \\ \vdots \\ \langle E_N \rangle / n_N \end{bmatrix} = \begin{bmatrix} \langle \Pi^{\mathrm{ext}}_{\mathrm{in,1}} \rangle \\ \vdots \\ \langle \Pi^{\mathrm{ext}}_{\mathrm{in,N}} \rangle \end{bmatrix}, \tag{2.33}$$

an inversion of the left matrix per frequency derives the ratio of the ensemble average energy and modal densities of every diffuse reverberant field involved in the system. If the vibrational energy is desired, a simple multiplication with the respective modal density computes the result (LE BOT, 2015).

2.3.4 Numerical implementation

Although Eq. 2.33 presents a proper power-flow balance between complex subsystems, in Hybrid FE-SEA method, it is often obtained a simplified solution for the subsystems due to implementation purposes. As a result from the small wavelength associated to the statistical subsystem's deformation, their coherence information between "distant" connection regions (contained in the deterministic boundary) can be neglected (COTONI; SHORTER; LANGLEY, 2007). This assumption reflects in energy flow coefficients ($\Pi^{ext}_{in,i}$, $h_{i,j}$ and $\mathcal{M}_{d,i}$) that can actually be computed using local direct field's information. Moreover, if we further assume that junctions are referred as point, straight line and flat area connections, then analytical formulations for the direct field dynamic stiffness $\mathbf{D_{dir}}$ of the statistical subsystems become available:

- Point (LANGLEY; SHORTER, 2003).
- Line (LANGLEY; HERON, 1990).
- Area (WILLIAMS; MAYNARD, 1982) and (LANGLEY, 2007a)

In case these local impedances are used, the external loads applied solely to statistical subsystems derive external input powers that can be direct computed from asymptotic expressions, similar to SEA. The same occurs to connection regions between solely statistical subsystems: due to Eq. 2.5 and Eq. 2.24, the power transfer coefficient $h_{i,j}$ can be directly computed from established coupling loss factor $\eta_{i,j}$ and modal density n_i expressions

$$h_{i,j} = \omega n_i \eta_{i,j}. \tag{2.34}$$

The degrees of freedom from these "statistical junctions" (not in contact with deterministic subsystems) become then unnecessary for the analysis and can be discarded from the model. The same can be applied to ones connected solely to external loads. Additionally, if no deterministic subsystems are considered in the system, the hybrid framework becomes equivalent to a wave-approach of SEA (SHORTER; LANGLEY, 2005b).

Although the analytical formulations greatly facilitate the definition of the power-flow model, known solutions for these expressions are only available for elementary configurations that may not accurately describe the energy flow of the system. Numerical descriptions become then strong alternatives to characterize the direct field and could be obtained through a modified version of the Boundary Element Method (SHORTER; LANGLEY, 2005b), however an analytical elementary dissipated power is still computed in Eq. 2.30. Therefore, a more generic power-flow definition is required to analyze complex systems that are outside of elementary configuration scope, and solid numerical alternatives for the statistical subsystem's descriptions have to be defined. Both topics are explored and discussed in the next section, where the novel method is presented.

3 GENERALIZED HYBRID FE-SEA METHOD

3.1 GENERALIZED POWER-FLOW BALANCE

It would be expected that the definition of a generic power-flow model should avoid the restricted usage of elementary analytical formulations to compute the statistical subsystem's energy flow and dynamic equilibrium. Ideally, this more generic method would be capable of handling numerical descriptions of the power-flow definition, expanding the possibilities for complex configurations of subsystems and deriving a more robust analysis. The method is denoted here as generalized hybrid FE-SEA method, or simply as generalized hybrid method.

The method defines a similar cross-spectral response for the coupled system (Eq. 2.14) and also ensures a diffuse characteristic to all reverberant fields ($\mathbf{f_{rev,i}} = 0$ and Eq. 2.15). However, the direct relation between diffuse amplitude and the ratio vibrational energy and modal density (Eq. 2.16) is not considered as it would require a known modal density to derive useful engineering units for the statistical subsystems. The cross-spectral response of the Generalized Hybrid method is then written as

$$\mathbf{S_{qq}} = \mathbf{D_{tot}}^{-1} \left[\mathbf{f_{ext}} \mathbf{f_{ext}^{H}} + \sum_{i} C_i \, \mathrm{Im} \left\{ \mathbf{D_{dir,i}} \right\} \right] \mathbf{D_{tot}}^{-H}. \tag{3.1}$$

The derivation of the power-flow balance is similar to the Hybrid FE-SEA Method. Assuming conservation of energy (Eq. 2.4), the ensemble average input power to the *ith* statistical subsystem is written as

$$\langle \Pi_{\mathrm{in},i} \rangle = \Pi_{\mathrm{in},i}^{\mathrm{ext}} + \pi\omega \sum_{j} h_{j,i} C_j. \tag{3.2}$$

The output power from the *ith* statistical subsystem is expressed as

$$\langle \Pi_{\mathrm{out},i} \rangle = \pi\omega C_i \left[\mathcal{M}_{d,i} + \sum_{j} h_{i,j} \right], \tag{3.3}$$

and the dissipated power by the *ith* subsystem is written as

$$\langle \Pi_{\mathrm{diss,i}} \rangle = \pi\omega \mathcal{M}_{\mathrm{i}} C_i. \tag{3.4}$$

Notice that if we assume the relation from Eq. 2.16, the equation above converges to Eq. 2.30. The computation of the dissipation coefficient $\mathcal{M}_i$ can be made analytically, similar to what the Hybrid FE-SEA method does, however, for more complex configurations,

it is suggested to be numerically computed. In the next section, a alternative numerical derivation is discussed. Similar to Eq. 2.32, the power-flow balance equation for the Generalized Hybrid framework is expressed as

$$\pi\omega \left[\left(\mathcal{M}_{\mathrm{i}} + \mathcal{M}_{\mathrm{d,i}} + \sum_{i \neq j} h_{\mathrm{i,j}} \right) C_{\mathrm{i}} - \left(\sum_{i \neq j} h_{\mathrm{j,i}} C_{\mathrm{j}} \right) \right] = \Pi^{\mathrm{ext}}_{\mathrm{in,i}}, \tag{3.5}$$

which if written in matrix form

$$\begin{bmatrix} \mathcal{M}_1 + \mathcal{M}_{\mathrm{d},1} + \sum_{j \neq 1} h_{\mathrm{j},1} & \dots & -h_{1,\mathrm{N}} \\ \vdots & \ddots & \vdots \\ -h_{\mathrm{N},1} & \dots & \mathcal{M}_{\mathrm{N}} + \mathcal{M}_{\mathrm{d,N}} + \sum_{j \neq N} h_{\mathrm{N,j}} \end{bmatrix} \begin{bmatrix} C_1 \\ \vdots \\ C_{\mathrm{N}} \end{bmatrix} = \frac{1}{\pi\omega} \begin{bmatrix} \Pi^{\mathrm{ext}}_{\mathrm{in},1} \\ \vdots \\ \Pi^{\mathrm{ext}}_{\mathrm{in,N}} \end{bmatrix}. \tag{3.6}$$

Again, a simple inversion of the left matrix per frequency is required to compute the diffuse amplitudes. The response of the deterministic degrees of freedom is then simply obtained in Eq. 3.1. In order to derive the vibrational energy contained in the reverberant wavefields, a simple equality between Eq. 2.8 and Eq. 3.4 is necessary to isolate the energy and compute it

$$E_i = \frac{\pi \mathcal{M}_i C_i}{\eta_i}. \tag{3.7}$$

The Generalized Hybrid Method presents a generic procedure to model and analyze a complex vibro-acoustic system, specially to mid and high frequency problems, where FEM struggles to derive a population of systems. The only consideration made to the model is regarding the statistics of the reverberant fields ensemble, which is reasonably acceptable for subsystems that perform low wavelength's deformation. Therefore, no major assumptions were made to the model regarding its geometry or configurations.

In order to fully describe the statistical subsystems in the model, two important parameters are required: the direct field dynamic stiffness $\mathbf{D_{dir,i}}$ and the dissipation coefficient $\mathcal{M}_i$. In the next section, a numerical derivation for these the two parameters is presented. It's important to point out that if analytical formulations are used to compute these two parameters, the generalized hybrid method becomes equivalent to the established Hybrid FE-SEA method.

3.2 NUMERICAL DESCRIPTIONS FOR STATISTICAL SUBSYSTEMS

These parameters can be derived in combination with other established numerical methods, e.g., standard FEM or periodic FEM. The choice of which approach to use in

combination will depend on the configuration of system, e.g., if it is composed of a irregular or a recurring cell structure. The standard/non-periodic case will be explored in more detail here in this text, for another discussion in this respective approach, it is suggested the reading of a different work that was conducted in the same research project of this present text (HINZ, 2021). It's important to point out that, although this standard/non-periodic approach is ideal for irregular configurations, it could also be used to model elementary or periodic structures, as it presents a generic formulation to characterize the subsystem.

In order to numerically describe the statistical subsystems, the standard/non-periodic approach assumes that a standard FE model for the respective subsystem is available. Prepossessing manipulations are performed to the statistical subsystem's FE model in order to derive the method's parameters before coupling it to the rest of the system. As discussed in the review section of FEM, a standard subsystem's FE model contains nodal degrees of freedom over its entire domain (figure 6a). However, two important sets of degrees of freedom for the *ith* statistical subsystem are required to be defined and are referred as: boundary degrees of freedom $\mathbf{q_i^B}$, similar to the ones from the Hybrid FE-SEA method that describe the deformation in connections to external loads or other subsystems, and the internal degrees of freedom $\mathbf{q_i^I}$ that describe the deformation for the rest of the statistical subsystem's domain (figure 6b).

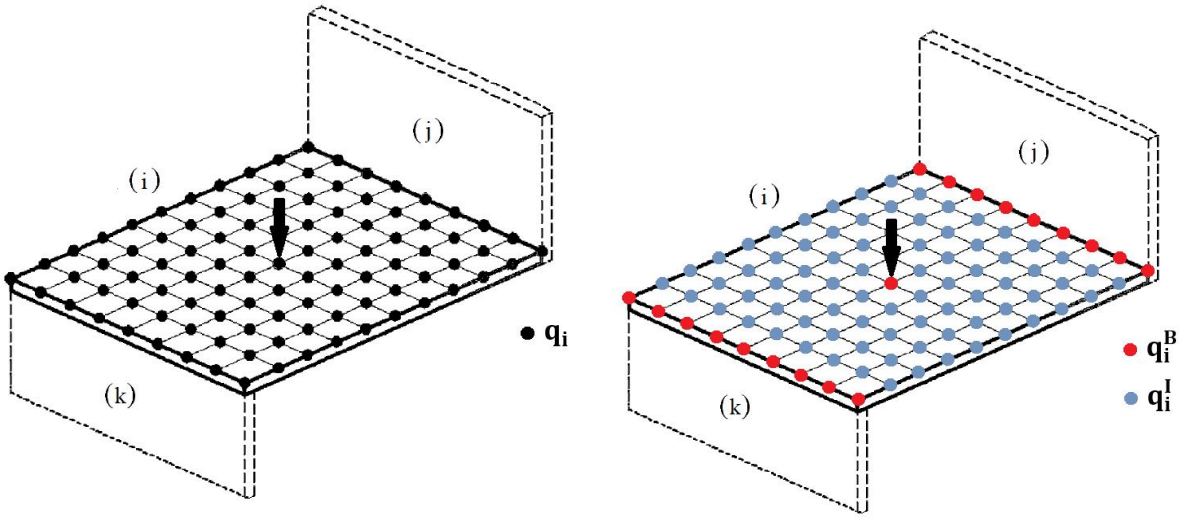

(a) Subsystem's FE nodes (b) Boundary and internal nodes

Figure 6 – Representation to which FE nodes the respective degrees of freedom are associated with. The *jth* and *kth* subsystems exhibited represent connected subsystems to the *ith* one.

Source: Modified from (SHORTER; LANGLEY, 2005b)

3.2.1 Direct field dynamic stiffness

The equation of motion associated to the *ith* statistical subsystem is expressed as (assuming harmonic motion and internal mechanic damping)

$$\left[-\omega^2\mathbf{M_i} + (1+\eta_i)\mathbf{K_i}\right]\mathbf{q_i} = \mathbf{D_i}\mathbf{q_i} = \mathbf{f_i}. \tag{3.8}$$

If we expand the set of degrees of freedom ($\mathbf{q_i} = \left[\mathbf{q_i^B}^T \mathbf{q_i^I}^T\right]^T$)

$$\begin{bmatrix} \mathbf{D_i^{BB}} & \mathbf{D_i^{BI}} \\ \mathbf{D_i^{IB}} & \mathbf{D_i^{II}} \end{bmatrix} \begin{bmatrix} \mathbf{q_i^B} \\ \mathbf{q_i^I} \end{bmatrix} = \begin{bmatrix} \mathbf{f_i^B} \\ \mathbf{f_i^I} \end{bmatrix}, \tag{3.9}$$

where $\mathbf{f_i^B}$ and $\mathbf{f_i^I}$ are the external loads applied to, respectively, the boundary and internal degrees of freedom. The dynamic stiffness $\mathbf{D_i}$'s submatrices describe contributions associated to a specific set of forces (first superscript) and degrees of freedom (second superscript), where "B" and "I" represent, respectively, the boundary and internal sets of generalized coordinates.

A simple manipulation is then performed to reduce the set of degrees of freedom, omitting the internal ones, however still retaining their influence over the subsystem's deformation. By performing the multiplication of the left side of Eq. 3.9, two equations are derived

$$\mathbf{D_i^{BB}}\mathbf{q_i^B} + \mathbf{D_i^{BI}}\mathbf{q_i^I} = \mathbf{f_i^B}, \tag{3.10}$$

and

$$\mathbf{D_i^{IB}}\mathbf{q_i^B} + \mathbf{D_i^{II}}\mathbf{q_i^I} = \mathbf{f_i^I}. \tag{3.11}$$

By isolating the interior degrees of freedom in the second equation and substituting in the first equation, we obtain the following expression

$$\mathbf{D_i^{BB}}\mathbf{q_i^B} + \mathbf{D_i^{BI}}(\mathbf{D_i^{II}}^{-1}\mathbf{f_i^I} - \mathbf{D_i^{II}}^{-1}\mathbf{D_i^{IB}}\mathbf{q_i^B}) = \mathbf{f_i^B}. \tag{3.12}$$

As mentioned, any degrees of freedom experiencing external loads is assumed to be part of $\mathbf{q_i^B}$, i.e, $\mathbf{f_i^I} = 0$, hence

$$(\mathbf{D_i^{BB}} - \mathbf{D_i^{BI}}\mathbf{D_i^{II}}^{-1}\mathbf{D_i^{IB}})\mathbf{q_i^B} = \mathbf{D_i^J}\mathbf{q_i^B} = \mathbf{f_i^B}. \tag{3.13}$$

The operation being performed in equation above is denoted Schur complement (more specifically taking the Schur complement of $\mathbf{D_i^{II}}$ to $\mathbf{D_i^{BB}}$) (DEVRIENDT et al., 2015), which derives the *ith* statistical subsystem's equation of motion using solely the boundary

degrees of freedom. By idealizing the subsystem's response as a superposition of a direct and reverberant field, the junction's dynamic stiffness matrix $\mathbf{D_i^J}$ contains both wavefields influences. The derivation of the direct field dynamic stiffness matrix in local coordinates $\mathbf{D_{dir,i}^L}$ can be seen as the removal of the influence of the reverberant wavefield from $\mathbf{D_i^J}$, retaining only the desired infinite propagating contribution.

This procedure is achieved by taking an ensemble average of the junction dynamic stiffness $\mathbf{D_i^J}$, i.e., $\mathbf{D_{dir,i}^L} = \langle \mathbf{D_i^J} \rangle$ (LANGLEY, 2007b). Moreover, as regions that allow energy flow from external or coupling interactions are assumed to be known precisely, the boundary dynamic stiffness $\mathbf{D_i^{BB}}$ is interpreted as deterministic. The correlation matrices $\mathbf{D_i^{BI}}$ and $\mathbf{D_i^{IB}}$ describe the coherence between the two sets of degrees of freedom. Therefore, no specific interactions directly related to the internal domain's uncertainty are regarded, which can be interpreted as representation of deterministic matrices (HINZ, 2021).

The only matrix from Eq. 3.13 that inherently contains influence from the uncertain interactions of the internal domain is the internal dynamic stiffness $\mathbf{D_i^{II}}$, therefore the direct field dynamic stiffness in (local coordinates) can be written as (HINZ, 2021)

$$\mathbf{D_{dir,i}^L} = \mathbf{D_i^{BB}} - \mathbf{D_i^{BI}} \langle \mathbf{H_i^{II}} \rangle \mathbf{D_i^{IB}}, \tag{3.14}$$

where $\mathbf{H_i^{II}}$ is the internal receptance ($\mathbf{H_i^{II}} = \mathbf{D_i^{II}}^{-1}$). This ensemble average to the internal matrix can be derived experimentally (CLOT et al., 2020), numerically or, if certain conditions are met, analytically (DEVRIENDT et al., 2015). This is discussed further in the next chapter. Assuming all alternatives are capable of obtaining a robust convergence, either one could be used to establish the required ensemble. Moreover, the direct field dynamic stiffness in global deterministic coordinates $\mathbf{q}$ is written as

$$\mathbf{D_{dir,i}} = \mathbf{B_i}^T \mathbf{D_{dir,i}^L} \mathbf{B_i}, \tag{3.15}$$

where the *ith* boolean matrix $\mathbf{B_i}$ translates the local deterministic coordinates to the global ones ($\mathbf{q_i^B} = \mathbf{B_i q}$).

3.2.2 Dissipation coefficient

In order to numerically define the dissipation coefficient for the *ith* statistical subsystem, a different derivation for the dissipated power is expressed (MACE; SHORTER, 2000)

$$\langle \Pi_{diss,i} \rangle = \frac{1}{2} \langle \mathrm{Re}\{ i\omega \mathbf{f}^{\mathbf{I}}_{\mathbf{diss,i}}{}^{H} \mathbf{q}^{\mathbf{I}}_{\mathbf{i}} \} \rangle. \tag{3.16}$$

Assuming only internal damping, the dissipated force can be expressed as

$$\mathbf{f}^{\mathbf{I}}_{\mathbf{diss,i}} = i\eta_i \mathbf{K}^{\mathbf{II}}_{\mathbf{i}} \mathbf{q}^{\mathbf{I}}_{\mathbf{i}}, \tag{3.17}$$

where $\mathbf{K}^{\mathbf{II}}_{\mathbf{i}}$ is the static stiffness contribution of the internal dynamic stiffness ($\mathbf{D}^{\mathbf{II}}(\omega) = -\omega^2 \mathbf{M}^{\mathbf{II}}_{\mathbf{i}} + (1 + i\eta)\mathbf{K}^{\mathbf{II}}_{\mathbf{i}}$), therefore

$$\langle \Pi_{diss,i} \rangle = -\frac{1}{2} \omega \eta_i \langle \mathbf{q}^{\mathbf{I}}_{\mathbf{i}}{}^{H} \mathbf{K}^{\mathbf{II}}_{\mathbf{i}} \mathbf{q}^{\mathbf{I}}_{\mathbf{i}} \rangle. \tag{3.18}$$

Using the same procedure from Eq. 2.20, equation above can be expressed as

$$\langle \Pi_{diss,i} \rangle = -\frac{1}{2} \omega \eta_i \mathrm{Tr} \left[\mathbf{K}^{\mathbf{II}}_{\mathbf{i}} \mathbf{S}_{\mathbf{q}^{\mathbf{I}}_{\mathbf{i}} \mathbf{q}^{\mathbf{I}}_{\mathbf{i}}} \right]. \tag{3.19}$$

The cross-spectral response from the internal degrees of freedom of the *ith* statistical subsystem $\mathbf{S}_{\mathbf{q}^{\mathbf{I}}_{\mathbf{i}} \mathbf{q}^{\mathbf{I}}_{\mathbf{i}}}$ can be approximated to the displacement generated by the ensemble average blocked loading from the respective subsystem's domain. In order to derive these forces, the deterministic boundary is assumed to be constrained ($\mathbf{q}^{\mathbf{B}}_{\mathbf{i}} = 0$), resulting in the following equation of motion

$$\mathbf{D}^{\mathbf{II}}_{\mathbf{i}} \mathbf{q}^{\mathbf{I}}_{\mathbf{i}} = 0. \tag{3.20}$$

The above expression was generated from Eq. 3.11, where it was also assumed that no external loads are applied to internal degrees of freedom ($\mathbf{f}^{\mathbf{I}}_{\mathbf{i}} = 0$). Following the same procedure adopted from Eq. 2.11 to Eq. 2.12, the internal forces can be represented by a deterministic direct field and a random reverberant contribution

$$\mathbf{D}^{\mathbf{II}}_{\mathbf{dir,i}} \mathbf{q}^{\mathbf{I}}_{\mathbf{i}} = \mathbf{f}^{\mathbf{I}}_{\mathbf{rev,i}}. \tag{3.21}$$

The cross-spectral internal response is then written as

$$\mathbf{S}_{\mathbf{q}^{\mathbf{I}}_{\mathbf{i}} \mathbf{q}^{\mathbf{I}}_{\mathbf{i}}} = \mathbf{D}^{\mathbf{II}}_{\mathbf{dir,i}}{}^{-1} \mathbf{S}_{\mathbf{f}^{\mathbf{I}}_{\mathbf{rev,i}} \mathbf{f}^{\mathbf{I}}_{\mathbf{rev,i}}} \mathbf{D}^{\mathbf{II}}_{\mathbf{dir,i}}{}^{-H}, \tag{3.22}$$

which by assuming a maximum entropy ensemble statistic to the internal domain of the subsystem ($\langle \mathbf{f}^{\mathbf{I}}_{\mathbf{rev,i}} \rangle = 0$ and $\mathbf{S}_{\mathbf{f}^{\mathbf{I}}_{\mathbf{rev,i}} \mathbf{f}^{\mathbf{I}}_{\mathbf{rev,i}}} = 4C_i \mathbf{Im}\{\mathbf{D}^{\mathbf{II}}_{\mathbf{dir,i}}\}$), the *ith* subsystem's cross-spectral internal response can be expressed as

$$\mathbf{S}_{\mathbf{q}^{\mathbf{I}}_{\mathbf{i}} \mathbf{q}^{\mathbf{I}}_{\mathbf{i}}} = 4C_i (\mathbf{D}^{\mathbf{II}}_{\mathbf{dir,i}}{}^{-1} \mathbf{Im}\{\mathbf{D}^{\mathbf{II}}_{\mathbf{dir,i}}\} \mathbf{D}^{\mathbf{II}}_{\mathbf{dir,i}}{}^{-H}). \tag{3.23}$$

Assuming the elegant mathematical relationship from (LANGLEY; CORDIOLI, 2009) to greatly simply the expression

$$\mathbf{S}_{\mathbf{q_i^I q_i^I}} = 4C_i \mathbf{Im}\{\mathbf{D}_{\mathbf{dir,i}}^{\mathbf{II}\ -1}\}. \tag{3.24}$$

Substituting the above expression into Eq. 3.19, the *ith* statistical subsystem's ensemble average dissipated power can then be expressed as

$$\langle \Pi_{diss,i} \rangle = \omega \pi \mathcal{M}_i C_i, \tag{3.25}$$

where the *ith* statistical subsystem's dissipation coefficient $\mathcal{M}_i$ is written as

$$\mathcal{M}_i = -\frac{2}{\pi} \eta_i \mathrm{Tr}\left[\mathbf{K}_\mathbf{i}^\mathbf{II} \mathbf{Im}\{\mathbf{D}_{\mathbf{dir,i}}^{\mathbf{II}\ -1}\}\right]. \tag{3.26}$$

Using the same previous analogy, the internal direct field dynamic stiffness $\mathbf{D}_{\mathbf{dir,i}}^{\mathbf{II}}$ is computed simply by the ensemble average of the internal dynamic stiffness

$$\mathbf{D}_{\mathbf{dir,i}}^{\mathbf{II}} = \langle \mathbf{D}_\mathbf{i}^\mathbf{II} \rangle. \tag{3.27}$$

.

4 NUMERICAL IMPLEMENTATION

Although the previous chapter presented formulation for the Generalized Hybrid method, a deeper discussion regarding its implementation is required in order to achieve competitive computational processing costs and reliable results.

4.1 INTERNAL MODAL BASIS - STATISTICAL SUBSYSTEMS

The greatest processing cost reduction for the Generalized Hybrid model is achieved by projecting the internal nodal degrees of freedom from the statistical subsystems into modal basis. The internal domain of these subsystems is constituted of regions that demand the finest configuration definition, resulting in an unfeasible number of degrees of freedom. If not projected/reduced, the computational cost can easily surpass the one of a full FE model analysis, due to the high number of matrices manipulations made in the method.

The degrees of freedom from deterministic boundaries remain nodal in order to enforce compatibility to connected subsystems. The relationship between the *ith* statistical subsystem's internal nodal $\mathbf{q^I}$ and modal $\mathbf{p^I}$ degrees of freedom is defined as

$$\mathbf{q_i^I} = \mathbf{U_i^I p_i^I}, \tag{4.1}$$

where $\mathbf{U_i^I}$ is the eigenvectors matrix for the internal domain. This matrix is derived by performing a modal analysis to the interior domain of the *ith* statistical subsystem, i.e.

$$\left[\mathbf{K_i^{II}} - \omega^2 \mathbf{M_i^{II}}\right] \mathbf{u_i^I} = \mathbf{0}, \tag{4.2}$$

where $\mathbf{U_i^I}$ is obtained from the collection of all eigenvectors from above equation, i.e. $\mathbf{U_i^I} = [\mathbf{u_{i,1}^I}, \ldots, \mathbf{u_{i,N}^I}]$. This internal modal basis affects the derivation of both the direct field dynamic stiffness $\mathbf{D_{dir,i}}$ and the dissipation coefficient $\mathcal{M}_i$. For the former parameter, the substitution of Eq. 4.1 in Eq. 3.11 results in

$$\mathbf{D_i^{IB} q_i^B} + \mathbf{D_i^{II} U_i^I p_i^I} = \mathbf{f_i^I}. \tag{4.3}$$

By multiplying over left side of equation above by $\mathbf{U_i^{I^T}}$ and eliminating the external loads to internal domain ($\mathbf{f_i^I} = 0$), the expression becomes

$$\mathbf{U_i^{I^T} D_i^{IB} q_i^B} + \mathbf{D_i^{II,p} p_i^I} = \mathbf{0}, \tag{4.4}$$

where $\mathbf{D_i^{II,p}}$ is the internal dynamic stiffness matrix projected over internal modal basis ($\mathbf{D_i^{II,p}} = \mathbf{U_i^{I}}^T \mathbf{D_i^{II}} \mathbf{U_i^{I}}$). By isolating the modal coordinates, we obtain

$$\mathbf{p_i^I} = -\mathbf{D_i^{II,p}}^{-1} \mathbf{U_i^{I}}^T \mathbf{D_i^{IB}} \mathbf{q_i^B}. \tag{4.5}$$

If we also change the internal basis to modal basis over Eq. 3.10, we obtain

$$\mathbf{D_i^{BB}} \mathbf{q_i^B} + \mathbf{D_i^{BI}} \mathbf{U_i^I} \mathbf{p_i^I} = \mathbf{f_i^B}, \tag{4.6}$$

which if we substitute Eq. 4.5 in Eq. 4.3 and put $\mathbf{q_i^B}$ in common, we obtain the definition of the junction dynamic stiffness with internal contribution projected over modal basis $\mathbf{D_i^{J,p}}$

$$(\mathbf{D_i^{BB}} - \mathbf{D_i^{BI}} \mathbf{U_i^I} \mathbf{D_i^{II,p}}^{-1} \mathbf{U_i^{I}}^T \mathbf{D_i^{IB}}) \mathbf{q_i^B} = \mathbf{D_i^{J,p}} \mathbf{q_i^B} = \mathbf{f_i^B}. \tag{4.7}$$

The computational efficiency from above equation above is far superior from Eq. 3.13 as lesser matrices manipulations are required per frequency. This is explained why in the following arguments. By defining two partially modal dynamic stiffness ($\mathbf{D_i^{BI,U}} = \mathbf{D_i^{BI}} \mathbf{U_i^I}$ and $\mathbf{D_i^{IB,U}} = \mathbf{U_i^I}^T \mathbf{D_i^{IB}}$) and by expanding one of them, we obtain

$$\mathbf{D_i^{BI,U}} = -\omega^2 \mathbf{M_i^{BI,U}} + (1 + i\eta) \mathbf{K_i^{BI,U}}, \tag{4.8}$$

where, although a internal eigenproblem is necessary for analysis, the mass ($\mathbf{M_i^{BI,U}} = \mathbf{M_i^{BI}} \mathbf{U_i^I}$) and stiffness ($\mathbf{K_i^{BI,U}} = \mathbf{K_i^{BI}} \mathbf{U_i^I}$) matrices are evaluated just once and are far smaller than their nodal counterparts (at Eq. 4.2). The derivation of $\mathbf{D_i^{IB,U}}$ is similar to the equation above, just exchanging the mass and stiffness matrices to the ones that correspond correctly to the related degrees of freedom. Furthermore, the most important computational aspect from Eq. 4.7 is the internal modal dynamic stiffness $\mathbf{D_i^{II,p}}$, which, as this is a diagonalized matrix, can be easily inverted. Similar to Eq. 3.14, the ensemble average of junction dynamic stiffness with internal modal basis (Eq. 4.7) is written as

$$\langle \mathbf{D_i^{J,p}} \rangle = \mathbf{D_i^{BB}} - \mathbf{D_i^{BI,U}} \langle \mathbf{H_i^{II,p}} \rangle \mathbf{D_i^{IB,U}}, \tag{4.9}$$

where $\mathbf{H_i^{II,p}} = \mathbf{D_i^{II,p}}^{-1}$. Due to the truncation of modes made in Eq. 4.2, the average dynamic stiffness $\langle \mathbf{D_i^{J,p}} \rangle$ does not converge directly to the direct field dynamic stiffness $\mathbf{D_{dir,i}}$. A correction is then necessary to obtain equivalence. The proposed method to obtain such correction uses a pseudostatic technique, which approximates strain contributions

from the dropped modes by the use of a residual flexibility matrix $\widetilde{\mathbf{K}}_{\mathbf{res,i}}$ (TOURNOUR; ATALLA, 2000). In the paper, the authors discuss and prove that these contributions are enough to correct structure-borne FE system's analysis. The residual flexibility is then computed as the difference between the pseudostatic contributions from $\mathbf{D_i^J}$ and $\mathbf{D_i^{J,P}}$, i.e. neglecting the inertial contribution ($\omega = 0$), which writes as

$$\widetilde{\mathbf{K}}_{\mathbf{res,i}} = \mathbf{D_i^J}(\omega = 0) - \mathbf{D_i^{J,P}}(\omega = 0). \tag{4.10}$$

The pseudostatic contribution from the dynamic stiffness consists essentially of the dissipative and restoration forces resistances. For example, in the case of the internal dynamic stiffness, its pseudostatic contribution is written as

$$\mathbf{D_i^{II}}(\omega = 0) = (1 + i\eta_i)\mathbf{K_i^{II}} = \widetilde{\mathbf{K}}_\mathbf{i}^\mathbf{II}. \tag{4.11}$$

All dynamic stiffness inside $\mathbf{D_i^J}(\omega = 0)$ and $\mathbf{D_i^{J,P}}(\omega = 0)$ represent a similar composition as Eq. 4.11. Consequently, by substituting Eq. 3.14 and Eq. 4.7 into above equation, the residual flexibility is computed as

$$\widetilde{\mathbf{K}}_{\mathbf{res,i}} = \widetilde{\mathbf{K}}_\mathbf{i}^\mathbf{BI}(\widetilde{\mathbf{K}}_\mathbf{i}^{\mathbf{II}-1} - \mathbf{U_i^I}\widetilde{\mathbf{K}}_\mathbf{i}^{\mathbf{II,p}-1}\mathbf{U_i^{I}}^T)\widetilde{\mathbf{K}}_\mathbf{i}^\mathbf{IB}, \tag{4.12}$$

and, therefore, the direct field dynamic stiffness in local coordinates is obtained by

$$\mathbf{D_{dir,i}^L} = \langle \mathbf{D_i^{J,P}} \rangle + \widetilde{\mathbf{K}}_{\mathbf{res,i}}. \tag{4.13}$$

Although the computation of the residual flexibility (Eq. 4.12) consists of large complex matrix manipulations, it's only required to be evaluated once, as opposed to the dynamic matrices. An important note to point out is that, when implementing Eq. 4.12 in a routine, it's more computationally efficient to compute all matrices multiplications and divisions before computing the difference from the two terms on the right side of the expression. Moreover, the direct field dynamic stiffness in global coordinates $\mathbf{D_{dir,i}}$ is derived similarly to Eq. 3.15.

In the case of the internal dissipation, by substituting the modal basis transformation (Eq. 4.1) into the dissipated power expression (Eq. 3.18)

$$\langle \Pi_{diss,i} \rangle = -\frac{1}{2}\omega\eta_i \langle \mathbf{p_i^I}^H \mathbf{U_i^I}^T \mathbf{K_i^{II}} \mathbf{U_i^I} \mathbf{q_i^I} \rangle = -\frac{1}{2}\omega\eta_i \langle \mathbf{p_i^I}^H \mathbf{K_i^{II,p}} \mathbf{p_i^I} \rangle. \tag{4.14}$$

By repeating the same process of Eq. 2.20, the dissipated power is then expressed as

$$\langle \Pi_{diss,i} \rangle = -\frac{1}{2}\omega\eta_i \mathrm{Tr}\left[\mathbf{K}_{\mathbf{i}}^{\mathbf{II,p}} \mathbf{S}_{\mathbf{p}_i^{\mathbf{I}},\mathbf{p}_i^{\mathbf{I}}}\right]. \tag{4.15}$$

The derivation of the cross-spectrum of internal modal basis is performed by substituting the modal basis transformation into Eq. 3.21 and multiplying by $\mathbf{U}_{\mathbf{i}}^{\mathbf{I}^T}$ at left side of the expression

$$\mathbf{D}_{\mathbf{dir,i}}^{\mathbf{II,p}} \mathbf{p}_{\mathbf{i}}^{\mathbf{I}} = \mathbf{U}_{\mathbf{i}}^{\mathbf{I}^T} \mathbf{f}_{\mathbf{rev,i}}^{\mathbf{I}}, \tag{4.16}$$

where $\mathbf{D}_{\mathbf{dir,i}}^{\mathbf{II,p}} = \mathbf{U}_{\mathbf{i}}^{\mathbf{I}^T} \mathbf{D}_{\mathbf{dir,i}}^{\mathbf{II}} \mathbf{U}_{\mathbf{i}}^{\mathbf{I}}$. Therefore, by computing the cross-spectrum of internal modal basis

$$\mathbf{S}_{\mathbf{p}_i^{\mathbf{I}},\mathbf{p}_i^{\mathbf{I}}} = \mathbf{D}_{\mathbf{dir,i}}^{\mathbf{II,p}\,-1} (\mathbf{U}_{\mathbf{i}}^{\mathbf{I}^T} \mathbf{S}_{\mathbf{f}_{\mathbf{rev,i}}^{\mathbf{I}},\mathbf{f}_{\mathbf{rev,i}}^{\mathbf{I}}} \mathbf{U}_{\mathbf{i}}^{\mathbf{I}}) \mathbf{D}_{\mathbf{dir,i}}^{\mathbf{II,p}\,-H}, \tag{4.17}$$

and substituting the same cross-spectral of the internal reverberant force ($\mathbf{S}_{\mathbf{f}_{\mathbf{rev,i}}^{\mathbf{I}},\mathbf{f}_{\mathbf{rev,i}}^{\mathbf{I}}} = 4C_i \mathbf{Im}\{\mathbf{D}_{\mathbf{dir,i}}^{\mathbf{II}}\}$), used in Eq. 3.23, into above equation and following the same matrices manipulations from Eq. 3.23, we obtain the following expression

$$\mathbf{S}_{\mathbf{p}_i^{\mathbf{I}},\mathbf{p}_i^{\mathbf{I}}} = 4C_i \mathbf{Im}\{\mathbf{D}_{\mathbf{dir,i}}^{\mathbf{II,p}\,-1}\}. \tag{4.18}$$

The *ith* statistical subsystem's dissipation coefficient $\mathcal{M}_i$ can then computed as

$$\mathcal{M}_i = -\frac{2}{\pi}\eta_i \mathrm{Tr}\left[\mathbf{K}_{\mathbf{i}}^{\mathbf{II,p}} \mathbf{Im}\{\mathbf{D}_{\mathbf{dir,i}}^{\mathbf{II,p}\,-1}\}\right], \tag{4.19}$$

which represents a far more computational efficient approach to derive the dissipated power from Eq. 3.25. The internal modal direct field dynamic stiffness $\mathbf{D}_{\mathbf{dir,i}}^{\mathbf{II,p}}$ is derived similarly to its nodal counterpart (Eq. 3.27)

$$\mathbf{D}_{\mathbf{dir,i}}^{\mathbf{II,p}} = \langle \mathbf{D}_{\mathbf{i}}^{\mathbf{II,p}} \rangle. \tag{4.20}$$

Although Eq. 4.13 and Eq. 4.19 are capable of fully describe the power flow from a statistical subsystem (in combination with the power-flow coefficient's expressions), a proper and efficient approach to derive the ensemble average internal dynamic stiffness $\langle \mathbf{D}_{\mathbf{i}}^{\mathbf{II,p}} \rangle$ is required for the analysis and is presented in the next section.

4.2 EFFICIENT AVERAGING METHODS - STATISTICAL SUBSYSTEMS

A direct approach to calculate the ensemble average of a FE dynamic stiffness is by generating a collection of randomized nominally identical samples and computing their frequency response function (FRF) mean, this is known as the FE Monte Carlo method.

However, every sample realization requires an unique eigenproblem, eventually demanding an impractical amount of processing time to derive a proper and converged ensemble average, regardless of the randomization technique adopted to the samples.

Two efficient averaging methods were explored at a parallel work to this thesis (HINZ, 2021), with each one presenting different attributes over their processing time and robustness to their ensemble average's results. The two methods are briefly presented in the following, if a detailed discussion is sought, head into the parallel work's reference. Results for the direct field receptance (Eq. 4.13 inverted) and vibrational energy (Eq. 3.7), using both averaging methods to derive $\langle \mathbf{D}_{\mathbf{i}}^{\mathbf{II,p}} \rangle$, were compared to a solid FE Monte Carlo model for evaluation.

4.2.1 Non-parametric random matrix averaging

The first method introduces the randomization of the FRF using techniques from random matrix theory (RMT) in combination with a maximum entropy non-parametric approach. Essentially, this approach allows for a randomization controlled by a single universal intensity parameter $\delta_{\mathbf{R,i}}$, disregarding possible physical or conceptual parameters that would require known information about the system's configuration. This data is usually not available due to the high level of uncertainty associated to the statistical subsystem's internal domain.

Assuming $\mathbf{A}$ as an arbitrary deterministic FRF matrix, the *ith* randomized sample $\mathbf{A}_{\mathbf{R,i}}$ is defined as

$$\mathbf{A}_{\mathbf{R,i}} = \mathbf{L_A}^T \mathbf{G_i} \mathbf{L_A}, \tag{4.21}$$

where $\mathbf{L_A}$ is the upper triangular matrix from a Cholesky factorization ($\mathbf{A} = \mathbf{L_A}^T \mathbf{L_A}$). $\mathbf{G_i}$ is a random matrix defined as the source of uncertainty to the FRF, which is derived accordingly to the universal parameter $\delta_{\mathbf{R,i}}$. In order to derive LA from the factorization, the original matrix A is required to be definitive positive, which applies for $\mathbf{D}_{\mathbf{i}}^{\mathbf{II,p}}$, as the *ith* subsystem's deterministic boundary is understood as constrained and, therefore, no rigid modes are defined. For a fully deterministic sample, the random matrix $\mathbf{G_i}$ equals identity ($\mathbf{G_i} = \mathbf{I}$).

The randomized FRFs conceptualize an ensemble of N samples, similar to FE Monte Carlo, which an average is then computed ($\langle \mathbf{A} \rangle = 1/N \sum_i^N \mathbf{A}_{\mathbf{R,i}}$). The major

computational advantage of this method, in comparison the standard FE Monte Carlo, is the possibility of the directly randomization of the modal matrices, neglecting the necessity of an eigenproblem for every sample, resulting in huge processing cost reduction.

In (HINZ, 2021), results for a Numerical SEA analysis using the non-parametric averaging method to derive $\langle \mathbf{D}_\mathbf{i}^{\mathbf{II}} \rangle$ exhibited robustness at mid and high frequency regions, due to the great convergence to the FE Monte Carlo result. However, at lower frequencies, the non-parametric results showed a nominal deterministic behavior, implying in a lack of randomization impact over these lower spectrum regions.

4.2.2 Lorentzian frequency averaging

The second method consists in assuming that the arbitrary deterministic FRF matrix $\mathbf{A}(\omega)$ displays a frequency-ensemble ergodicity property, implying an average of the matrix over the frequency ω converges into the desired ensemble average. Furthermore, a weighted frequency average of $\mathbf{A}(\omega)$ is defined as

$$\langle \mathbf{A}(\omega) \rangle_W = \int_{-\infty}^{+\infty} W(\omega)\mathbf{A}(\omega)\mathrm{d}\omega, \tag{4.22}$$

where $W(\omega)$ is denoted as weighting function. In general, this integral is computed numerically over the spectrum domain, which, depending on the frequency resolution, demands a considerable amount of processing cost. However, the weighting function that is adopted here in this approach, the Lorentzian weighting function $L(\omega, \gamma)$, has a specific distribution that invokes a powerful mathematical feature, allowing for the integral to be analytically computed. Therefore, reducing considerably the amount of processing cost required. The Lorentzian weighting function $L(\omega, \gamma)$ has a peculiar bell shaped distribution and γ is the parameter that calibrates its bandwidth.

After some manipulations (DEVRIENDT et al., 2015), the analytical derivation for the weighted frequency integral is defined as

$$\int_{-\infty}^{+\infty} L(\omega, \gamma)\mathbf{A}(\omega) = \mathbf{A}(\omega - \mathrm{i}\gamma). \tag{4.23}$$

In the case of $\mathbf{A}(\omega)$ is defined as the dynamic stiffness with structural damping (our case here), a causality issue must be concerned, as Eq. 4.23 is no longer an exact equivalence to the ensemble average, but actually an reasonable approximation (HINZ, 2021)

$$\langle \mathbf{A}(\omega) \rangle \approx \mathbf{A}(\omega - \mathrm{i}\gamma). \tag{4.24}$$

In this approach, the shape of the Lorentzian weighting function, defined by γ, will directly affect the randomization of the $\mathbf{A}(\omega)$ matrix. For a small γ, the distribution will be concentrated over a narrow region, resulting in lack of variability to the average. In contrast, a large number will flatten the distribution and will most likely affect regions out of local stationarity. Therefore, defining a optimal value for γ is critical for a proper average.

The proposed definition for the shape parameter is written as (DEVRIENDT et al., 2015)

$$\gamma_{\mathbf{A}} = \frac{N_\gamma}{n_{\mathbf{A}}}, \tag{4.25}$$

where N_γ is an integer that quantify how many modes the weighting function covers around its peak. For (DEVRIENDT et al., 2015), the nominator is usually set as a constant, e.g. for flat plates the optimal value of 3 was suggested. However, for (HINZ, 2021), the integer as a function of frequency $N_\gamma(\omega)$ is used. The denominator $n_{\mathbf{A}}(\omega)$ is the modal density related to the subsystem associated to $\mathbf{A}$, which can be analytically calculated, however, due to generalization, it is more appropriated to be numerically computed by the number of modes obtained in the eigenproblem (Eq. 4.2) divided by the respective band-widths.

Another possibility for γ is to relate it directly to the band-width of analysis. In the case of a 1/3 octave frequency band, the shape parameter can be written as

$$\gamma_{1/3} = \left[\Delta\omega_{1/3}^1 \quad \Delta\omega_{1/3}^2 \quad \dots \quad \Delta\omega_{1/3}^{N_\omega}\right], \tag{4.26}$$

where $\Delta\omega_{1/3}^i$ is the band-width of the ith one-third octave band of analysis and N_ω is the number of frequency bands. This approach is employed when no modal density is available, either when no known analytical formulations are known or no modes were numerically obtained at lower frequency bands (this is usually not the case here, as we are dealing with the interior domains of statistical subsystems that are highly populated with resonant modes, however, in the next section, there is a scenario where Eq. 4.26 becomes necessary). Both the first approach, using a numerically derived modal density, and the second approach assume a broad-band frequency resolution, however it is possible to derive a γ over a narrow-band one if interpolation is used between the bands' center frequencies.

In (HINZ, 2021), a Numerical SEA model using the Lorentzian averaging method was also evaluated, similar to the evaluation made for the non-parametric averaging

method. The results using this method were able to achieve convergence to the FE Monte Carlo curves over the entire frequency region, exhibiting superior robustness against the previously discussed method.

4.3 WAVEFIELD'S PARTITION - STATISTICAL SUBSYSTEMS

Until now, every subsystem was associated to a single direct field dynamic stiffness $\mathbf{D_{dir,i}}$ and a single dissipation coefficient $\mathcal{M}_i$, meaning that each is linked to a single lumped wavefield. This type of wavefield concentrates all dynamics and internal forces of a subsystem into a single energy container. However, as mentioned, in SEA or Hybrid FE-SEA method, the subsystems are actually portioned into a set of wavefields, e.g., in the case of plates: flexure, extensional and shear wavefields are usually defined.

In general, defining groups of wavefields per subsystem, instead of a single lumped one, is mostly motivated by: limitations of analytical formulations to cover complex mechanisms, therefore splitting it into simpler physics to be able to fully describe the subsystem, and due to the disparity of energy influence from different wavefields to the system's power-flow framework, as, e.g., the in-plane wavefields dissipate far less energy than the out-of-plane ones (otherwise, in some situations, the lumped wavefield would impose a misguiding equipartition of energy around the wavefields). This separation of wavefields is not a universal approach, as only some elementary configurations present manners of splitting their physical mechanism without lost of generality.

The necessity of wavefield's partition is also not obvious, as depending on the structure's configuration, different types of wavefields could be intrinsically mixed and, therefore, impossible to be partitioned. Moreover, this intrinsic blend end up supporting a more even distribution of energy influence over the wavefields, disregarding the need of their partition. In general, a irregular configuration tends to support more even distributed wavefields, as a result of the wave scattering that arise from its discontinuities, whereas a elementary configuration tends in defining a clear distinction between different wavefield's energy influence.

Apart from the subsystem's configuration, the wavefield's definition will also be affected by the method used to model the subsystem. As mentioned, analytical formulations require wavefield partitions to derive proper solutions. If however, the subsystem's configuration obeys a cycle of repetition, it could be modelled by a Wave FE method,

which defines the set of wavefields based on the dispersion curves. In this approach, a greater number of wavefields could be obtained. Nonetheless, a standard FE method could be used to model the subsystem and is the case discussed here in the thesis. Although a lumped wavefield is generally obtained from defining a subsystem from a standard FE model, post-processing manipulations could be performed to partition this respective wavefield. This is what is discussed in the following.

It is possible that the post-processing to partition the lumped wavefield could be a generalized procedure, applying to every sort of configuration. However, the presented formulation here will only be concerned with the elementary configuration of flat plates, which is a clear representation of a subsystem with two or more decoupled wavefields. A set of direct field dynamic stiffness $\mathbf{D_{dir,i}}$ and dissipation coefficient $\mathcal{M}_i$ is then derived for each wavefield. Consequently, additional energy containers C_i are defined, increasing the number of energy paths in the power-flow framework. This results in also increased number of coefficients ($h_{i,j}$, $\mathcal{M}_{d,i}$ and, as mentioned, $\mathcal{M}_i$) and size of Eq. 3.6.

For the case of flat plates, the out-of-plane and in-plane contributions were selected to derive the partitioned wavefields. These wavefields represent, respectively, transverse and parallel wave contributions relative to the flat plate's plane. The process consists in separating these contributions directly from the subsystem's FE matrices, compute the framework's power flow coefficients for each wavefield and solve the system to determine the energy containers (Eq. 3.6). Consider a first scenario of a flat plate's FE model with its normal vector $\hat{\mathbf{v}}_\mathbf{n}$ parallel to the $\hat{\mathbf{k}}$ vector of the global coordinate system ($\hat{\mathbf{i}}, \hat{\mathbf{j}}, \hat{\mathbf{k}}$), like the one exhibited in Fig. 7.

Assuming six degrees of freedom per node (three displacements u_x, u_y, u_z and three rotations θ_x, θ_y, θ_z), the out-of-plane and in-plane contributions can be easy separated from the FE matrices by a simply separation of degrees of freedom. In this case, the out-of-plane is solely associated to normal displacement u_z and to the orthogonal vector's rotations θ_x and θ_y, whereas the in-plane is associated to rest of degrees of freedom u_x, u_y and θ_z. This easy separation is also possible when the plate's normal is parallel to either $\hat{\mathbf{i}}$ or $\hat{\mathbf{j}}$ vectors, the only difference would be the set of degrees of freedom each wavefield is associated.

Consider now a second scenario of a plate that has the normal vector $\hat{\mathbf{v}}_\mathbf{n}$ with arbitrary direction in the global coordinate system and, therefore, probably with out-of-plane and in-plane contributions mixed over the sets of six degrees of freedom per node. In order

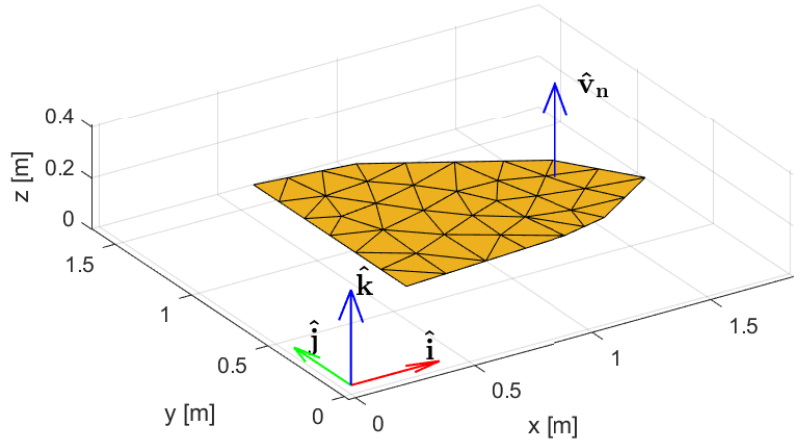

Figure 7 – Plate on x-y plane

Source: Matlab

to separate the *ith* subsystem matrices in this general case, a local coordinate system $(\hat{\mathbf{i}}_\mathbf{i}^\mathbf{L}, \hat{\mathbf{j}}_\mathbf{i}^\mathbf{L}, \hat{\mathbf{k}}_\mathbf{i}^\mathbf{L})$ is defined, where it is assumed that the plate's normal vector $\hat{\mathbf{v}}_\mathbf{n}$ is parallel to any of the three local coordinate system's vectors. Just for clarification reasons, the $\hat{\mathbf{k}}_\mathbf{i}^\mathbf{L}$ is chosen here. The other two vectors directions are arbitrary, as long as they remain orthogonal to the plate's normal and to each other. This second scenario is illustrated at Fig. 8. The values defined for $\hat{\mathbf{j}}_\mathbf{i}^\mathbf{L}$ and $\hat{\mathbf{k}}_\mathbf{i}^\mathbf{L}$ are arbitrary.

The process then consists in projecting the *ith* subsystem 's FE matrices from global coordinates $\mathbf{q_i}$ (second scenario) to local coordinates $\mathbf{q_i^L}$ (similar to the first scenario), where out-of-plane and in-plane set of the degrees of freedom are decoupled, and, therefore, allowing for easy contribution's separation from the FE matrices. Thereafter, the separated matrices are projected back to global coordinate system to enforce compatibility to neighbor subsystems. The formulation of the process in presented in the following.

The projection from local coordinates to global ones is expressed as

$$\mathbf{q_i} = \mathbf{T_i} \mathbf{q_i^L}, \tag{4.27}$$

where the *ith* subsystem's transformation matrix $\mathbf{T_i}$ is derived from the inner products between the global and local coordinate system of *ith* subsystem. Although all FE elements of a flat plate assume the same normal vector $\hat{\mathbf{v}}_\mathbf{n}$, the other two orthogonal basis have

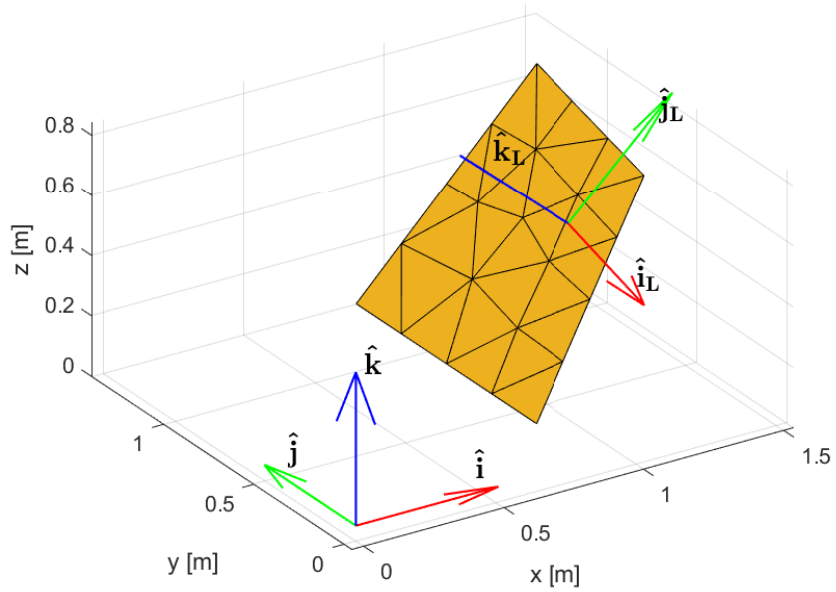

Figure 8 – Plate on arbitrary plane

Source: Matlab

distinct vector directions. Nonetheless, assuming the same local coordinate system's vectors (in this case, arbitrary and orthogonal) for every element is not a problem as it is intended to return to global coordinate system at the end, reverting any possible dubious and erroneous projection. The *ith* subsystem's transformation matrix $\mathbf{T_i}$ is then constructed as a diagonal concatenation of several identical nodal transformation matrices $\mathbf{T_{nodal,i}}$

$$\mathbf{T_i} = \begin{bmatrix} \mathbf{T_{nodal,1}} & & \\ & \ddots & \\ & & \mathbf{T_{nodal,N_i}} \end{bmatrix}, \tag{4.28}$$

where N_i is the total number of nodes inside the *ith* subsystem and the nodal transformation matrices $\mathbf{T_{nodal,i}}$ is written as (SHABANA, 2010)

$$\mathbf{T_{nodal,i}} = \begin{bmatrix} \hat{\mathbf{i}} \cdot \hat{\mathbf{i}}_\mathbf{i}^\mathbf{L} & \hat{\mathbf{i}} \cdot \hat{\mathbf{j}}_\mathbf{i}^\mathbf{L} & \hat{\mathbf{i}} \cdot \hat{\mathbf{k}}_\mathbf{i}^\mathbf{L} \\ \hat{\mathbf{j}} \cdot \hat{\mathbf{i}}_\mathbf{i}^\mathbf{L} & \hat{\mathbf{j}} \cdot \hat{\mathbf{j}}_\mathbf{i}^\mathbf{L} & \hat{\mathbf{j}} \cdot \hat{\mathbf{k}}_\mathbf{i}^\mathbf{L} \\ \hat{\mathbf{k}} \cdot \hat{\mathbf{i}}_\mathbf{i}^\mathbf{L} & \hat{\mathbf{k}} \cdot \hat{\mathbf{j}}_\mathbf{i}^\mathbf{L} & \hat{\mathbf{k}} \cdot \hat{\mathbf{k}}_\mathbf{i}^\mathbf{L} \end{bmatrix}, \tag{4.29}$$

where $\langle \cdot \rangle$ symbolizes the inner product operator. By substituting Eq. 4.27 in Eq. 3.8 and also multiplying by the left side the latter by $\mathbf{T_i}^T$, the subsystem's FE matrices are projected over local coordinates, resulting in the following equation of motion

$$\mathbf{D_i^L q_i^L} = \mathbf{f_i^L}. \tag{4.30}$$

where the dynamic stiffness ($\mathbf{D_i^L} = \mathbf{T_i}^T\mathbf{D_i}\mathbf{T_i}$) matrix and the force ($\mathbf{f_i^L} = \mathbf{T_i}^T\mathbf{f_i}$) vector admit decoupled out-of-plane and in-plane contributions. The partitioned matrices are then generated by simply separating the contributions from the decoupled degrees of freedom associated to each wavefield into different matrices

$$\mathbf{D_i^L} = \mathbf{D_{in,i}^L} + \mathbf{D_{out,i}^L}. \tag{4.31}$$

The in-plane $\mathbf{f_{in,i}}$ and out-of-plane $\mathbf{f_{out,i}}$ force vectors follow the same principle from above. Consequently, the decoupled equation of motion for the in-plane is written as

$$\mathbf{D_{in,i}^L}\mathbf{q_i^L} = \mathbf{f_{in,i}^L}, \tag{4.32}$$

and for the out-of-plane as

$$\mathbf{D_{out,i}^L}\mathbf{q_i^L} = \mathbf{f_{out,i}^L}. \tag{4.33}$$

Moreover, due to the orthogonality from the transformation matrix ($\mathbf{T_i}^T\mathbf{T_i} = \mathbf{I}$ (SHABANA, 2010) and, therefore, $\mathbf{q_i^L} = \mathbf{T_i}^T\mathbf{q_i}$), the decoupled equations of motion in global coordinates can be derived by simply multiplying by the left side of Eq. 4.32 and Eq. 4.33 by $\mathbf{T}$, which are then expressed as

$$\mathbf{D_{in,i}}\mathbf{q_i} = \mathbf{f_{in,i}}, \tag{4.34}$$

and

$$\mathbf{D_{out,i}}\mathbf{q_i} = \mathbf{f_{out,i}}, \tag{4.35}$$

where $\mathbf{D_{in,i}} = \mathbf{T_i}\mathbf{D_{in,i}^L}\mathbf{T_i}^T$ and $\mathbf{f_{in,i}} = \mathbf{T_i}\mathbf{f_{in,i}^L}$. The out-of-plane matrices follow the same logic of derivation. In the global coordinate system, the matrices and vectors probably have contributions populating all six types of degrees of freedom, however is not a problem anymore, as the in-plane and out-of-plane contributions are already separated. The force vectors $\mathbf{f_{in,i}}$ and $\mathbf{f_{out,i}}$ are then used in Eq. 3.2 to derive external input power $\Pi_{in,i}^{ext}$ to each partitioned wavefield.

The previous two expressions concentrate all the dynamics involved for each partitioned wavefield in the isolated *ith* subsystem. They have enough information to follow the derivation steps from Eq. 3.8 and Eq. 3.16, and derive separately the remaining framework parameters for each wavefield. Therefore, the direct field dynamic stiffness for the in-plane wavefield $\mathbf{D_{in,dir,i}}$ is written as

$$\mathbf{D_{in,dir,i}} = \mathbf{D_{in,i}^{BB}} - \mathbf{D_{in,i}^{BI,U}}\langle\mathbf{H_{in,i}^{II,P}}\rangle\mathbf{D_{in,i}^{IB,U}} + \mathbf{K_{in,res,i}}, \tag{4.36}$$

where the partially modal dynamic stiffness matrices are derived as $\mathbf{D_{in,i}^{BI,U}} = \mathbf{D_{in,i}^{BI}}\mathbf{U_{in,i}^{I}}$ and $\mathbf{D_{in,i}^{IB,U}} = \mathbf{U_{in,i}^{I}}^{T}\mathbf{D_{in,i}^{IB}}$. All the boundary $\mathbf{B}$ and internal $\mathbf{I}$ nodal matrices are derived from the same analogy of Eq. 3.9 to the in-plane equation of motion (Eq. 4.34), as they both assume the same generalized coordinates vector $\mathbf{q_i}$. The same logic of above is applied to derive $\mathbf{D_{out,dir,i}}$. Although the formulation for nodal dynamic stiffness matrices was already defined, due to numerical characteristics of $\mathbf{D_{in,i}}$ and $\mathbf{D_{out,i}}$, the derivations for the modal internal receptances ($\mathbf{H_{in,i}^{II,P}}$ and $\mathbf{H_{out,i}^{II,P}}$), modal internal shapes ($\mathbf{U_{in,i}^{I}}$ and $\mathbf{U_{out,i}^{II}}$) and residual flexibility ($\mathbf{K_{in,res,i}}$ and $\mathbf{K_{out,res,i}}$) require further discussions to be defined.

Perhaps the most intuitive approach to derive the modal internal receptance and shape matrices would be performing an eigenproblem to the respective internal nodal matrices ($\mathbf{D_{in,i}^{II}}$ and $\mathbf{D_{out,i}^{II}}$). However, the process of projecting them into local coordinates, separating the contributions and then reverting back to global coordinates unwittingly inserts numerical errors into the partitioned matrices, resulting in inaccurate modes' derivations. In general, these partitioned nodal matrices are slightly non-symmetrical, resulting in complex eigenvalues and eigenvectors. Even if symmetry is enforced for linear analysis, erroneous results are still obtained. Therefore, the solution to derive the modal matrices relies on partitioning the contributions only after the lumped wavefield's eigenproblem is performed.

Remembering that the internal equation of motion (obtained when the deterministic boundary is constrained Eq. 3.20) is written as

$$\mathbf{D_i^{II}}\mathbf{q_i^{I}} = 0,$$

which by performing a projection over modal internal basis (Eq. 4.1) and multiplying by the left side of the equation by $\mathbf{U_i^{I}}^{T}$, the modal internal equation of motion is obtained

$$\mathbf{U_i^{I}}^{T}\mathbf{D_i^{II}}\mathbf{U_i^{I}}\mathbf{p_i^{I}} = 0. \tag{4.37}$$

The separation of the wavefield's contribution is actually made directly to the modal internal shape matrices in local coordinates, similar to the process made for the dynamic stiffness matrices. The internal projection from local coordinates $\mathbf{q_i^{I,L}}$ is then defined as

$$\mathbf{q_i^{I}} = \mathbf{T_i^{I}}\mathbf{q_i^{I,L}}, \tag{4.38}$$

where $\mathbf{T_i^I}$ is similar to the transformation matrix derived in Eq. 4.28, however with N_i equal to the number of nodes outside of the ith subsystem's deterministic boundary. In order to properly project the modal shape matrices in local coordinates, the orthogonality properties from the transformation matrices is used in our favor ($\mathbf{T_i^I T_i^{I}}^T = \mathbf{I}$). Consequently, by inserting $\mathbf{T_i^I T_i^{I}}^T$ between the dynamic stiffness and the modal shape functions in Eq. 4.37, the following expression is obtained

$$\mathbf{U_i^{I}}^T(\mathbf{T_i^I T_i^{I}}^T)\mathbf{D_i^{II}}(\mathbf{T_i^I T_i^{I}}^T)\mathbf{U_i^{I,L}p_i^I} = 0, \tag{4.39}$$

or after manipulating it

$$\mathbf{U_i^{I,L}}^T\mathbf{D_i^{II,L}U_i^{I,L}p_i^I} = 0, \tag{4.40}$$

where $\mathbf{U_i^{I,L}} = \mathbf{T_i^{I}}^T\mathbf{U_i^I}$ and $\mathbf{D_i^{II,L}} = \mathbf{T_i^{I}}^T\mathbf{D_i^{II}T_i^I}$. Similar to Eq. 4.31, the local modal internal shape matrix can be separated into two distinct matrices based on the selected sets of degrees of freedom ($\mathbf{U_i^{I,L}} = \mathbf{U_{in,i}^{I,L}} + \mathbf{U_{out,i}^{I,L}}$). The projection of the internal dynamic stiffness matrix in modal basis is then expressed as

$$\mathbf{U_i^{I,L}}^T\mathbf{D_i^{II,L}U_i^{I,L}} = \mathbf{D_{in,i}^{II,P}} + \mathbf{D_{out,i}^{II,P}} + \mathbf{D_{cor,i}^{II,P}}. \tag{4.41}$$

The in-plane ($\mathbf{D_{in,i}^{II,P}} = \mathbf{U_{in,i}^{I,L}}^T\mathbf{D_{in,i}^{II}U_{in,i}^{I,L}}$) and out-of-plane ($\mathbf{D_{out,i}^{II,P}} = \mathbf{U_{out,i}^{I,L}}^T\mathbf{D_i^{II,L}U_{out,i}^{I,L}}$) modal internal dynamic stiffness are then defined and decoupled, as the correlation matrix ($\mathbf{D_{cor,i}^{II,P}} = \mathbf{U_{in,i}^{I,L}}^T\mathbf{D_i^{II,L}U_{out,i}^{I,L}} + \mathbf{U_{in,i}^{I,L}}^T\mathbf{D_i^{II,L}U_{in,i}^{I,L}}$) is negligible, due to the orthogonality between different modes of the same subsystem, resulting in a matrix consisting of solely numerical errors. The robustness regarding the choice of the local coordinate system ($\mathbf{\hat{i}_i^L}, \mathbf{\hat{j}_i^L}, \mathbf{\hat{k}_i^L}$) for the flat plate is evaluated here in the partitioned modal internal matrices, as the matrices should be accurately diagonalized and decoupled, i.e., if the lumped internal modal shape matrix was mass normalized, there should be zeros values (or numerical errors) on diagonal elements that represent in-plane modes in the out-of-plane matrix, and vice versa.

The identification of these modes could be easy visualized by plotting the partitioned internal modal shapes. Figure 9 and Fig. 10, respectively, exhibit a clear representation of a specific in-plane mode in $\mathbf{U_{in,i}^{I,L}}$ and out-of-plane mode in $\mathbf{U_{out,i}^{I,L}}$. If by any means, the opposite partitioned internal modal shape matrix was plotted for the respective mode, a static mode is exhibited, as negligible contribution is present. Moreover, in order to compute the modal internal receptance $\mathbf{H_{in,i}^{II,P}}$ used in Eq. 4.36, an inversion of $\mathbf{D_{in,i}^{II,P}}$ is

required. However, as this matrix present specific columns and rows fully populated with zero values (due to decoupling), matrix singularity becomes a concern. The solution is then to remove these columns and rows from the matrix (consequently from the partitioned internal modal shape matrix $\mathbf{U}^{\mathbf{I,L}}_{\mathbf{in,i}}$ columns as well), when used in Eq. 4.36, retaining only contributions associated to the respective wavefield. This same analogy is also applied to derive the direct field dynamic stiffness of the out-of-plane wavefield.

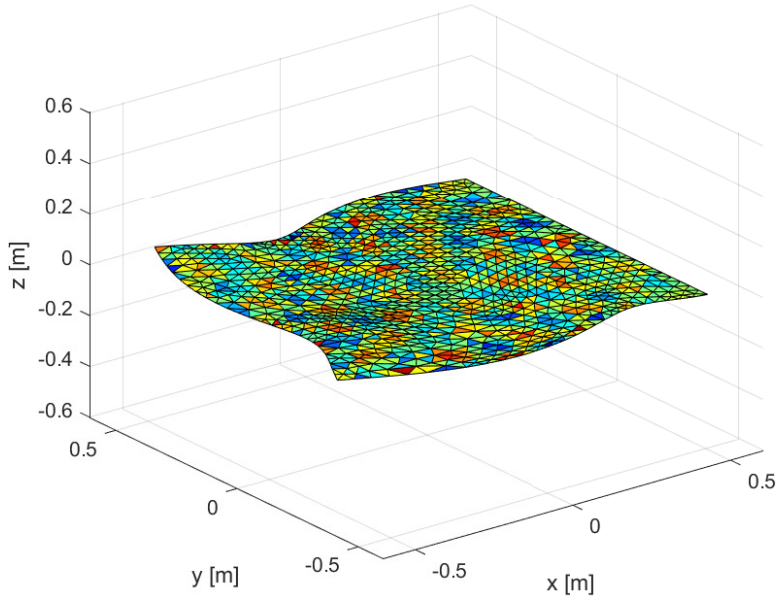

Figure 9 – An in-plane mode of an arbitrary plate (colors related to out-of-plane displacement)

Source: Matlab

Although deriving the average internal receptance $\langle \mathbf{H}^{\mathbf{II,P}}_{\mathbf{out,i}} \rangle$ by the use of the frequency Lorentzian averaging technique (Eq. 4.23) (assuming the shape parameter as a function of modal density (Eq. 4.25)) being a simple task, in the case of the in-plane receptance $\langle \mathbf{H}^{\mathbf{II,P}}_{\mathbf{in,i}} \rangle$, it is not. This is issue is mostly caused by the lack of modes numerically obtained from the modal analysis, therefore obtaining a zero valued modal density. Determining the shape parameter as a function of the band-width (Eq. 4.26) is then suggested. The use of the non-parametric average is not advised for this scenario as an alternative, due to the inefficient influence of the technique over lower frequency regions (which is where the lack of modes issue is addressed).

Regarding the definition of $\mathbf{K}_{\mathbf{in,res,i}}$ and $\mathbf{K}_{\mathbf{out,res,i}}$, their derivation using partitioned matrices is not possible due to the inversion of a nodal matrix on Eq. 4.12, as the

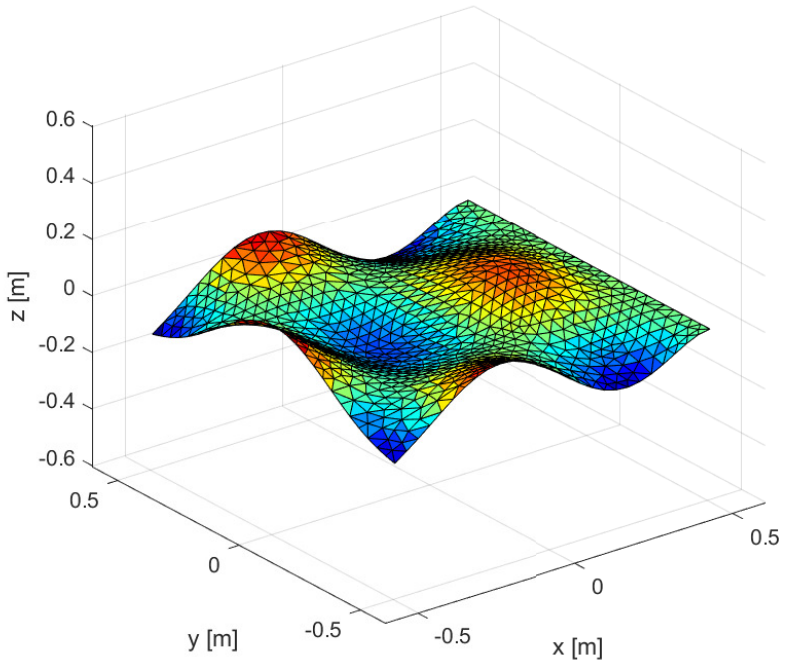

Figure 10 – An out-of-plane mode of an arbitrary plate (colors related to out-of-plane displacement)

Source: Matlab

partitioned matrices present bad matrix conditioning and, consequently, singular matrix inversions. The solution to derive the in-plane and out-of-plane residual flexibility matrices is then made by directly partitioning the respective lumped matrix $\mathbf{K_{res,i}}$. This process is performed similarly to the approach presented in Eq. 4.31, where the residual flexibility is projected into local boundary coordinates $\mathbf{q_i^{B,L}}$ (as it is associated to the deterministic boundary), separated based on the set of degrees of freedom associated to the respective wavefield and then retrieved back to the original global coordinate system to enforce compatibility along the neighbor subsystems. The projections of the boundary coordinates over local coordinates systems is obtained similarly to Eq. 4.38, respectively, the difference is in the size of the transformation matrix, as here it considers only nodes inside the deterministic boundary.

The remaining coefficient to be defined is the dissipation coefficient for the partitioned wavefields ($\mathcal{M}_{in,i}$ and $\mathcal{M}_{out,i}$). The coefficients are eventually obtained by following the steps of Eq. 4.16 using the dynamics represented in Eq. 4.40. The dissipation coefficient for the in-plane wavefield is then written as

$$\mathcal{M}_{in,i} = -\frac{2}{\pi}\eta_i \mathrm{Tr}\left[\mathbf{K}^{\mathbf{II,P}}_{\mathbf{in,i}} \mathbf{Im}\{\mathbf{H}^{\mathbf{II,P}}_{\mathbf{in,dir,i}}\}\right], \tag{4.42}$$

and for the out-of-plane as

$$\mathcal{M}_{out,i} = -\frac{2}{\pi}\eta_i \mathrm{Tr}\left[\mathbf{K}^{\mathbf{II,P}}_{\mathbf{out,i}} \mathbf{Im}\{\mathbf{H}^{\mathbf{II,P}}_{\mathbf{out,dir,i}}\}\right]. \tag{4.43}$$

where the $\mathbf{K}^{\mathbf{II,P}}_{\mathbf{in,i}}$ and $\mathbf{K}^{\mathbf{II,P}}_{\mathbf{out,i}}$ are the stiffness matrices contained in the dynamic stiffness matrices $\mathbf{D}^{\mathbf{II,P}}_{\mathbf{in,i}}$ and $\mathbf{D}^{\mathbf{II,P}}_{\mathbf{out,i}}$, respectively.

4.4 MODAL BASIS - DETERMINISTIC SUBSYSTEMS

One more model reduction is possible in order to achieve competitive processing costs, which is by projecting the deterministic subsystem's degrees of freedom into their modal basis. These deterministic components tend to admit fewer modes, resulting in a change of basis that greatly reduces the number of generalized coordinates. This is reflected on the reduced size of the framework matrices ($\mathbf{D_d}$, $\mathbf{D_{dir,i}}$ and $\mathbf{D_{tot}}$) that require fewer matrix manipulation for processing.

The modes used for projection could be arbitrary determined, still, in this work, only the free and specific clamped modes of the deterministic subsystems were explored. Both modal projection approaches affect the system's analysis differently and are discussed separately in the following subsections. Anyhow, this projection over the deterministic subsystem's degrees of freedom develops a new set of global generalized coordinates $\mathbf{q^h}$ that is related to the nodal global one $\mathbf{q}$ as

$$\mathbf{q} = \mathbf{T_U} \mathbf{q^h}. \tag{4.44}$$

where $\mathbf{T_U}$ is the transformation matrix responsible for projection of the generalized coordinates and it will be explained shortly. Remembering the system's deterministic degrees of freedom were defined as $\mathbf{q} = [\mathbf{q_d}^T \, \mathbf{q^B}^T]^T$ (discussed above Fig. 4) and assuming the $\mathbf{q_d}$ vector is expressed as

$$\mathbf{q_d} = \left[\mathbf{q_{d,i}}^T \ldots \mathbf{q_{d,N^d}}^T\right]^T, \tag{4.45}$$

where $\mathbf{q_{d,i}}$ is the *ith* deterministic subsystem's nodal degrees of freedom and $\mathrm{N_d}$ is the number of deterministic subsystems. The new set of coordinates $\mathbf{q^h}$ is constituted of groups of projected degrees of freedom $\mathbf{q^h_{d,i}}$ that represent each *ith* decoupled deterministic

subsystem's modal or partially modal coordinates (depending on the approach used for projection) and a sole group of nodal degrees of freedom $\mathbf{q^B}$, which are the generalized coordinates that remained as nodal from $\mathbf{q}$ (they are related to nodes that do not interact to any selected modal shape). Therefore, if expanded, the new coordinate vector is expressed as

$$\mathbf{q^h} = \begin{bmatrix} \mathbf{q^h_{d,i}}^T & \dots & \mathbf{q^h_{d,N_d}}^T & \mathbf{q^B}^T \end{bmatrix}^T. \tag{4.46}$$

As $\mathbf{q^h}$ comprises both modal and nodal degrees of freedom, it is considered to be a partially modal coordinate vector and should be smaller than its fully nodal counterpart $\mathbf{q}$, justifying the process discussed here. The global transformation matrix $\mathbf{T_U}$ is then derived according to the definition of $\mathbf{q}$ and $\mathbf{q^h}$, and is written as

$$\mathbf{T_U} = \begin{bmatrix} \mathbf{T_{U,i}} & & & \\ & \ddots & & \\ & & \mathbf{T_{U,N^d}} & \\ & & & \mathbf{I_b} \end{bmatrix}, \tag{4.47}$$

where $\mathbf{I_b}$ is the identity matrix that retains specific coordinates into nodal basis. Therefore, its size should be defined according to the length of $\mathbf{q^B}$. The local transformation matrix $\mathbf{T_{U,i}}$ is related directly to the *ith* deterministic subsystem ($\mathbf{q_{d,i}} = \mathbf{T_{U,i}} \mathbf{q^h_{d,i}}$) and is derived accordingly to the basis used for projection. Their derivations are discussed in the following subsections.

Having the global transformation matrix $\mathbf{T_U}$ properly derived, the next step is to project the framework's matrices into these more efficient bases. In the case of the deterministic subsystem's dynamic stiffness $\mathbf{D_d}$, its representation in partially modal global coordinates $\mathbf{q^h}$ is obtained similarly to Eq. 3.15, and written as

$$\mathbf{D^h_d} = \mathbf{T_U}^T \mathbf{D_d} \mathbf{T_U}. \tag{4.48}$$

The total dynamic stiffness $\mathbf{D^h_{tot}}$, *ith* statistical subsystem's direct field dynamic stiffness $\mathbf{D^h_{dir,i}}$ and the cross-spectral external force $\mathbf{S^{ext,h}_{ff}}$ in partially modal global coordinates are obtained similarly to the equation above. This results in the partially modal deterministic response

$$\mathbf{S_{q^h q^h}} = \mathbf{D_{tot}^h}^{-1}\Big(\mathbf{S_{ff}^{ext,h}} + \sum_i^N 4C_i \mathrm{Im}\{\mathbf{D_{dir,i}^h}\}\Big)\mathbf{D_{tot}^h}^{-H}. \tag{4.49}$$

All power-flow framework's coefficients ($h_{i,j}$, $\mathcal{M}_{d,i}$ and Π_i^{ext}) are then computed using these projected matrices (except for the dissipation coefficient $\mathcal{M}_i$, which is computed using the previous discussed expressions for lumped nodal Eq. 3.26, lumped modal Eq. 4.19 or partitioned modal Eq. 4.42-4.43 scenarios). The power-flow coefficients can then be more efficiently derived with following expressions. For the external input power to the ith statistical subsystem

$$\Pi_{\mathrm{in,i}}^{\mathrm{ext}} = \frac{\omega}{2}\,\mathrm{Tr}\left[\mathrm{Im}\left\{\mathbf{D_{dir,i}^h}\right\}\mathbf{D_{tot}^h}^{-1}\mathbf{S_{ff}^{ext,h}}\mathbf{D_{tot}^h}^{-H}\right], \tag{4.50}$$

for the power transfer coefficient from the ith to the jth statistical subsystem

$$h_{\mathrm{i,j}} = \frac{2}{\pi}\,\mathrm{Tr}\left[\mathrm{Im}\left\{\mathbf{D_{dir,i}^h}\right\}\mathbf{D_{tot}^h}^{-1}\,\mathrm{Im}\left\{\mathbf{D_{dir,j}^h}\right\}\mathbf{D_{tot}^h}^{-H}\right] = h_{\mathrm{j,i}}. \tag{4.51}$$

and for the deterministic damping coefficient

$$\mathcal{M}_{d,i} = \frac{2}{\pi}\,\mathrm{Tr}\left[\mathrm{Im}\left\{\mathbf{D_d^h}\right\}\mathbf{D_{tot}^h}^{-1}\,\mathrm{Im}\left\{\mathbf{D_{dir,i}^h}\right\}\mathbf{D_{tot}^h}^{-H}\right]. \tag{4.52}$$

The discussion regarding each of the two approaches (using either free or clamped modes) to properly define $\mathbf{T_{U,i}}$ and $\mathbf{q_{d,i}^h}$ are discussed next.

4.4.1 Clamped modes

Assuming the ith deterministic subsystem's nodal basis could be defined simply as $\mathbf{q_{d,i}} = \begin{bmatrix}\mathbf{q_{d,i}^I} & \mathbf{q_{d,i}^B}\end{bmatrix}$, the first approach projects the deterministic subsystem based on a fixed interface configuration (MACE; SHORTER, 2000), where the degrees of freedom related to nodes contained in junctions to other subsystems or external excitations $\mathbf{q_{d,i}^B}$ are retained in nodal coordinates. The rest of the ith deterministic subsystem's nodal coordinates $\mathbf{q_{d,i}^I}$ are projected to modal bases $\mathbf{p_{d,i}^I}$ (all the interior domain is projected). This change of coordinates is expressed as

$$\mathbf{q_{d,i}^I} = \mathbf{U_{d,i}^I}\mathbf{p_{d,i}^I}. \tag{4.53}$$

The ith deterministic subsystem's internal modal shape matrix $\mathbf{U_{d,i}^I}$ is generated from the respective internal eigenproblem

$$\left[\mathbf{K_{d,i}^{II}} - \omega^2\mathbf{M_{d,i}^{II}}\right]\mathbf{u_{d,i}^I} = \mathbf{0}, \tag{4.54}$$

where $\mathbf{U^I_{d,i}}$ is obtained from the collection of all eigenvectors from above equation, i.e. $\mathbf{U^I_{d,i}} = [\mathbf{u^I_{d,i,1}}, \ldots, \mathbf{u^I_{d,i,N}}]$. This approach is denoted as clamped modes because the modal shape obtained from the above eigenproblem represents the deformation that the *ith* deterministic subsystem would have if the boundary was constrained. The *ith* deterministic subsystem's stiffness and mass matrix ($\mathbf{K^{II}_{d,i}}$ and $\mathbf{M^{II}_{d,i}}$, respectively) are simply derived by separating the subsystem's coordinates into boundary and internal degrees of freedom in the respective subsystem's matrices $\mathbf{K_{d,i}}$ and $\mathbf{M_{d,i}}$, similar to what was applied in Eq. 3.9. After projection, the *ith* deterministic subsystem's degrees of freedom are expressed as

$$\mathbf{q^h_{d,i}} = \begin{bmatrix} \mathbf{p^I_{d,i}}^T & \mathbf{q^B_{d,i}}^T \end{bmatrix}^T, \tag{4.55}$$

which, in order to satisfy the relation between $\mathbf{q_{d,i}}$ and above expression, its local transformation matrix should be defined as

$$\mathbf{T_{U,i}} = \begin{bmatrix} \mathbf{U^I_{d,i}} & \mathcal{X}_{\mathbf{d,i}} \\ \mathbf{0} & \mathbf{I_{d,i}} \end{bmatrix} \tag{4.56}$$

where $\mathbf{I_{d,i}}$ is the identity matrix that retains the junction node's coordinates of the *ith* deterministic subsystem into nodal basis, its size is defined according to the number of degrees of freedom contained in the junctions. The constrained modal shape $\mathcal{X}_{\mathbf{d,i}}$ was defined in order to apply the internal forces from the junction boundary to the interior modes. Otherwise, the projected internal degrees of freedom would interpret the junction nodes as constrained, which is unintended. The constrained modal shape is then written as

$$\mathcal{X}_{d,i} = -\mathbf{K^{II}_{d,i}}^{-1}\mathbf{K^{IB}_{d,i}}, \tag{4.57}$$

where $\mathbf{K^{IB,i}_{d,i}}$ was also obtained by expanding the subsystem's coordinates in $\mathbf{K_{d,i}}$. Notice that, as this approach only changes nodal bases that are contained in the interior domain of deterministic subsystems, the coordinates in the boundary of connected statistical subsystems remain as nodal basis, resulting in a projection over direct field dynamic stiffness matrices that only rearranges their respective nodal matrices in the newly defined set of partially modal degrees of freedom.

4.4.2 Free modes

The second approach presents a simpler projection, where the entire domain of the *ith* deterministic subsystem is projected into free modal basis $\mathbf{p_{d,i}}$. The projection is then

expressed as

$$\mathbf{q_{d,i}} = \mathbf{U_{d,i}} \mathbf{p_{d,i}}, \tag{4.58}$$

where $\mathbf{U_{d,i}}$ is the free modal shape matrix obtained from the following eigenproblem

$$\left[\mathbf{K_{d,i}} - \omega^2 \mathbf{M_{d,i}}\right] \mathbf{U_{d,i}} = \mathbf{0}. \tag{4.59}$$

After projection, the *ith* deterministic subsystem's partially modal degrees of freedom are expressed as

$$\mathbf{q^h_{d,i}} = \mathbf{p_{d,i}}, \tag{4.60}$$

resulting in the following local transformation matrix

$$\mathbf{T_{U,i}} = \mathbf{U_{d,i}}. \tag{4.61}$$

As the free eigenproblem covers the projection of the entire *ith* deterministic subsystem's domain, nodal degrees of freedom from statistical subsystems that are connected to deterministic subsystems are also projected into the respective connected deterministic subsystem's modal basis. For this reason, the global partially modal coordinate vector $\mathbf{q^h}$ becomes considerable smaller, when compared to the first approach, as several nodal degrees of freedom vanish, resulting in also smaller matrices and higher computational efficiency. These two projection approaches do not need to be applied to all deterministic subsystems, only to those intended for model reduction. Moreover, the same modal projection approach does not need to be applied to every selected deterministic subsystems, a mix of approaches could be applied.

4.5 VIBRATIONAL ENERGY - DETERMINISTIC SUBSYSTEMS

This section presents a derivation for the deterministic subsystem's vibrational energies, which are composed as a superposition of a kinetic and strain contributions, using the newly presented partially modal degrees of freedom. As $\mathbf{K_{d,i}}$ and $\mathbf{M_{d,i}}$ were defined according to the deterministic subsystem's degrees of freedom $\mathbf{q_{d,i}}$, an additional boolean matrix $\mathbf{B_{d,i}}$ is defined to arrange the subsystem's matrices into global nodal degrees of freedom $\mathbf{q}$. This arrangement is expressed as

$$\mathbf{q_{d,i}} = \mathbf{B_{d,i}} \mathbf{q}. \tag{4.62}$$

Therefore, in combination with Eq. 4.44, the *ith* deterministic subsystem's mass matrix in global partially modal coordinates $\mathbf{q^h}$ can be expressed as

$$\mathbf{M_i^h} = \mathbf{T_U}^T \mathbf{B_{d,i}}^T \mathbf{M_{d,i}} \mathbf{B_{d,i}} \mathbf{T_U}, \tag{4.63}$$

resulting in the following *ith* deterministic subsystem's kinetic energy expression

$$K_{d,i} = \frac{1}{4} \dot{\mathbf{q}}^{\mathbf{h}H} \mathbf{M_{d,i}^h} \dot{\mathbf{q}}^{\mathbf{h}}. \tag{4.64}$$

By assuming a harmonic motion ($\dot{\mathbf{q}}_i^h = \mathrm{i}\omega \mathbf{q}_i^h$), the expression could be rewritten as

$$K_{d,i} = \frac{\omega^2}{4} \mathbf{q}^{\mathbf{h}H} \mathbf{M_{d,i}^h} \mathbf{q}^{\mathbf{h}}, \tag{4.65}$$

or in index notation representation

$$K_{d,i} = \frac{\omega^2}{4} \sum_{k,m} M^{h,(k,m)} q^{h,(k)} q^{h,(m)^*}. \tag{4.66}$$

The above expressions only considers deterministic results, neglecting the random behavior from statistical subsystems. In order to derive ensemble average contributions, the same steps from Eq. 2.21 to 2.23 could be performed, resulting in the expression written as

$$\langle K_{d,i} \rangle = \frac{\omega^2}{4} \operatorname{Tr} \left\{ \mathbf{M_{d,i}^h} \mathbf{S_{q^h q^h}} \right\}. \tag{4.67}$$

As for the *ith* deterministic subsystem's strain energy, it obtained by the following expression

$$U_{d,i} = \frac{1}{4} \mathbf{q}^{\mathbf{h}H} \mathbf{K_{d,i}^h} \mathbf{q}^{\mathbf{h}}, \tag{4.68}$$

where the *ith* deterministic subsystem's stiffness matrix in global partially modal coordinates is expressed as (exacly the same process used for the mass matrix)

$$\mathbf{K_i^h} = \mathbf{T_U}^T \mathbf{B_{d,i}}^T \mathbf{K_{d,i}} \mathbf{B_{d,i}} \mathbf{T_U}, \tag{4.69}$$

By following the same steps above, the ensemble average strain energy is given by

$$\langle U_{d,i} \rangle = \frac{1}{4} \operatorname{Tr} \left\{ \mathbf{K_{d,i}^h} \mathbf{S_{q^h q^h}} \right\}. \tag{4.70}$$

The ensemble average vibrational energy of the *ith* deterministic subsystem is then computed as

$$\langle E_{d,i} \rangle = \langle K_{d,i} \rangle + \langle U_{d,i} \rangle. \tag{4.71}$$

5 NUMERICAL EXAMPLES

To evaluate the performance of the discussed vibro-acoustic methods, including the novel generalized hybrid method, four cases were selected to explore different aspects of each methods: two mid-frequency and two high-frequency problems. Low-frequency cases were disregarded from analysis, as the Finite Element Method is the most suggested and used method, when compared to other ones in this frequency region (HAMBRIC; SUNG; NEFSKE, 2017). For the rest, the choice of method for analysis will depend on the characteristics of the system, as they may directly influence on the performance of each method differently. The analysis performed here in this chapter could serve as a guideline for this concern.

The evaluation will mainly concern the robustness of the results and the computational expense demanded to derive the results. A FE Monte Carlo model was defined as reference for comparison. The methods that presented better convergence to the FE Monte Carlo's results were considered the ones with better performance on representing the system results. The FE Monte Carlo ensemble was derived using standard FE models in combination with random constrains applied into the domain of the statistical subsystems in each sample. Additionally, for the subsystems excited by a transverse point force, the latter is applied at random positions on the excited subsystem in each sample. This whole process is discussed in more detail on Appendix. A convergence analysis was performed in order to determine the ensemble's size for each problem. As for the computational performance's evaluation, the processing time demanded from each method to derive their results were used for comparison.

The results for the established methods (SEA and Hybrid FE-SEA) were derived from the commercial software VAOne (ESI GROUP, 2019). The same software generated the FE Matrices used for the FE Monte Carlo and Generalized Hybrid Method, which were extracted and post-processed in Matlab scripting routines (MATHWORKS, 2020). Figure 11 display the relationship of the four methods' derivation with the mentioned softwares. The novel method's results were derived according to the implementation chart displayed on Fig. 12. As it can be seen, modal projection is performed to both statistical subsystems' interior domains and deterministic subsystems. In the latter case, free mode shapes were assumed, due to smaller nodes retained after projection. Regarding the averaging technique used to derive the direct field dynamic stiffness $\mathbf{D_{dir,i}}$, the Lorentzian frequency approach

was adopted, due to its superior result convergence and computational performance. Lastly, if any subsystem assumes a flat plate geometry, its lumped wavefield is partitioned into in-plane and out-of-plane before introducing it to the power-flow framework, otherwise lumped wavefield is assumed.

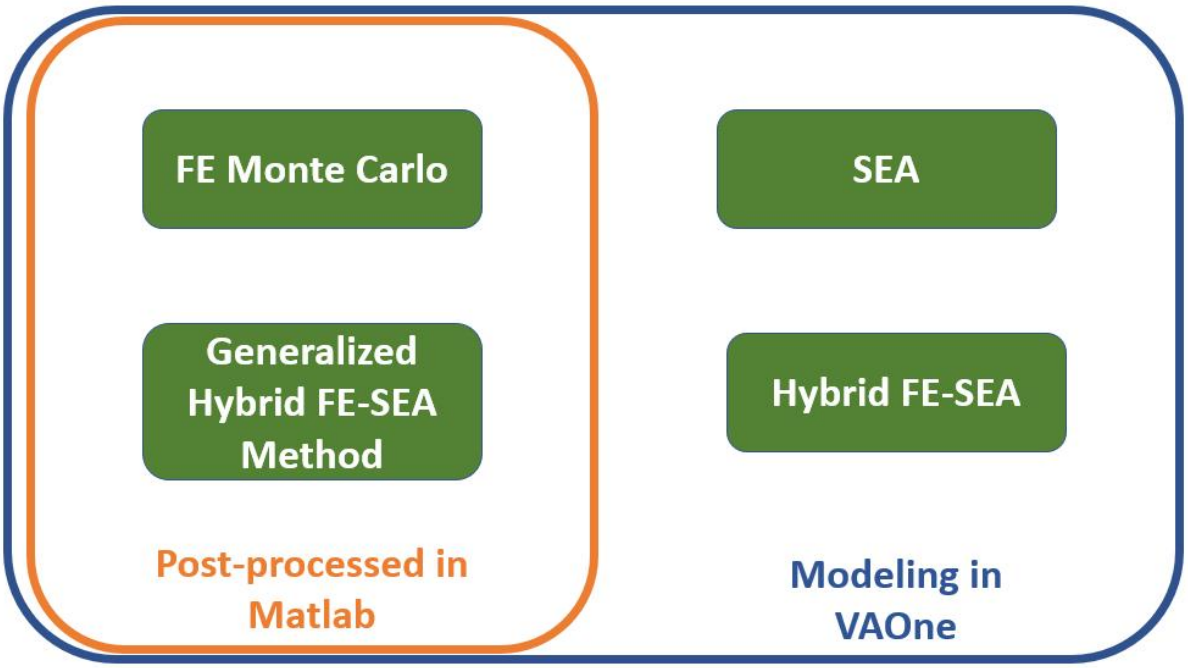

Figure 11 – Relationship between methods and softwares

The analysis's frequency spectrum was limited from 50Hz to 4000Hz with a 10Hz step frequency ($\Delta f = 10Hz$), which was enough to enforce low and high wavelength motion to (some or all) components from the selected cases. In order to guarantee robustness for the FE models, the modal extraction performed extracted modes with natural frequencies up to twice the maximum analyzed frequency (8kHz) and the FE meshes admitted, at least, six elements per wavelength. Moreover, the FE Meshes were generated with triangular elements (CTRIA3) with simply 3 nodes with 6 degrees of freedom per each.

All the components presented in the following cases will be constituted by either steel or aluminum with a 1% (0.01) damping loss factor η_i, their material properties are presented in Tab. 1. Each case presented a single excitation to a particular subsystem, represented by a $1N$ rms transverse point force (in the following figures exhibiting the 3d visualization of the systems, the excitations are pictured as purple arrows).

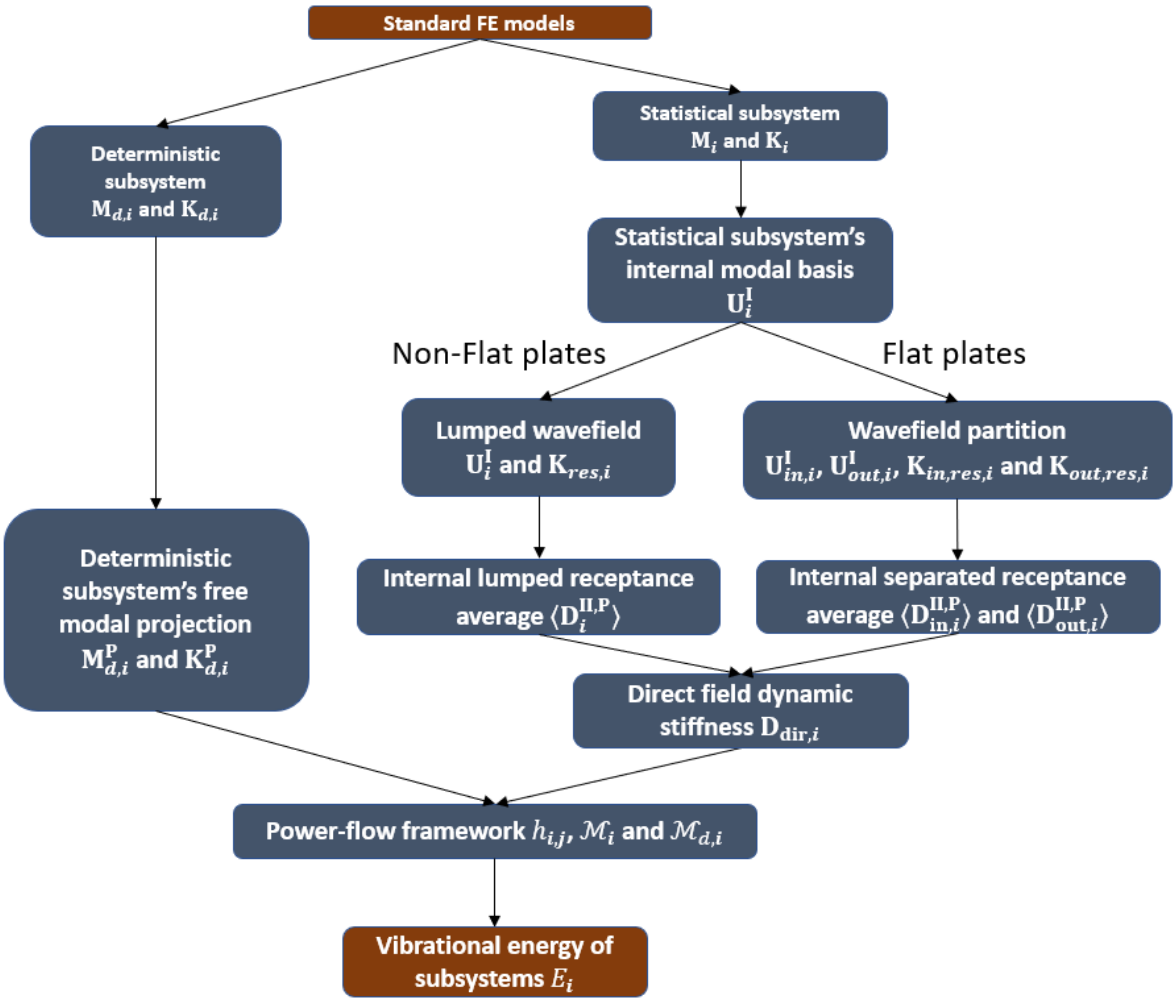

Figure 12 – Novel method's process flowchart

Table 1 – Aluminum and Steel material properties

Properties	Aluminum	Steel
Density ρ $[kg/m^3]$	2700	7800
Young's Modulus E [GPa]	71	210
Shear Modulus G	26.7	80
Poisson's Ratio ν	0.3296	0.3125

5.1 CO-PLANAR FLAT PLATES COUPLED BY A BEAM

The first case consists of a mid-frequency problem (shown in Fig. 13), involving two aluminum co-planar plates coupled at four specific points (two for each plate) to a stiff steel beam with rectangular cross section. These connections are exhibited in the figure as dark yellow circles (one is hidden behind the beam). Regarding their geometry, both plates have an area of $0.723m^2$ with the excited and the receiver plate admitting, respectively, a thickness of $1mm$ and $2mm$. The beam of $1.1m$ length has a cross section shape of $0.1m$ x $0.08m$ with $10mm$ thickness.

The thin plates are ideally identified as statistical subsystems in both standard and generalized Hybrid FE-SEA method, due to their diffuse motion and high modal density associated to their wavefield. In contrast, the beam admits a stiff and coherent behavior, resulting in an efficient and reliable deterministic definition. In SEA, the beam had to be defined as statistical subsystem due to the assumptions made be the framework, therefore, in order to properly couple it to the plates, offsets were defined on connections.

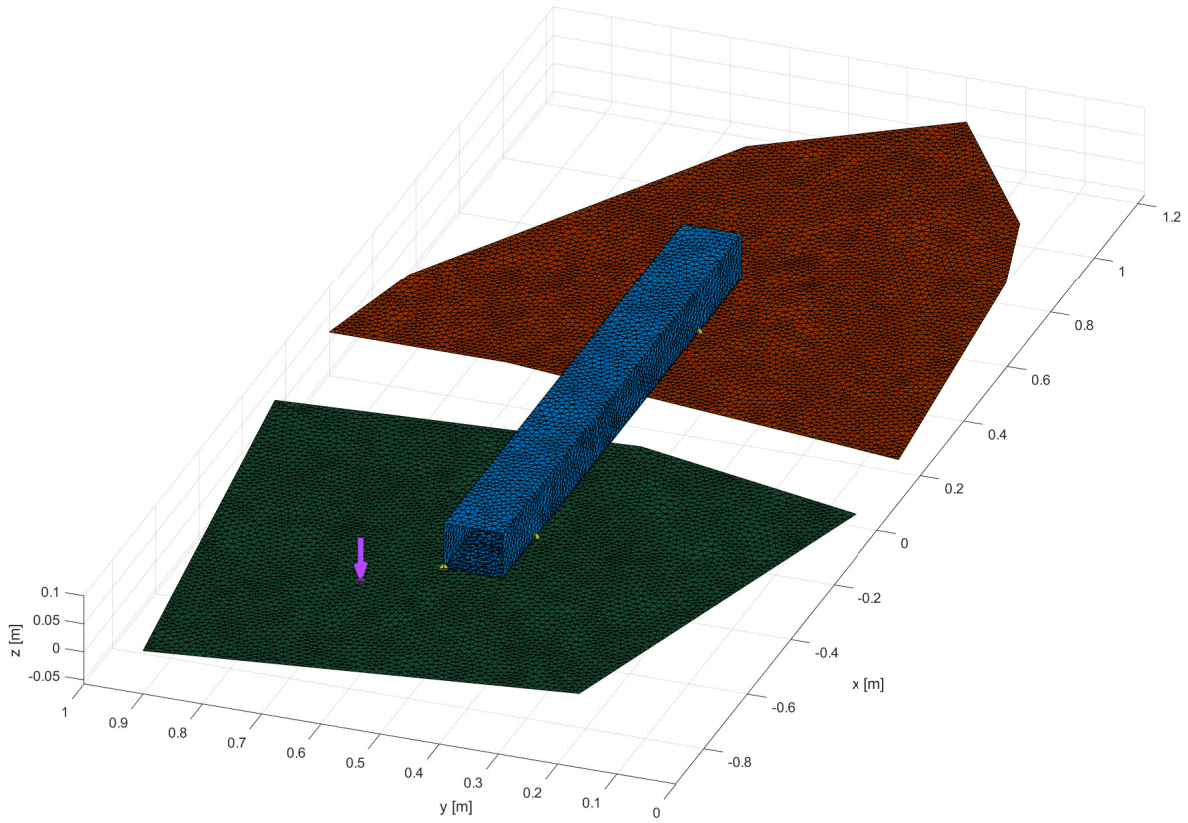

Figure 13 – First case - Co-planar plates and a beam

Results for the excited plate, beam and receiver plate are exhibited, respectively, in Fig. 14, Fig. 15 and Fig. 16. In combination with the FE Monte Carlo's ensemble mean results (in black), the curves from all samples (in gray) are exhibited, in order to have clearer understanding of the samples' randomization and ensemble convergence. Nonetheless, when a FE Monte Carlo result is mentioned, it is the ensemble mean result being referred to. For the excited plate's results, where the response is predominantly influenced by the external loads and the respective subsystem properties, a simple decay over frequency is obtained from all methods, resulted from the highly overlapped modal behavior of the flat plate. Moreover, the analytical formulations, used in SEA and Hybrid FE-SEA method, were capable of deriving a proper description for the wavefields, as can be observed by the convergence of these methods to the more generalized ones, i.e. the Generalized Hybrid method and FE Monte Carlo, which used standard FE models to describe the wavefields.

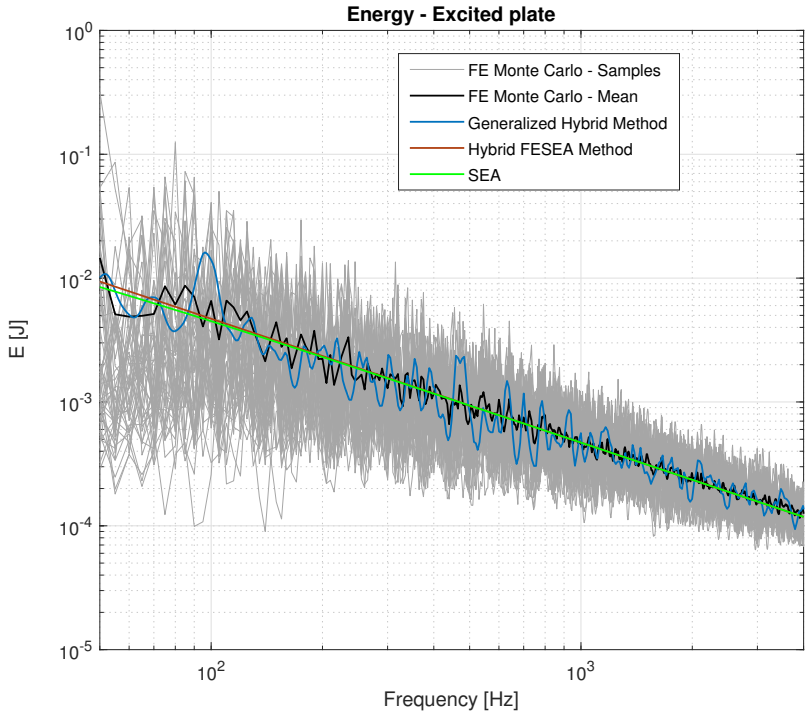

Figure 14 – Excited plate's energy results in the first case

Regarding the beam's results, a different curve's shape is presented for most of the methods. This is a consequence of the predominant influence of the beam's dynamics in the derivation. Moreover, as the beam possess a low modal density behavior, the results presented a strong influence to specific modes with reasonable small modal overlapping.

This is observed from the reference result (FE Monte Carlo) and also on both hybrid method results, as they modeled the highly coherent beam with a standard FE model, allowing for a proper definition of the its wavefield. By contrast, in order to fulfill the framework's analytical formulation's requirements, the SEA assumes the beam's wavefields are fully diffusive, thus underestimating the beam's response. Nevertheless, the SEA's result is still capable of giving useful information about the system's response. The framework's curve presents the average decay tendency of the response and could give an estimation of a maximum response's amplitude for an analyzed real-life system to, for example, avoid a possible fatigue.

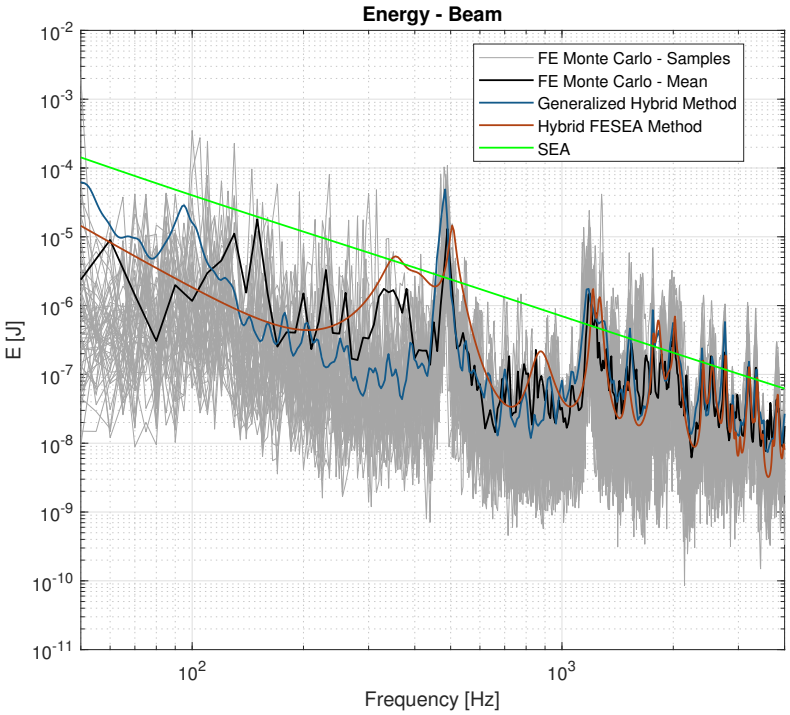

Figure 15 – Beam's energy results in the first case

An analogous conclusion could be obtained from the receiver plate's results, as the energy that flows into the subsystem comes from the beam's point junctions and, therefore, is also influenced by the beam's modal behavior. Regarding the novel hybrid method, it was only possible to derive such robust results due to the use of partitioned wavefields, i.e. enforcing a power-flow definition for the in-plane and out-of-plane contributions separately. Figure 17 exhibits the receiver's plate energy results if each plate's wavefield was modeled as a single lumped wavefield, compressing all power flow's contributions into unique coefficients per subsystems. A similar deviant curve is obtained for the beam's energy

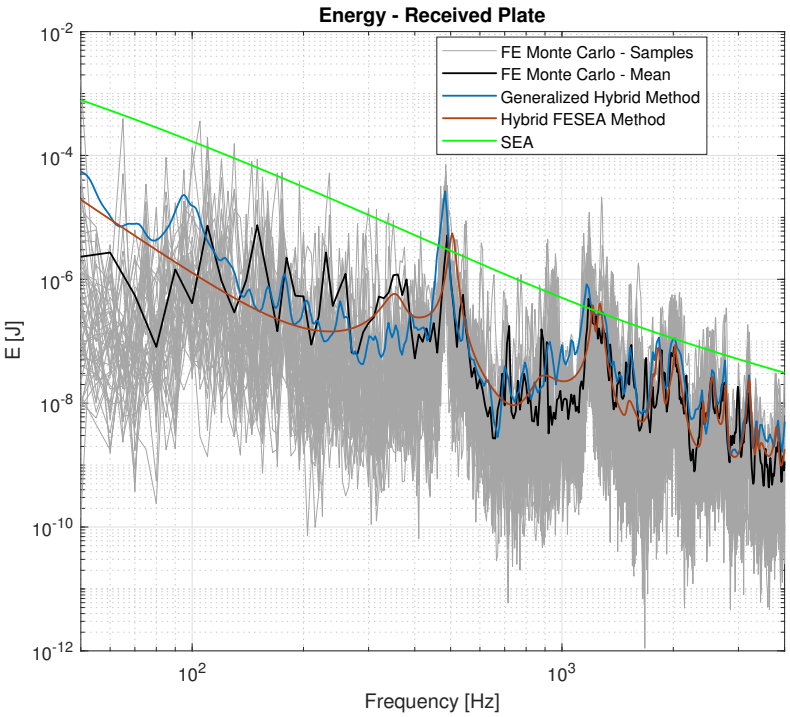

Figure 16 – Receiver plate's energy results in the first case

results. Only the reference and the hybrids curves were plotted for comparison.

This difference is caused by the overestimation of the in-plane's response, as the in-plane wavefield stores significantly less energy than its out-of-plane pair and the lumped wavefield assumes equipartition of energy between both. The overestimation is only presented to subsystems that have their in-plane wavefield excited, consequently the excited plate's results are not affected, as the transverse force applied to this plate only excites the out-of-plane wavefield (the excited plate results with a lumped wavefield is analogous to the one exhibited in Fig. 14). The in-plane wavefield's contributions start to become relevant after the power-flow interacts to discontinuities, which are presented at the beam's junctions and edges. For this reason, this overestimation becomes present only to the beam and receiver plate's subsystems.

The processing time required by each method to derive their results is exhibited in Fig 18. As expected, the method that used the larger quantity of detail in the model (FE Monte Carlo) demanded, at large scale, the most processing time just for a single sample, when compared to the other methods. The novel hybrid method was able to derive results in far lesser time, although presenting, simultaneous, very similar curves to the Monte Carlo Method. In the case of the Hybrid FE-SEA and SEA, both had minimal processing

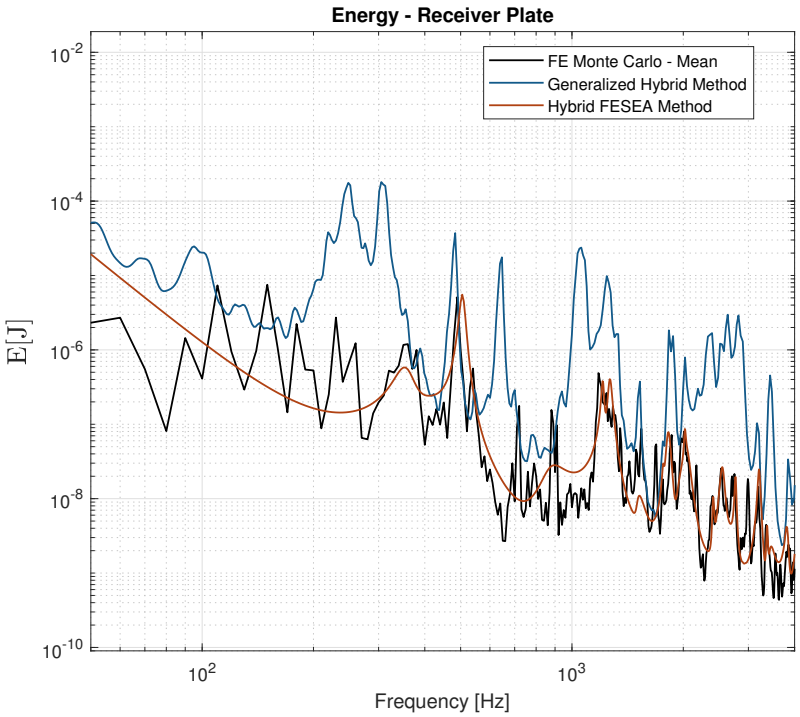

Figure 17 – Receiver plate's energy results with lumped wavefields in the first case

time, resulted from the efficient use of analytical formulations. Their difference in duration is due to the beam's FE model used in the Hybrid FE-SEA, which increased the size of information contained in the model by a considerable scale. Furthermore, as the SEA was unable to provide a proper definition for all subsystems and the Hybrid FE-SEA exhibited robust performance regarding both processing time and result's curves, the established Hybrid method is inferred as the selected method with optimal performance along the ones discussed here in the work to this specific case's analysis.

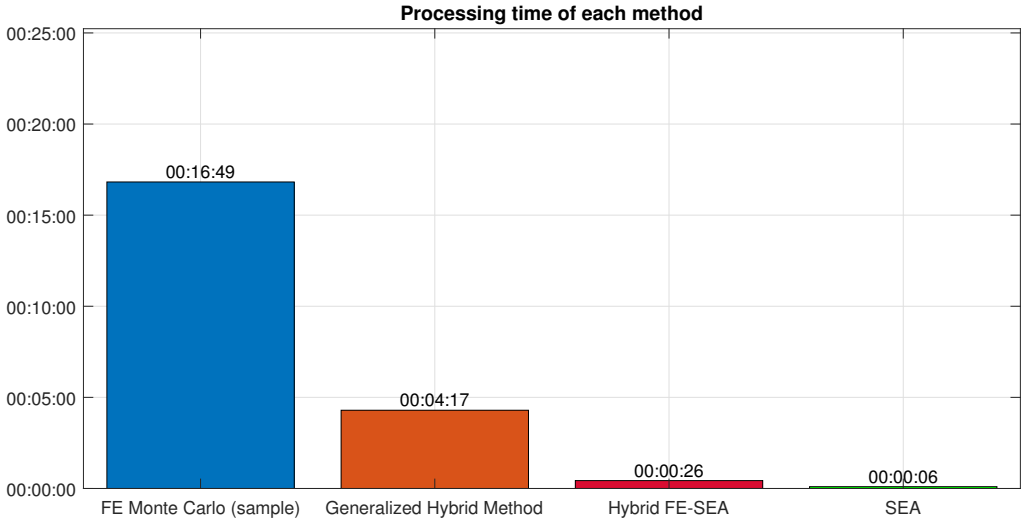

Figure 18 – Processing time for each method in the first case

5.2 CUBE BEAM FRAMEWORK

The second case is, again, a mid-frequency problem (shown in Fig. 19) that consist of four flat plates (green) connected by their edges to a single beam framework (brown), resulting into a similar cube shaped system (with its top and bottom sides open). It is assumed that these plates have their whole edges connected to the framework and one of them is excited. The beam framework has a hollow structure with a squared cross section of $2.52cm$ side, $3mm$ of thickness and is made of steel. As for the plates, they are identical, having a squared area of $0.4724m^2$, thickness of $2mm$ and are made of aluminum. Moreover, in this second case, a clamped boundary condition (all translational and rotational degrees of freedom of the respective nodes are set to zero) is applied to two bottom outer edges of the beam framework, as shown in Fig. 20. The white circles represent the clamped nodes.

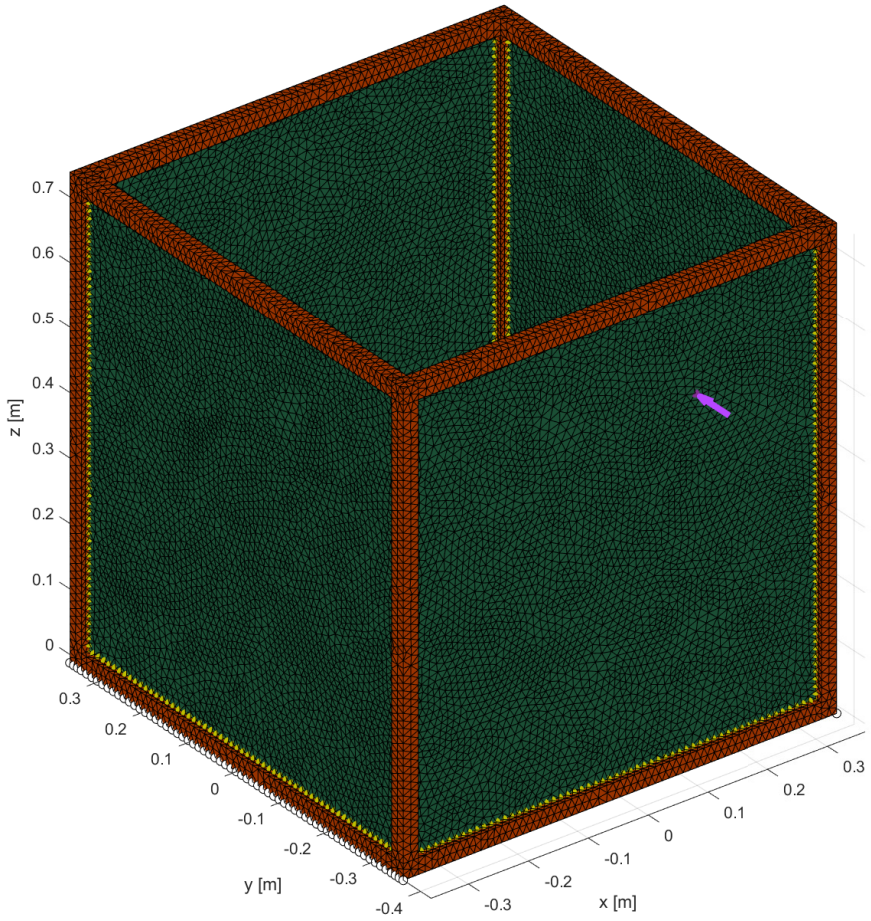

Figure 19 – Second case - Cube beam framework with side plates

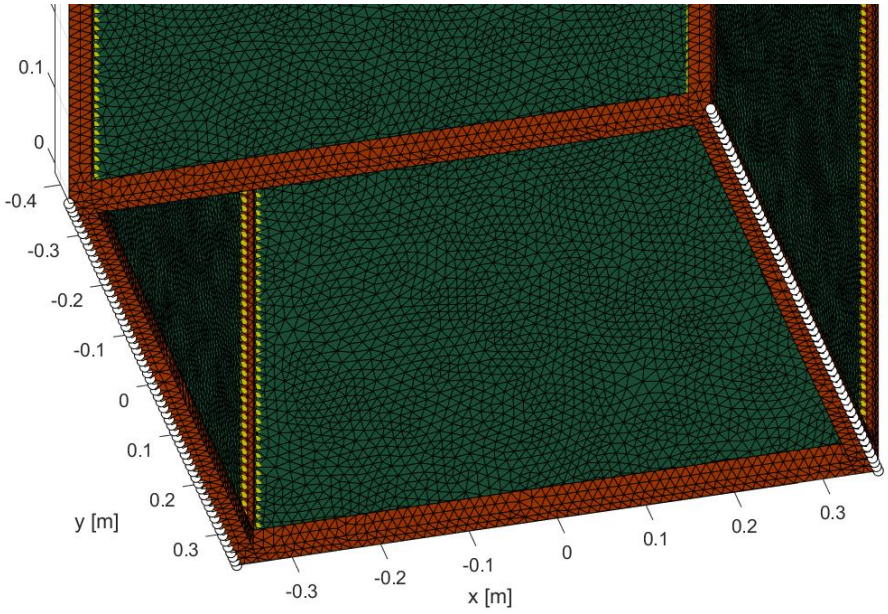

Figure 20 – Second case - Boundary condition on detail

By a similar manner of the previous numerical example, the flat plates are modeled as statistical subsystems and the beam framework as deterministic. No SEA results were derived for this case, as the same conclusion of the last numerical example would be obtained. Moreover, no acoustic cavity is considered. Results for the excited front plate, side plate and rear side plate are exhibited, respectively, in Fig. 21, Fig. 22 and Fig. 23. The other side plate's results derive a similar conclusion of the considered side one, therefore it is not necessary to be shown here. The beam framework's result is shown in Fig. 24. Again, the excited subsystem's response is predominantly controlled by the external load and its internal dynamics. Here, all methods were capable of converging to the same energy decay over frequency.

In the case of the side plate's results, the curve's shape was considerably altered due to the more prevalent influence from the beam framework's modal behavior. It can be observed that the Generalized Hybrid Method was capable of deriving a similar curve to the FE Monte Carlo's one, showing robust definition of the system's energy flow. In contrast, the Hybrid FE-SEA method exhibits an underestimated curve at high frequency regions. This is mostly due to the simplified junction definition that the method assumes, where, in order to support analytical derivations, the method interprets the square junction as either four incoherent straight line junctions or a single big straight line junction, resulting in loss of energy flow characterization. Due to the general junction definition supported by the FE models in the Generalized Hybrid method, this coherence information is extracted

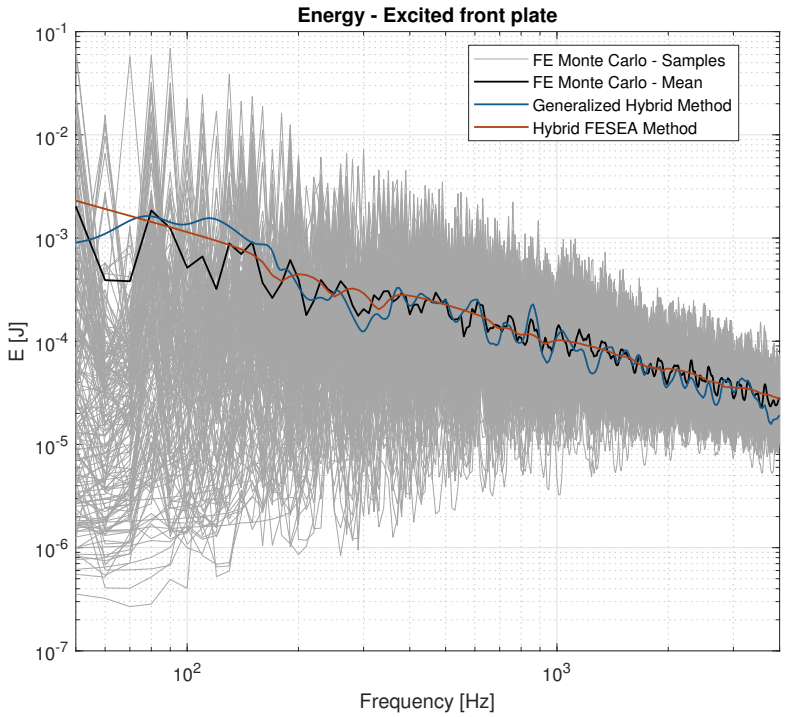

Figure 21 – Excited front plate's energy results in the second case

in the derivation, therefore obtaining a more robust characterization for the model's power flow. The same underestimation is experienced in the plate's results from the rear side and in the beam framework's results, although the latter in a less intense manner.

Figure 25 shows each method's processing time required to derive the results. Again as expected, the FE Monte Carlo sample demands the larger amount of time. In the case of the Generalized Hybrid method, a smaller processing time was necessary for derivation when compared to the established Hybrid one, even though the latter one uses analytical formulations. This is probably caused by definition of the four straight junctions' per plate (this definition is not confirmed), in comparison to the single generic junction per plate in the Generalized method, demanding more processing costs. It is important to point out that this difference between the novel generalized and established hybrid methods could be accentuated if more irregular configurations was adopted to the junctions and/or plates.

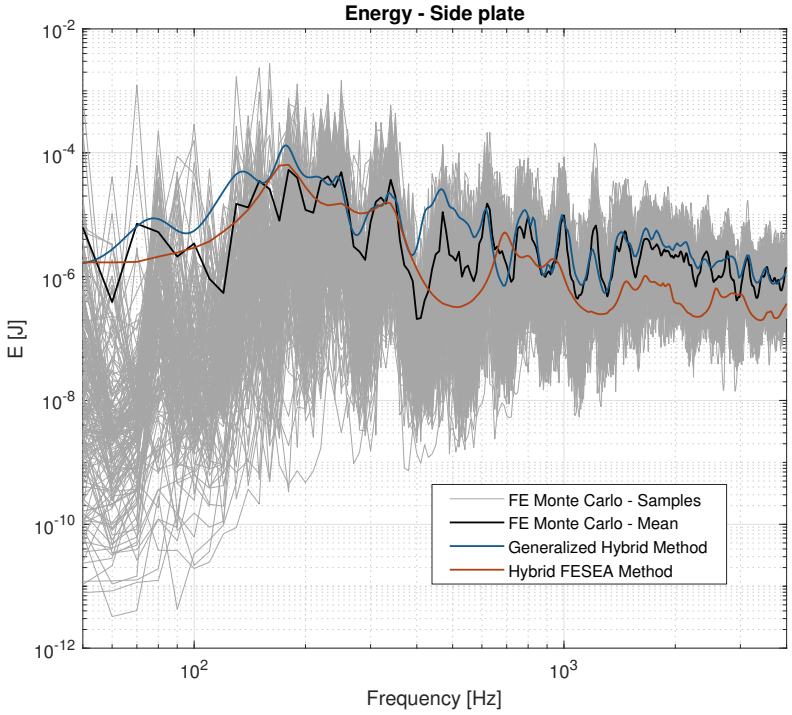

Figure 22 – Side plate's energy results in the second case

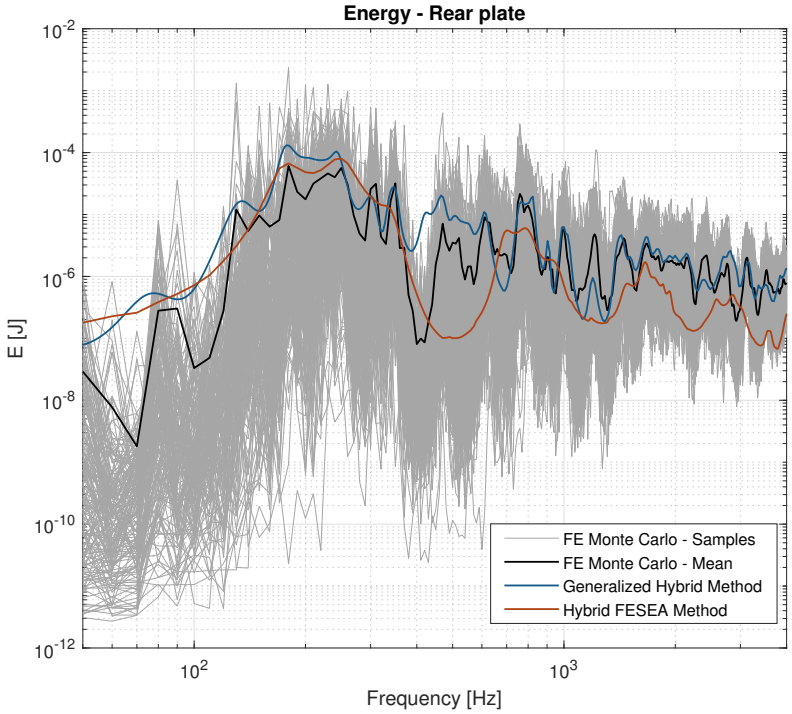

Figure 23 – Rear plate's energy results in the second case

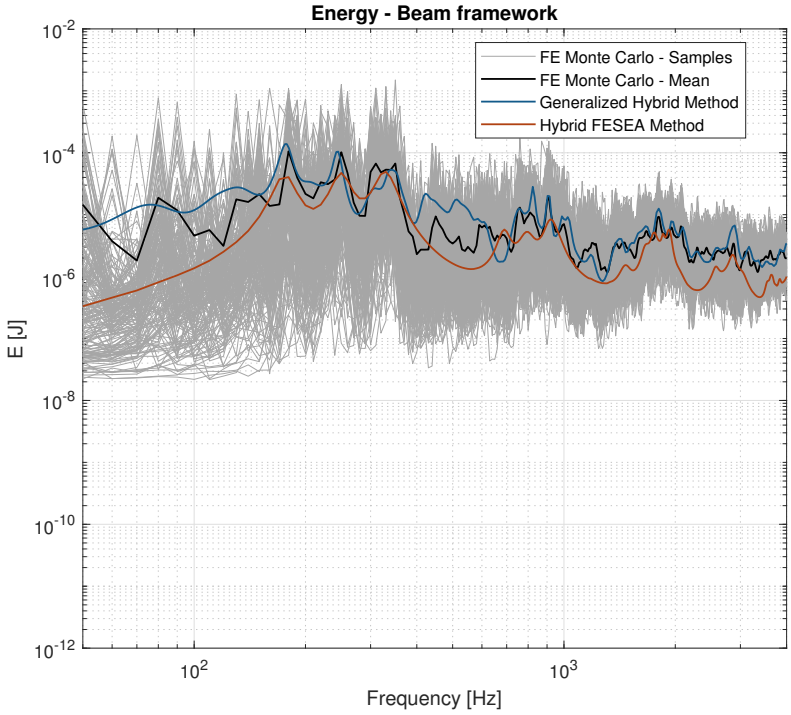

Figure 24 – Beam framework's energy results in the second case

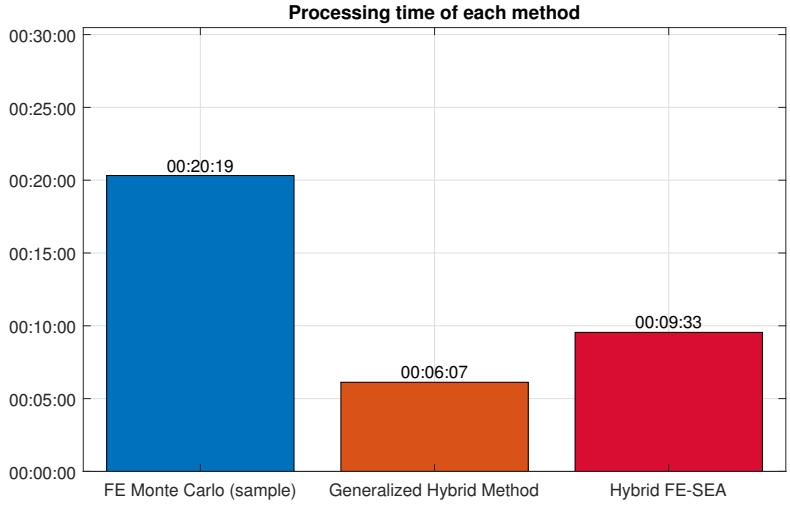

Figure 25 – Processing time for each method in the second case

5.3 FUSELAGE

The third case is a classical representation of a high frequency problem (exhibited in Fig. 26), frequently employed in the aerospace and space areas. The system consists two curved plates connected at their straight edge, portraying a fuselage structure. Both plates assume the same area, are made of aluminum and have $1m$ radius curve. Their difference is defined at their thickness, where the excited plate has $1mm$ and the receiver one has $2mm$.

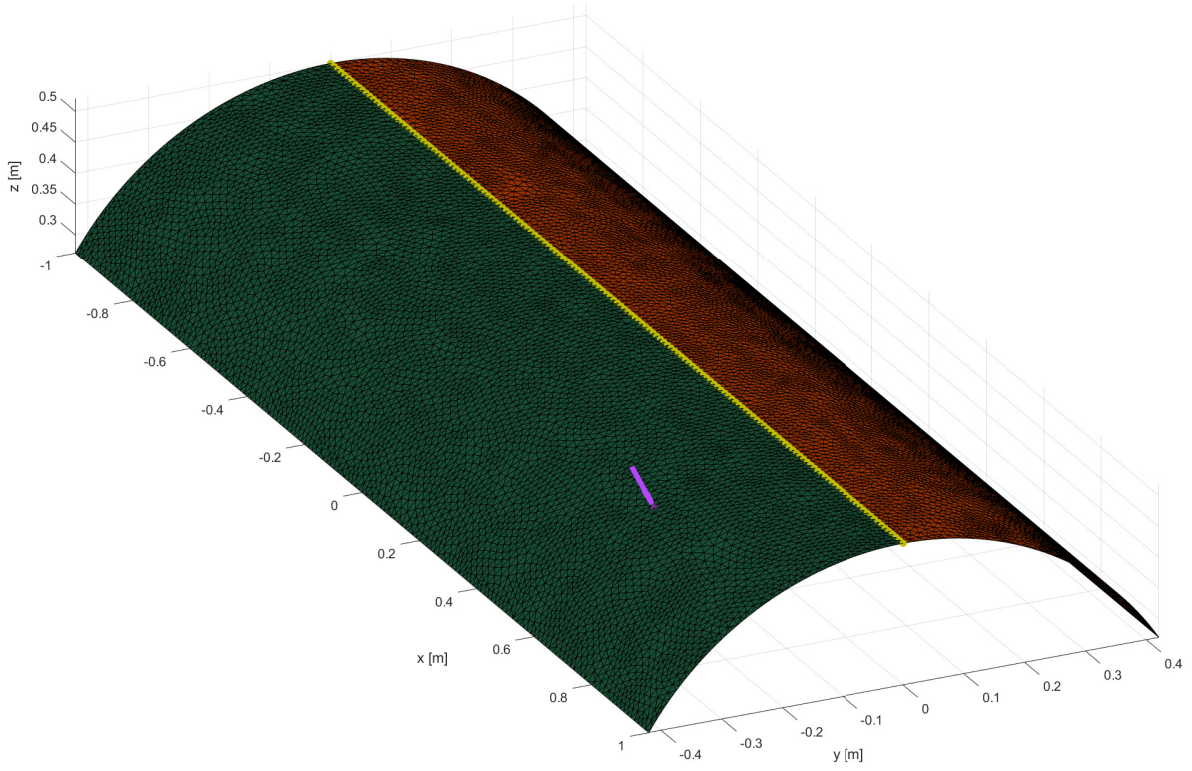

Figure 26 – Third case - Fuselage

Although the plates are curved, which increases their stiffness over frequency regions before the ring frequency, they are modeled as statistical subsystem, as their model densities are considerably high and support the SEA framework requirements. The ring frequency is a critical transition point where curved plates start to behave similarly to flat plates, this frequency is mainly a function of the plates' radius curve. No Hybrid FE-SEA results were derived, as no deterministic subsystems were defined, which, in this scenario, the method becomes equivalent to SEA. In the case of the novel method, due to its generalized formulation, a proper description of a high frequency problem is

also capable to be derived. As mentioned, in this context, the method is more commonly denoted as Numerical SEA (HINZ, 2021). The partition of the plate's wavefields was not adopted in this case, as no appropriate approach had been defined for curved plates.

Results for the excited and receiver plate are exhibited, respectively, in Fig. 27 and Fig. 28. Here, both plates' results assume a characteristic peak, which is a consequence of the subsystem's curvature and takes place at the ring frequency. SEA and Numerical SEA were capable of converging to FE Monte Carlo's results, demonstrating a robust derivation of the system's power flow. This is expected as the plate's configuration is fairly simple to be modeled with both analytical and numerical formulations.

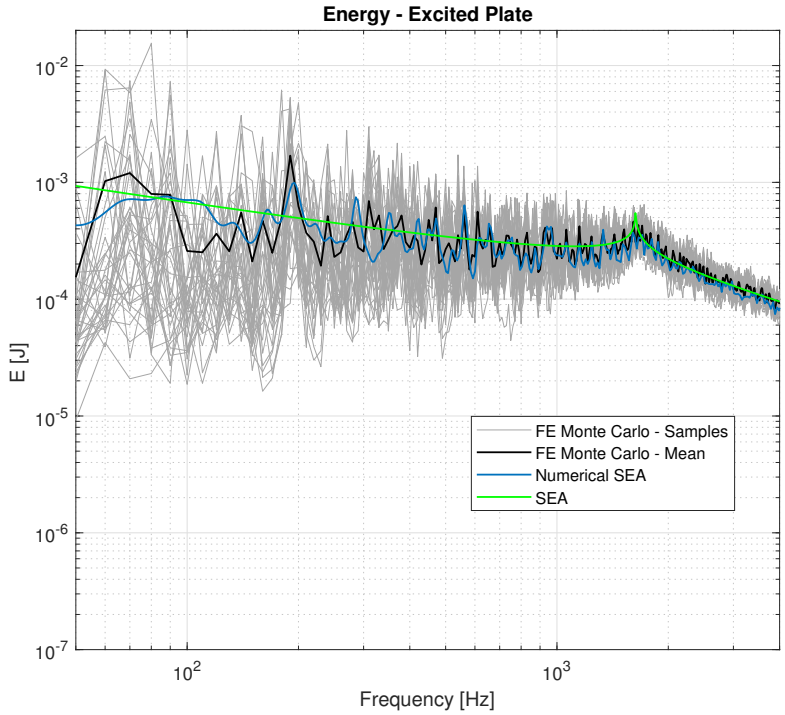

Figure 27 – Excited plate's energy results in the third case

When analyzing the processing time demanded for each method (Figure. 29), their difference becomes clear, as the analytical formulations from SEA allow for a seamlessly processing cost, surpassing by far the efficiency of the two numerical methods. This is a huge benefit for the method and is why it is vastly used in the industries. It can be observed from Fig. 26, more specifically from really dense mesh, that most of the amount of processing time from the numerical methods came from the huge amount of nodes required to match the desired element size (when compared to the minimum analyzed wavelength).

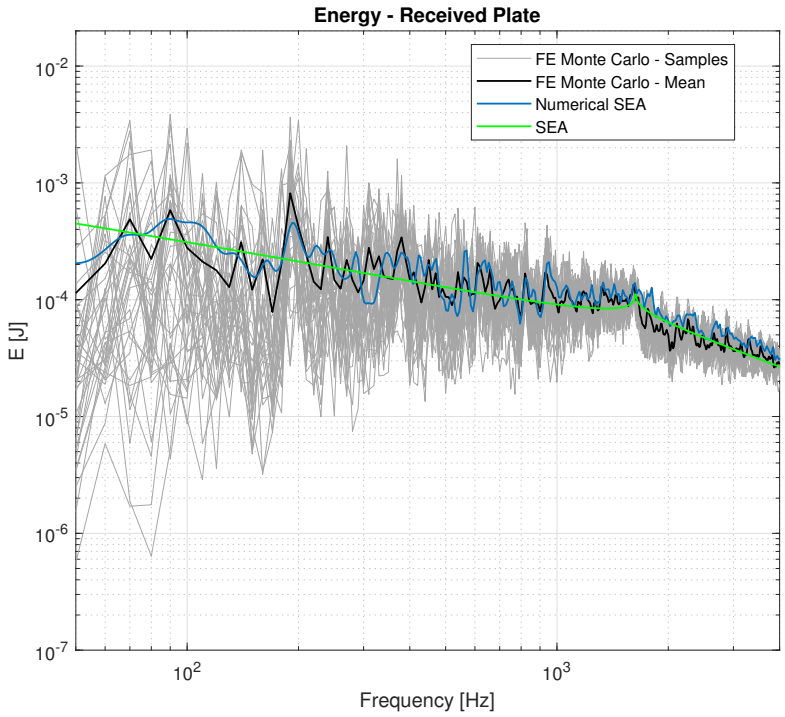

Figure 28 – Receiver plate's energy results in the third case

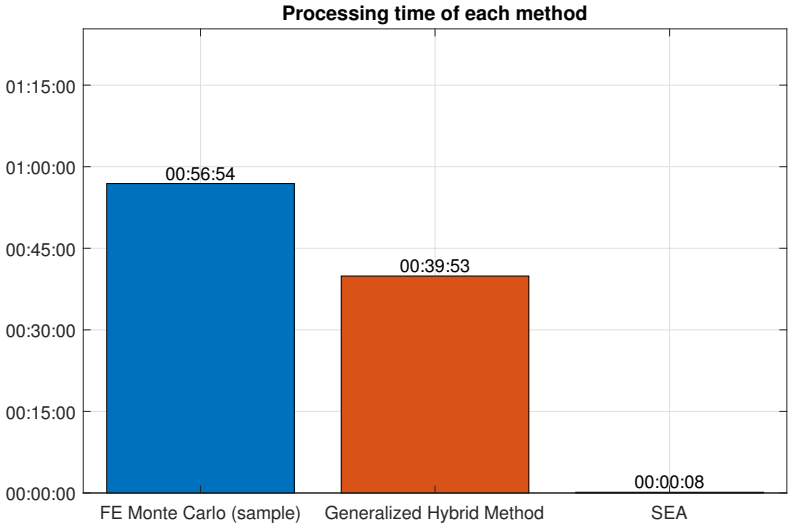

Figure 29 – Processing time for each method in the third case

5.4 VEHICLE BODY'S STRUCTURE

The last and fourth case was extracted from a real-life vehicle model, more specifically the outer structure from it floor structure. Figure 30 shows the system, which is divided in a top excited plate and a lower receiver plate, both admitting a very irregular configuration. The junction also possess an irregular geometry. Both the excited and receiver plates are made of aluminum and have, respectively, $1.2mm$ and $2.4mm$ of thickness, and 0.1928 m^2 and 0.2061 m^2 of area.

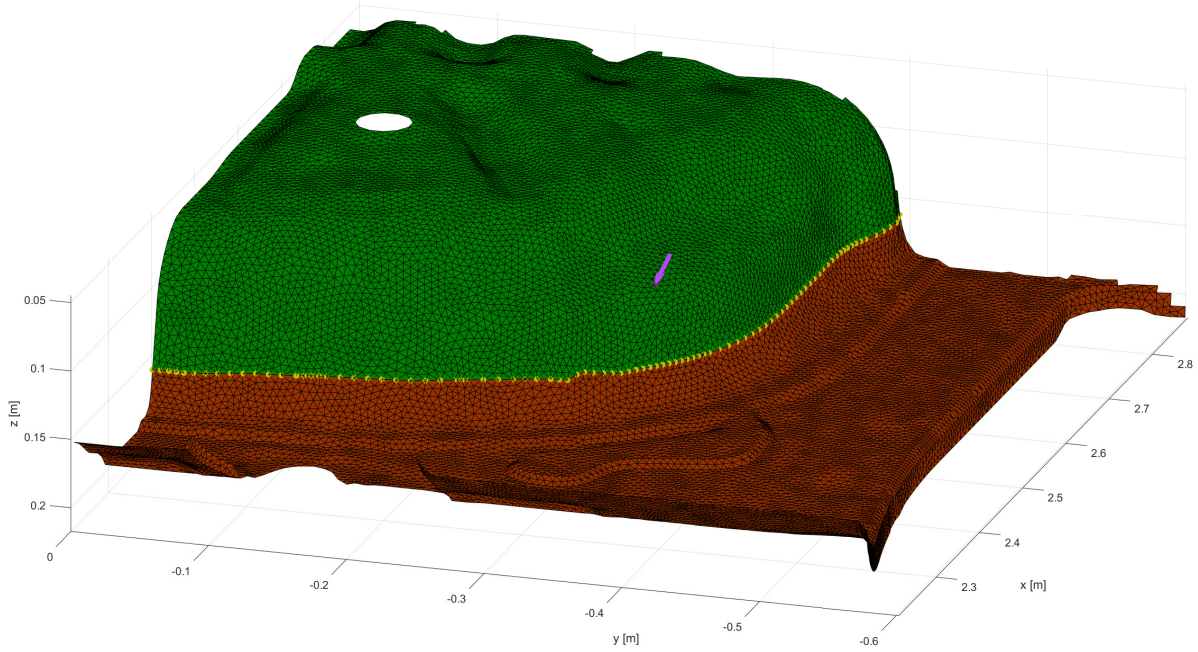

Figure 30 – Fourth case - Vehicle body structure's section

Similarly to the last presented case, both plates were modeled as statistical subsystems due to their high modal density. Although the fully numerical methods have no problem in describing the subsystems' configurations of this specific case, SEA needs to approximate their wavefields from a selection of possible elementary configurations. In this specific case, a singly curved configuration was observed to best model both subsystems. The VAOne software approximated the excited and receiver plates' radius by, respectively, 3.466 m and 0.156 m. Again, no Hybrid FE-SEA model was derived and a Numerical SEA model was used for the Generalized hybrid method. Lumped wavefield definition was used for each both plates.

Figure 31 and Fig. 32 exhibit the results, respectively, for the excited and receiver

plates. Here, the novel method was capable of smoothly converging to the FE Monte Carlo's curve, which is expected as the methods uses standard FE models. However, it is clear that the analytical formulations from SEA were not capable of deriving such robust wavefield definitions for the subsystems. As such, in the excited subsystem's results, there is an overall overestimation, when compared to the reference FE Monte Carlo curve. This is a consequence from the erroneous derivation of the input power to the subsystem (shown in Fig. 33).

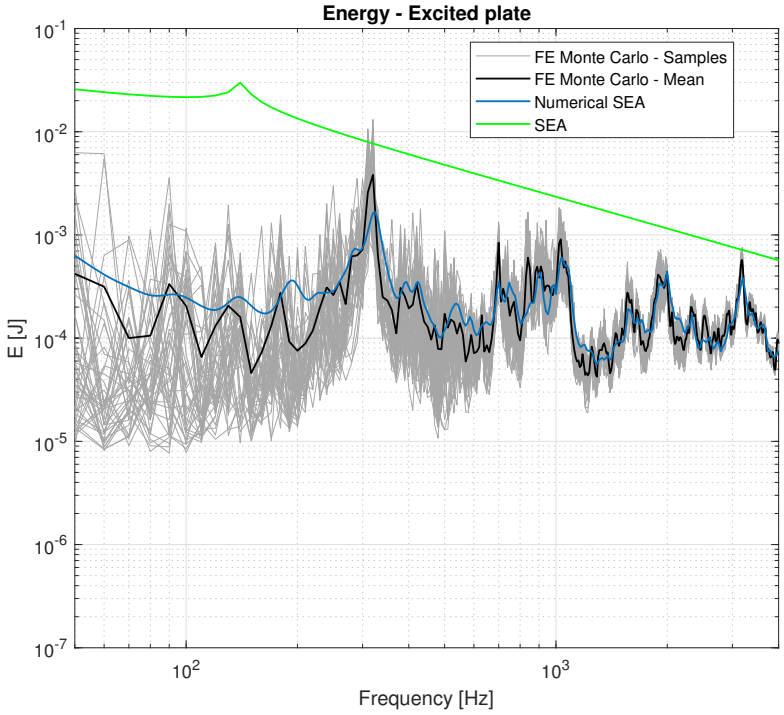

Figure 31 – Excited plate's energy results in the fourth case

In the processing cost's point of view, shown in Fig. 34, the expected times demanded from each method were obtained: the FE Monte Carlo's sample requiring the most of them to derive a single sample result, SEA requiring seamlessly costs and the Generalized Hybrid in mid-way. However, while the order was anticipated, the novel method was capable of requiring solely a fifth of the FE sample cost, exhibiting competitive efficiency for systems with irregular configurations. Furthermore, as SEA did not met a reliable result, its short processing time was meaningless. The novel method would be then the optimal method to model such irregular system in high frequency regions.

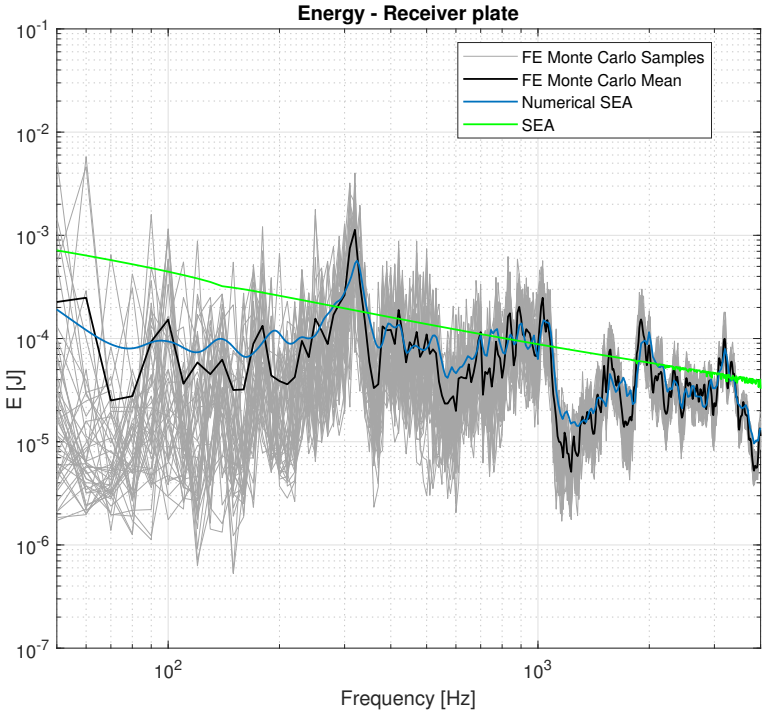

Figure 32 – Receiver plate's energy results in the fourth case

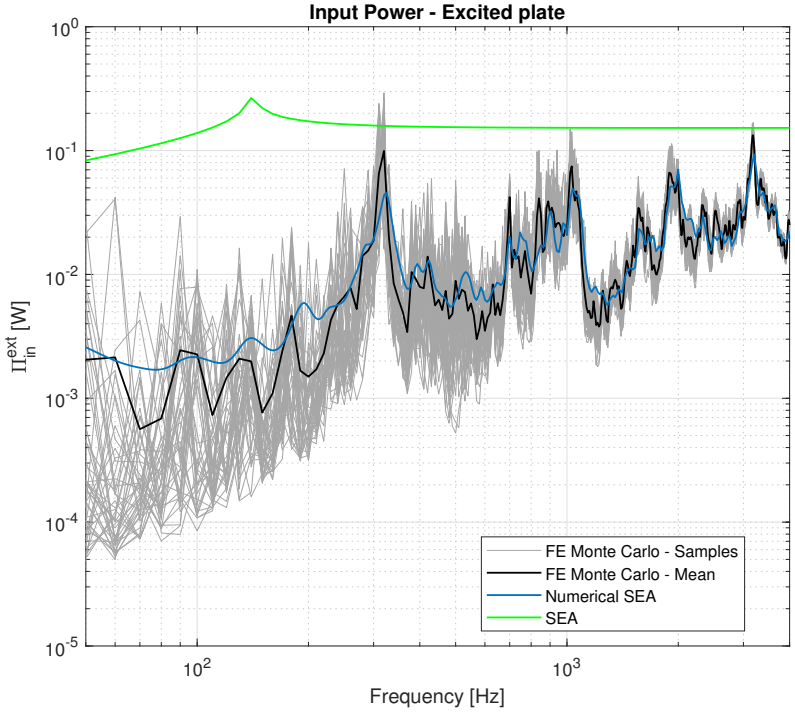

Figure 33 – Excited plate's input power in the fourth case

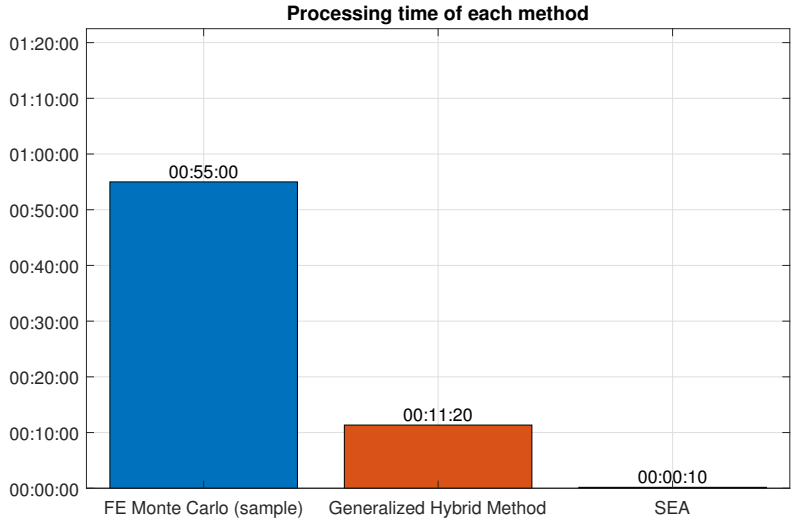

Figure 34 – Processing time for each method in the fourth case

6 CONCLUSION AND FUTURE WORKS

The thesis was planned to present, in both theory and results, the performance of established and novel vibroacoustic methods when applied to complex vibro-acoustic systems. The most employed methods used for structural vibrations were selected, ranging from the ones recommended low-frequency problems, to the ones associated to mid and high frequency problems. The novel generalized method was introduced, given by its formulation derivation and, after, by its implementation processes required for optimal efficiency. A set of mid and high-frequency problems were then selected to evaluate the methods' performance.

For complex structural systems associated purely to low frequency motions, the Finite Element Method (FEM) has the optimal performance of all methods, as it has the greatest capacity of modeling details from the system's configuration. Also, at this frequency range, the system's wavelength is considerably large, demanding only coarse mesh to properly characterize the subsystem's wavefields. This limits the necessary computational processing cost to a lower level. Lastly, the system is mostly deterministic, and therefore, statistical ensembles becomes unnecessary, resulting in additional processing cost saving to the model.

In the case of mid-frequency problems, an ensemble of samples and a dense mesh are demanded for a proper definition of specific components of the system, which mostly discourages the use of FEM for practical applications. This thesis's first and second examples explored such scenario. For cases consisting entirely of elementary configurations, such as homogeneous and isotropic properties with well behaved geometry and point/flat junctions, the analytical formulations used in the Hybrid FE-SEA Method are capable of deriving a robust wavefield characterization. This is case of the first numerical example, where the optimal performance is achieved by the established hybrid method. Although the generalized method was also capable creating a proper wavefield definition, the computational effort became excessive for such a simple system.

For mid-frequency problem's systems that surpass the elementary scope to their components configurations, a numerical derivation becomes necessary to avoid loss of generality, which is addressed in the second numerical example. The flow of energy between the subsystems is the contribution that is underestimated when derived through analytical formulations, as to the closed squared junction definition assumes an additional coherence contribution that is neglected by the straight approximation. Moreover, in order

to approximate the complex junctions of the system, the established hybrid had to split them into several simpler connections, which made the demanded processing cost for the method surpass the one from the generalized method that defines a single generalized junction per subsystems. This presented a simple example where the generalized hybrid method can outperforms the established hybrid method in both robustness of model and computational efficiency aspects.

In the high-frequency problem scenario, diffuse wavefields are assumed for every subsystems in the system, this condition makes the Hybrid FE-SEA method and the generalized hybrid method equivalent to, respectively, the SEA and the Numerical SEA. This scenario was explored in the third and fourth numerical examples. For these two cases, the same analogy made in the mid-frequency problems could be applied to derive a conclusion from their results: for the case consisting of solely elementary configurations, the method that uses analytical formulations (SEA) is likely to be choice for analysis, wheres, when more complex configurations are assumed, the generalized one (Numerical SEA) tends to be the choice.

Similarly to the second case, where the fully numerical method (Generalized hybrid) and the one that supports analytical formulations (Hybrid FE-SEA) were compared, the fourth case explores a system with much more irregular configurations, which then, as expected, resulted in a lot more divergence between the two methods (SEA and Numerical SEA), as the wavefield became very difficult to be approximated by analytical formulations. In contrast to the second case, here the novel method had a much larger processing cost when compared to the one from the established method. This mostly due to the fact the no projection over modal basis were possible to be performed in the junction's degrees of freedom. This aspect should be taken with care, as with the increasing number of statistical subsystems, the number of junctions with no possible modal projections can make the method unfeasible for practical analysis.

In short, the idea extracted in the thesis's numerical analysis was that no single vibro-acoustic method has a optimal performance for every possible scenario. It will mainly depend on the system's characteristics and on the context of the analysis. The thesis managed to present some guidelines regarding the choice for the most suitable method to be used in some specific case scenarios. Clearly, there will be cases where neither method presents the desired performance. In this scenario, their features should be weighted.

The novel method presented solid and promising results for mid-frequency problems,

as well as it was able to reaffirm its robustness to model high-frequency cases. Nevertheless, a deeper evaluation of the framework's contributions could be performed, such as analyzing deeper the partitioned wavefield's contributions and results. Moreover, this partition process was necessary for modeling the power-flow of flat plate's wavefields, which are ideally uncorrelated. A generalization of this process or a derivation of partitioned wavefields for more complex configurations is of great interest. Lastly, although the novel method is intended for vibro-acoustics analysis, it was only evaluated, here in the thesis, with structural vibrations, thus the performance of the method in modeling a system containing both acoustic cavities and area junctions remains as intended. More generic formulations and implementation procedures would be required to be defined, in order to derive a solid and efficient representation for these different components.

REFERENCES

ALIMONTI, L. et al. The diffuse field reciprocity relationship as a framework for a general power flow model. **NOISE-CON**, 2019.

CLOT, A. et al. An experimental exploration of the properties of random frequency response functions. **Journal of Sound and Vibration**, 2020.

COTONI, V.; SHORTER, P. J.; LANGLEY, R. S. Numerical and experimental validation of a hybrid finite element-statistical energy analysis method. **Journal of Acoustical Society of America**, 2007.

CREMER, L.; HECKL, M.; PETERSSON, B. **Structure-Borne Sound**: Structural Vibrations and Sound Radiation at Audio Frequencies. 3. ed. United States: Springer, 2005.

DEVRIENDT, H. et al. Coupling Loss Factor Calculation Through Lorentzian-Weighted Frequency Averaging of the Direct Field Dynamic Stiffness, 2015.

ESI GROUP. **VAOne 2019.1**. Paris, France, 2019.

FAHY, F.; GARDONIO, P. **Sound and Structural Vibration**: Radiation, Transmission and Response. 2. ed. United States: Elsevier, 2007.

HAMBRIC, S. A.; SUNG, S. H.; NEFSKE, D. J. **Engineering Vibroacoustic Analysis**: Methods and Applications. 1. ed. United Kingdom: Wiley, 2017.

HANSEN, C. H. **Foundations of Vibroacoustics**. 1. ed. United Kingdom: Taylor and Francis Group, 2018.

HINZ, M. **Statistical Energy Analysis Modeling of Deterministic Subsystems**. 2021.

LANGLEY, R.; CORDIOLI, J. Hybrid deterministic-statistical analysis of vibro-acoustic systems with domain couplings on statistical components. **Journal of Sound and Vibration**, 2009.

LANGLEY, R. S.; HERON, K. H. Elastic Wave Transmission Through Plate/Beam Junctions. **Journal of Sound and Vibration**, 1990.

LANGLEY, R. S.; SHORTER, P. J. The wave transmission coefficients and coupling loss factors of point connected structures. **Acoustical Society of America**, 2003.

LANGLEY, R. Numerical evaluation of the acoustic radiation from planar structures with general baffle conditions using wavelets. **Journal of the Acoustical Society of America**, 2007.

LANGLEY, R. On the diffuse field reciprocity relationship and vibrational energy variance in a random subsystem at high frequencies. **Acoustical Society of America**, 2007.

LE BOT, A. **Foundation of Statistical Energy Analysis in Vibroacoustics**. 1. ed. United Kingdom: Oxford University Press, 2015.

LYON, R. H.; DEJONG, R. G. **Theory and application of statistical energy analysis**. 1. ed. United States: Butterworth-Heinemann, 1995.

MACE, B. R.; SHORTER, P. J. Energy Flow Models from Finite Element Analysis. **Journal of Sound and Vibration**, 2000.

MARCELLA, F. **Calculation of the Coupling Loss Factors for a Hybrid FEM/SEA Line Junction**. 2018.

MATHWORKS. **Matlab 2020b**. Natick, MA, US, 2020.

MEIROVITCH, L. **Fundamentals of Vibrations**. 1. ed. United States: Waveland Press, 2010.

PAPADRAKAKIS, M.; PAPADOPOULOS, V. Robust and efficient methods for stochastic finite element analysis using Monte Carlo simulation. **Computer methods in applied mechanics and engineering**, 1996.

PETYT, M. **Vibration of Discrete and Continuous Systems**. 3º. Unided Kingdom: Springer, 2019.

SHABANA, A. **Fundamentals of Vibrations**. 1. ed. Switzerland: Waveland Press, 2010.

SHORTER, P. J.; LANGLEY, R. S. On the reciprocity relationship between direct field radiation and diffuse reverberant loading. **Journal of Acoustical Society of America**, 2005.

SHORTER, P. J.; LANGLEY, R. S. Vibro-acoustic analysis of complex systems. **Journal of Sound and Vibration**, 2005.

TOURNOUR, M.; ATALLA, N. Pseudostatic corrections for the forced vibroacoustic response of a structure-cavity system, 2000.

WILLIAMS, E.; MAYNARD, J. Numerical evaluation of the Rayleigh integral for planar radiators using the FFT. **Journal of the Acoustical Society of America**, 1982.

APPENDIX

The FE Monte Carlo model was used as reference for the evaluation of the numerical methods in this work. It generated an ensemble average response from a collection of nominal identical samples, which each was randomized to simulate the effects of manufacturing imperfection in the vibro-acoustic system. This is vital for high frequency problems as deformations at this frequency range are very sensible to imperfections, hence they should be considered in the model. The randomization process applied to each sample is essentially directed to dynamics of the system (dynamic stiffness matrix) and external loads (force vector). The former is randomized by the application of (clamped or pinned) constrains at random groups of nodes on the statistical subsystems (the ones sensitive to imperfections). Figure 35, Fig. 36 and Fig. 37 present examples of these constrains (white nodes for clamped and green for pinned) applied to samples. Here, the beam was understood was deterministic, therefore no constrains were applied to it. Only the plates were defined as statistical subsystems.

These constrained nodes were elected from all possible nodes positioned at a maximum distance from (randomly) selected locations. Care was taken to make sure the systems were not extensively clamped, which would inadequately impact the statistics and energetics of the system. Therefore, a maximum size for constrained regions and minimum distances between different constrained regions were defined and manually calibrated for each different system. In the case of the randomly applied transverse force, care was taken only to ensure that the excitation was not applied near discontinuities (junctions, holes or constrains) to avoid coupling of the in-plane and out-of-plane wavefields to the input power. Examples of external forces locations applied to samples are exhibited on Fig. 35, Fig. 36 and Fig. 37 as well.

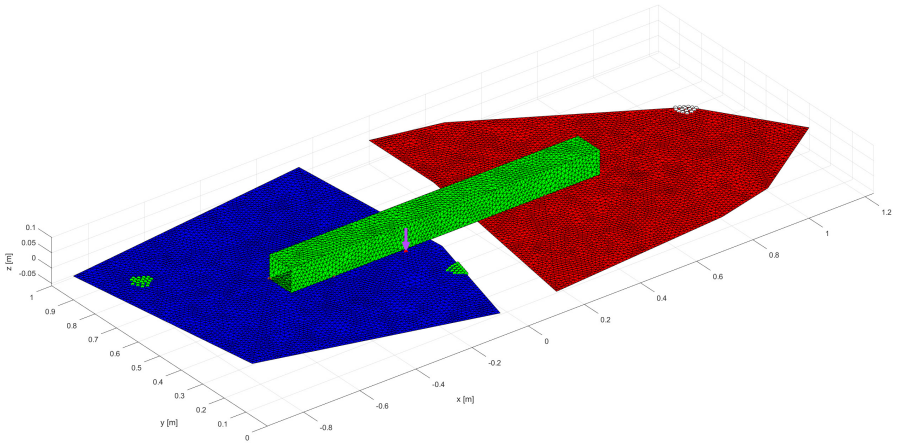

Figure 35 – First example of a randomized FE Monte Carlo sample.

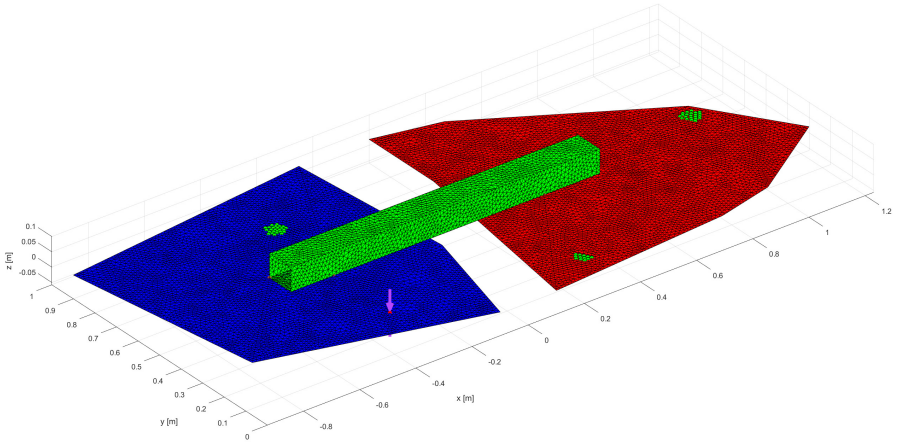

Figure 36 – Second example of a randomized FE Monte Carlo sample.

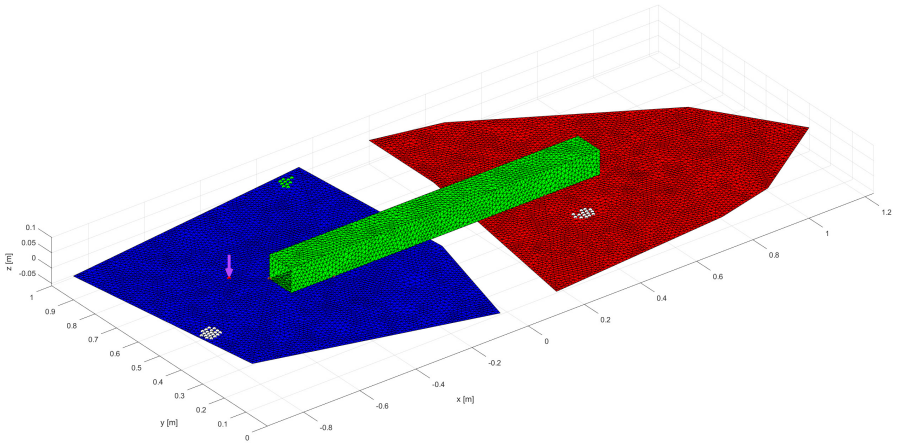

Figure 37 – Third example of a randomized FE Monte Carlo sample.